EXPERIMENTAL INVESTIGATION OF MIXING ENHANCEMENT IN A SMALL MIXING LAYER FACILITY AT LOW REYNOLDS NUMBER

By

Rohit Somnath Nehe

A DISSERTATION

Submitted to
Michigan State University
in partial fulfillment of the requirements
for the degree of

Mechanical Engineering – Doctor of Philosophy

2013

ABSTRACT

EXPERIMENTAL INVESTIGATION OF MIXING ENHANCEMENT IN A SMALL MIXING LAYER FACILITY AT LOW REYNOLDS NUMBER

By

Rohit Somnath Nehe

Many chemical and biological analyses are carried out in small devices which require rapid mixing of reactants. These miniaturized devices involve low speed flow wherein mixing occurs in the absence of turbulence. Microfluidic mixing devices are known to be poor mixers since molecular diffusion at the interface of flow streams forms the only mechanism of mixing. The key to enhance the mixing in such a low speed regime is to manipulate the contact area of two initially segregated flow streams.

In regards to the above mentioned problem, an experimental investigation is performed to understand the mixing field in a low Reynolds number forced wake flow. The flow velocity is so low that, in the absence of the imposed perturbation, mixing is primarily governed by interfacial diffusion mechanism which is similar to the situations commonly seen in microfluidic applications. To enhance the mixing interfacial area, flow perturbation is provided over a range of frequencies and amplitudes. The chemically reacting laser induced fluorescence technique (LIF) is used to quantify the level of mixedness, while single component molecular tagging velocimetry (MTV) technique is used to measure the amplitude of perturbation velocity. A non-reacting LIF technique is utilized for few selected forcing cases to study the distribution of mixed fluid composition.

Each forcing frequency creates a unique interfacial mixed fluid structure with different levels of chemical product. For low forcing frequencies, mixed and unmixed fluid regions were noticed

wherein mixed fluid was found on the interfacial structures. A large amount of chemical product was observed for certain high forcing frequencies which also corresponded to the highest perturbation velocity amplitudes, highlighting the large velocity dynamics involved in these cases. These highly mixed cases are also found to show asymmetric mixing characteristics. A chemically reacting LIF was also performed at lower forcing amplitude over all the forcing frequencies, and the amount of mixedness is seen to be directly connected to the forcing amplitude.

In addition to quantifying the mixedness, a stationary and reverse flow behavior of the mixed fluid structure was observed in certain forced cases. This phenomenon is discussed in detail by utilizing phase resolved streamwise chemically reacting LIF concentration fields.

DEDICATION

I dedicate this dissertation to my mother, grandmother and (late) grandfather for their love, support and guidance throughout my life.

ACKNOWLEDGEMENTS

I would like to acknowledge my advisor, Dr. Manoochehr M. Koochesfahani (Dr. K) for his continuous guidance during my PhD studies. His mentorship and encouragement throughout my research has always motivated me to work hard and strive for excellence. Also, I would sincerely thank Dr. K for providing me an opportunity to work on a "*gas phase photochemistry*" problem, in addition to the fluid dynamics research described in this dissertation. Photochemistry project allowed me to enhance my knowledge and broaden the research experience at Michigan State University.

I am very grateful to my doctoral committee members, Dr. Farhad Jaberi, Dr. Charles Petty and Dr. Ahmed Naguib for the comments and suggestions recommended by them during the course of Ph.D. program. I would also like to extend special thanks to Dr. Ahmed Naguib for all the valuable discussion during the first year of PhD program as my co-advisor.

Gratitude is also due to Michael Mclean, Roy Baliff and Alan Lawrenz for all the technical assistance related to various aspect of the experimental setup.

I would like to extend my thanks to all of the current as well as the previous members of ERC fluids group which includes laboratories TMUAL, FPaCL and TSFL for creating a very lively and friendly research environment. I would like to specially acknowledge Dr. Shahram Pouya for mentoring me throughout my PhD on operating different instruments in the laboratory and providing me his inputs whenever it was needed. I would also like to thank David Olson for helping me with the MTV and LIF data processing programs and also for many other stimulating technical and non-technical discussions. Special

thanks to Kyle and Lisa Bade, Dr. Bruno Monnier and Rachel for being good friends in and out of the lab and also for the valuable words of encouragement throughout my PhD.

Last, but not the least, I would like to take this opportunity to thank my family, which includes, my mother, grandparents, uncles and aunts for their support, patience and tacit understanding yet warm enough to motivate me to achieve my dream of attending a graduate school and performing scientific research.

TABLE OF CONTENTS

LIST OF TABLES

LIST OF FIGURES

KEY TO SYMBOLS

Symbol	Description
A	Cross sectional area
A_1, A_2, A_3	Bellows forcing amplitudes
A_p	Chemical product area
C_d	Local instantaneous dye concentration
C_o, C_{do}	Free stream dye concentration
C_p	Chemical product
$C_{p(max)}$	Maximum chemical product
C_P^*	Normalized chemical product
$\overline{C_P^*}$	Average normalized chemical product
D	Molecular diffusivity
d	Span length
F	Forcing frequency
I_B	Background signal
I_{corr}	Corrected intensity
I_f, I	Fluorescence intensity
I_o	Reference intensity

I_{ref}, $I_{f\,(max)}$	Maximum fluorescence intensity
l	Length of channel
L_d	Characteristic length scale for diffusive mixing
n	Number of active dye molecules
n_o	Initial total number of dye molecules
N	Number of images
Pe	Peclet Number
Q_b	Bleaching quantum efficiency
Re	Reynolds number based on channel width
Re_θ	Reynolds number based on momentum thickness
S	Length of one zig-zag pattern
t	Time
T	Time period
T_d	Characteristic time scale for diffusive mixing
U	Streamwise velocity
U_M	Spatially averaged streamwise velocity
U_{min}	Minimum streamwise velocity in wake
U_{max}	Maximum streamwise velocity in wake
U_{RMS}	Streamwise RMS velocity
W, w	Width of channel
x	Co-ordinate, streamwise direction

y	Co-ordinate, direction normal to wall
z	Co-ordinate, spanwise direction
α	Absorption coefficient
δ_p	Product thickness
Δt, t_d	Time between undelayed and delayed image (MTV measurements)
ε_0	Dye molar absorption coefficient
λ	Wavelength of laser
ξ_B	Base volume fraction
ξ	Normalized concentration
ξ_s	Stoichiometric base volume fraction
σ	Dye absorption cross section
τ_b	Photobleaching time constant
Φ	Phase
ϕ_p	Laser photon flux

1. INTRODUCTION

This study involves the experimental investigation of mixing field developed from a forced wake of a very low Reynolds number flow. Motivation of this mixing enhancement study arises from the requirement of rapid mixing in miniaturized devices commonly used in biological and chemical analyses. Many biological processes at small scale involve reactions which require mixing of reactants for initiation. The challenge in a low speed flow regime is the absence of mixing due to turbulence. Microfluidic devices are poor mixers since the interfacial contact area is usually small. So in this case, molecular diffusion at the interface of flow streams forms the primary mechanism of mixing. Consider a flow in a channel of width W (see Figure 1-1), wherein the streamwise velocity U is so low such that mixing is limited to molecular diffusion mechanism.

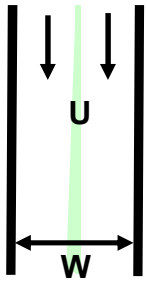

Note: For interpretation of the references to color in this and all other figures, the reader is referred to the electronic version of dissertation.

Figure 1-1. Schematic of flow through a microfluidic channel
(green color indicates mixing due to diffusion)

The Peclet number for this flow is $Pe = \frac{UW}{D}$, where D is the molecular diffusivity. The characteristic time scale for diffusive mixing is $T_d = \frac{W^2}{D}$, and the characteristic length scale is $L_d = \frac{W^2 U}{D} = Pe \times W$ or $\frac{L_d}{W} = Pe$. Thus, the distance along the channel

required to mix the flow streams solely by the diffusion process grows linearly with Peclet number, which is unacceptably high for the flows of practical interest to the microfluidic community. For example, consider the diffusivities shown in Table 1-1, for a small protein flowing in a 100 μm width channel at 100 μm/s requires $Pe \sim 250$ channel widths for complete mixing by molecular diffusion alone (Squires et al. 2005). The key to enhance the mixing in such a low speed regime is to increase the contact area of two initially segregated flow streams or to decrease the length scale over which diffusion acts. (This is the reason we usually stir the fluid to mix the two different species e.g. stirring of cream by spoon in a coffee mug reduces the diffusion length scale and thus it quickly reduces the mixing time).

Table 1-1. Typical diffusivities for various tracers at room temperature (Squires et al. 2005)

Particle	Typical size	Diffusion constant
Solute Ion	10^{-1} nm	2×10^{3} $\mu m^2/s$
Small Protein	5 nm	40 $\mu m^2/s$
Virus	100 nm	2 $\mu m^2/s$
Bacterium	1 μm	0.2 $\mu m^2/s$
Mammalian/Human Cell	10 μm	0.02 $\mu m^2/s$

The present investigation utilizes an active method to enhance the mixing in a very low speed flow. A high amplitude sinusoidal perturbation is applied on one of the flow stream of the mixing layer facility. Prior to this work, a preliminary flow visualization performed in TMUAL (Turbulent Mixing and Unsteady Aerodynamics Laboratory, East

Lansing, MSU) showed that the perturbed mixing layer exhibits local flow dynamics near the splitter plate tip enhancing the interfacial area to increase the mixedness (see Figure 1-2). This forms the main motivation of utilizing a small mixing layer facility as a mixing device. Another main reason for choosing a mixing layer facility for the mixing study is the geometric resemblance with some of the small scale mixing devices e.g. Y- mixer which are commonly used in microfluidic assay devices.

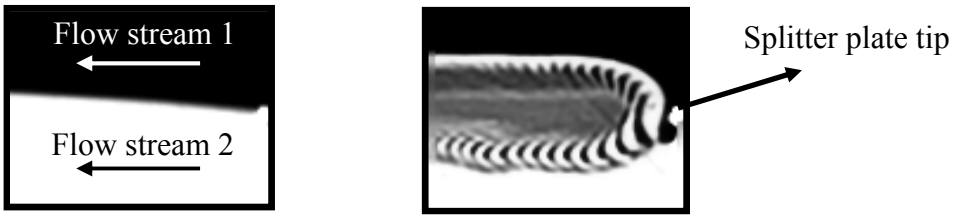

Figure 1-2. Mixing of two water streams downstream of a splitter plate tip
(a) A natural flow showing a passive (unperturbed) diffusion layer (b) Actively perturbed flow showing a large increase in the mixing interface.
(Unpublished data by Jason Smith (1999) at TMUAL)

A mixing layer facility can be operated as a wake or a two stream shear layer facility. A mixing layer is said to be a shear layer when the two streams of different velocity interact downstream of splitter plate. A wake flow is seen in a mixing layer when the two streams have the same velocity (Figure 1-3). For the experiments described in this study, the mixing layer facility is operated as a wake flow.

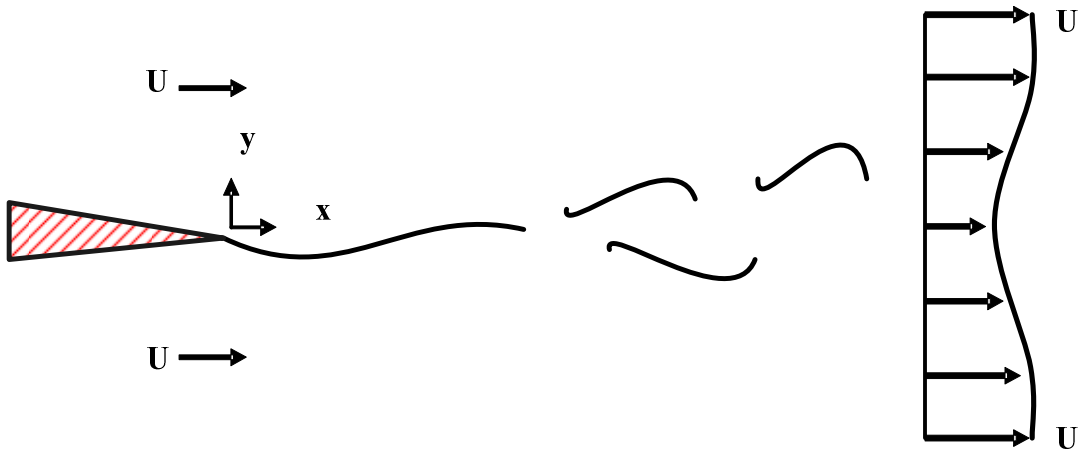

Figure 1-3. Sketch of a wake flow

1.1. PREVIOUS WORK

Several research groups have been studying mixing control and enhancement strategies in shear layers and wakes. Most of the previous studies are focused on higher Reynolds number compared to the Reynolds number flow studied in this report ($Re = 75$, based on channel width and streamwise velocity). Although much of the previous studies performed by researchers in the mixing layer do not relate to the current flow regime ($Re = 75$), it does provide background information on the mechanism used for mixing enhancement. The following two subsections will cover the literature review on forced mixing layers and mixing in microfluidic devices.

1.1.1. Forced mixing layer

Oster & Wygnanski (1982) is one of the earliest research work performed on a forced mixing layer. The main impetus of this work was to understand the sensitivity of the mixing layer (growth rate) to the finite amplitude oscillations introduced at the origin of the flow. Oster & Wygnanski (1982) showed the different growth characteristics of the turbulent shear layer depending upon the forcing frequency and amplitude used for the

given velocity ratio. Koochesfahani and Dimotakis (1989) studied the flow structure of a turbulent plane mixing layer by introducing two dimensional disturbances at some distance downstream of the splitter plate. The response of the mixing layer in the upstream and downstream region of the disturbance was investigated. The result showed that the upstream and downstream region can be selectively forced by the proper choice of the frequency. Although this study didn't quantify the molecular level mixedness, the results provided sufficient reasoning and motivation for researchers to manipulate and to control the spreading rate of the mixing layer by introducing artificial excitation of different frequency and amplitude.

Roberts and Roshko (1985) and Roberts (1985) used external forcing to study the mixing in a wake flow (Re_θ = 160, based on momentum thickness) perturbed at different frequencies. The forced wake studied by Roberts (1985) showed a great variety of interesting flow features. In the case of unforced wake, flow structure appeared to be a Karman vortex street with mixing product appearing at the interface. When the flow was forced at a frequency equal to its natural frequency (5 Hz) a well-organized flow structure was observed. Forcing at the frequency less than the natural frequency produced a double Karman vortex street. When the wake was forced at frequencies greater than the natural frequencies, the breakdown of the initial street was observed followed by a dramatic increase in mixing. The finite width of the test section and the thick side wall boundary layer were considered to be responsible for the three dimensional nature of the flow, causing enhanced level of mixing.

Koochesfahani and MacKinnon (1991) studied the influence of forcing on the mixed fluid composition of two stream shear layer using the non-reacting LIF technique. For the

cases they studied, the distribution of mixed fluid composition was found uniform across the width of the shear layer and an increase in the amount of mixed fluid was noted. Another mixing study was performed by MacKinnon and Koochesfahani (1993) to examine the effect of forcing amplitude on the mixing field of a low Reynolds number wake flow, the same flow studied by Roberts (1985). The forcing frequency was fixed at the natural frequency (F = 6 Hz), and Reynolds number was measured as Re_θ = 100 (based on momentum thickness). A significant increase in mixing was noted for a forced flow compared to unforced flow. Nelson (1996) performed chemically reacting LIF experiments at the same experimental conditions as mentioned in MacKinnon and Koochesfahani (1993). In his study, a high amplitude 2-D perturbation of the wake was used to generate strong spanwise vortices. Similar to Roberts, they also observed spanwise vortices - side wall interaction resulting in a dramatic increase in the three - dimensionality and chemical product. The quantitative measurements made in this study indicated an increase in mixing product by a factor of 40 over the unforced case. Also, the maximum level of mixing for a forced wake flow was recorded as three times higher than that observed for higher Reynolds number shear flow. A major conclusion of this study was that a forced low Reynolds number flow can mix much better than an unforced high Reynolds number flow.

1.1.2. Mixing in microfluidic devices

Microfluidic research groups have been working actively on improving the performance of mixing in microfluidic devices. In general, microfluidic devices used for mixing (micromixers) are classified as passive or active micromixers. Mixing in passive micromixers is obtained without using any moving part or external energy input. Passive

micromixers use the modifications in the geometry to introduce chaotic particle paths, ultimately increasing the mixing. An active micromixer uses an external source of energy for mixing process. The external source of energy or disturbance could be pressure, temperature, electrokinetics, magneto hydrodynamics or acoustics. The detail review of both passive and active micromixers used in microfluidics community could be found in Stone et al. (2004) and Nguyen et al. (2005).

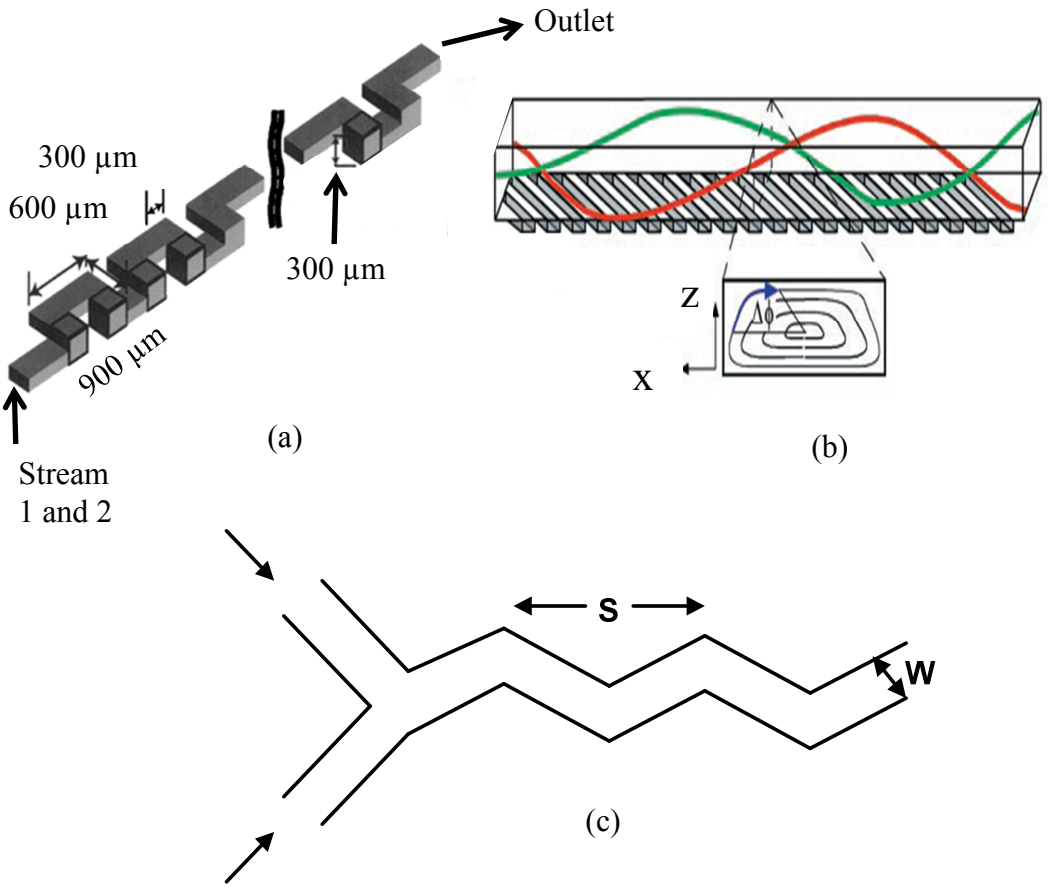

Figure 1-4. Schematic of various passive micromixers
(a) Three dimensional serpentine channel (Liu et al. 2000) (b) Herringbone channel (Strook et al. 2002) (c) Zigzag channel (Mengeaud et al. 2002).

Liu et al. (2000) designed a three dimensional serpentine microchannel (twisted channel) leading to chaotic advection mechanism to passively enhance fluid mixing (For details about chaotic advection phenomenon see Aref 1984, 1990, 2002; Ottino 1989).

The basic building blocks of this channel were the "*C-shaped*" mixing segments connected in series (Figure 1-4a). Mixing measurements were performed, and a comparison of mixing performance of serpentine channel was made with respect to "square-wave" and straight channel. Serpentine channel produced 16 times more mixed product than a straight channel and 1.6 times more than a "square-wave" channel.

The distortion of the interface, twisting and turning of the flow through the serpentine channel (chaotic advection) was explained as a reason for mixing enhancement. In general an increase in the mixing was observed with the increase in *Re* for the serpentine channel, and it was always higher than that observed for straight and square wave channels.

Strook et al. (2002) used a herringbone channel to generate transverse flows in a microchannel to induce chaotic stirring (Figure 1-4b). Channel geometry consisted of ridges on the floor at an oblique angle with respect to the axis of the channel. As a result, flow had less resistance in the direction parallel to ridges than in the orthogonal direction leading to a transverse component of velocity. Repeated helical motion of fluid volumes within channel produced a chaotic motion increasing the mixing. Another method to generate chaotic advection is to use a zigzag geometry to produce flow with recirculation regions along the channel (Figure 1-4c). Mengeaud et al. (2002) found the highest mixing efficiency for a geometry ratio $S/W = 4$ using numerical simulation for *Re* 0.26 to 267. For $S/W = 4$, below the critical Reynolds number of 80, mixing was found to be entirely dependent on molecular diffusion mechanism. For higher Reynolds number, ($80 < Re < 267$) the recirculation regions observed in the channel induced a transversal component of velocity, improving the mixing process. Lin et al. (2007) designed a planar serpentine

convergent-divergent channel and studied mixing using numerical simulation at *Re* = 160. Alternating convergent-divergent pattern of channel caused a local rotating flow at the turns and as a result, stretching and folding of interfaces was enhanced. This created irregular and chaotic flow trajectories along the channel promoting the fluid mixing. Figures 1-5 and 1-6 show few examples of active micromixers. Mensing et al. (2004) showed an in-expensive and easy–to-fabricate magnetic mixer (see figure 1-5a). The basic working principle of this mixer was to use a mixing blade in the mixing chamber and to control the rotation of this blade using externally applied magnetic field. This mixer was tested in a small channel and it was found to operate up to a flow rate of 10 ml/min.

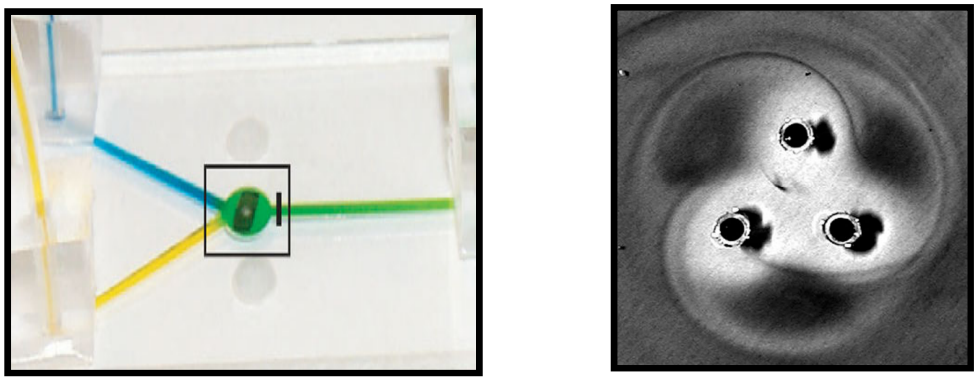

(a) (b)

Figure 1-5. Schematic of various active micromixers
(a) A magnetic mixing device using a blade in its mixing chamber. (b) Magnetic micromixers using doped magnetic particles.

Campbell et al. (2004) used magnetically doped particles to introduce the mixing. Polymeric particles were doped with magnetite and were made to rotate in the liquid using a magnetic field of a permanent rotating bar magnet (Figure 1-5b). As a result of externally applied magnetic field and the hydrodynamic forces, a system of rotating particles was formed to enhance the mixedness. Bau et al. (2001) presented the

theoretical and experimental investigation of a magneto-hydrodynamic stirrer. In his experiments, arrays of electrodes were deposited on a conduit wall. The conduit was filled with electrolyte solution and a potential difference was applied across the pair of electrodes establishing a flow of current in the solution. In presence of magnetic and electric field a body force (Lorentz) was generated to drive the fluid. This principle was utilized to create a complex flow field to enhance the mixing. Glasgow et al. (2003) introduced a time pulsing cross flow into a main channel to enhance the level of mixing. In this work, a liquid is pulsed from one inlet to periodically distort the interface between the two flow streams. A study was also performed wherein both of the flow streams where pulsed at a different phase. Mixing in this work was studied only at one pulsing frequency using Fluent 6 software and it was found that the pulsed flow with 90 degree phase difference provided the better mixing performance.

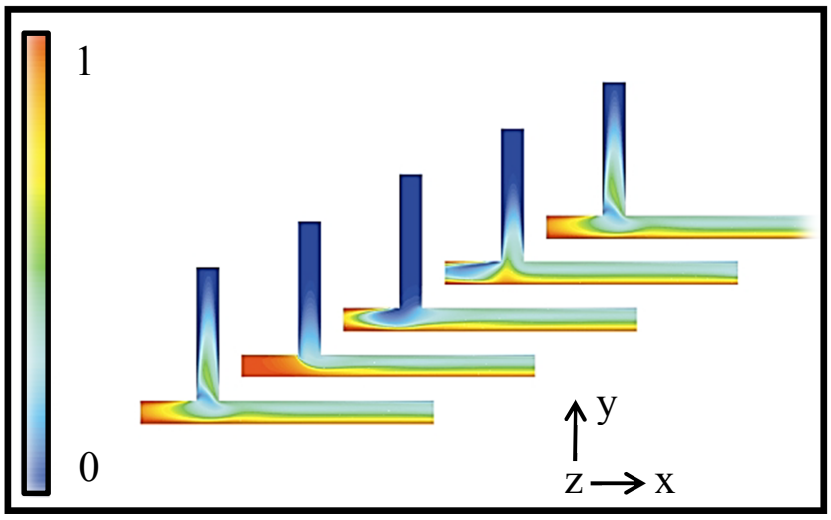

Figure 1-6. Numerical simulation result of two inlet flows pulsed at a 90 phase difference (Contour plot of mass fraction from Glasgow et al. 2003)

1.2. OBJECTIVE OF THE CURRENT WORK

The objective of this project is to quantify the amount of chemical product formed in a forced wake of a low Reynolds number flow. The flow studied in this dissertation is at such a low velocity that the natural flow (i.e. unperturbed flow) has mixing only across a planar diffusion layer, commonly seen in microfluidic geometries. To enhance the level of mixedness we use an active method of mixing. All the mixing measurements are made using chemically reacting laser induced fluorescence (LIF) technique. The amount of chemical product or the degree of mixedness is calculated from the time series data obtained through spanwise planar measurements.

Some of the questions which will be addressed through this dissertation are as follows:

1) What is the maximum amount of chemical product for a forced mixing layer at a very low Reynolds number?
2) How does the chemical product vary along and across the flow channel?
3) What is the range of mixing control parameters (perturbation amplitude and frequency) to enhance the mixing at the given Reynolds number?
4) What is the flow structure dynamics within a forcing cycle?

2. EXPERIMENTAL FACILITY AND INSTRUMENTATION

All the experiments were performed in a small mixing layer facility located in Turbulent Mixing and Unsteady Aerodynamics Laboratory (TMUAL). This chapter will provide details about the experimental facility, forcing mechanism and conditions and the imaging system used for both chemically reacting LIF and MTV experiments.

2.1. EXPERIMENTAL FACILITY

The experiments were performed in a gravity-driven liquid two-stream mixing layer facility with a test section of size 5 mm (w-width) × 10 mm (d-span) × 50 mm (l-length). A schematic of the facility is shown in Figure 2-1(a). Water was pumped from two separate reservoirs to constant head tanks, located approximately 0.4 m above the inlet of the test section. The constant head tanks were connected to the contraction chamber by tygon tubes. The contraction chamber housed a splitter plate separating the two streams. Here, the contraction chamber is designed such that it follows 5^{th} order polynomial with ratio of inlet width to outlet as approximately 4. Beyond the contraction chamber, flow was allowed to mix in the test section. The test section was constructed from quartz glass allowing optical access for LIF and MTV measurements. The flow from the test section entered the end section and finally it was discharged into the dump tank. An important aspect in terms of flow quality is the air bubble entrapment or the air pockets formed in the facility. This problem was eliminated by filling the facility with water from end section at the start of every experiment. The flow rate through the facility was controlled using three valves: one each along the two fluid supply lines and one at the end section.

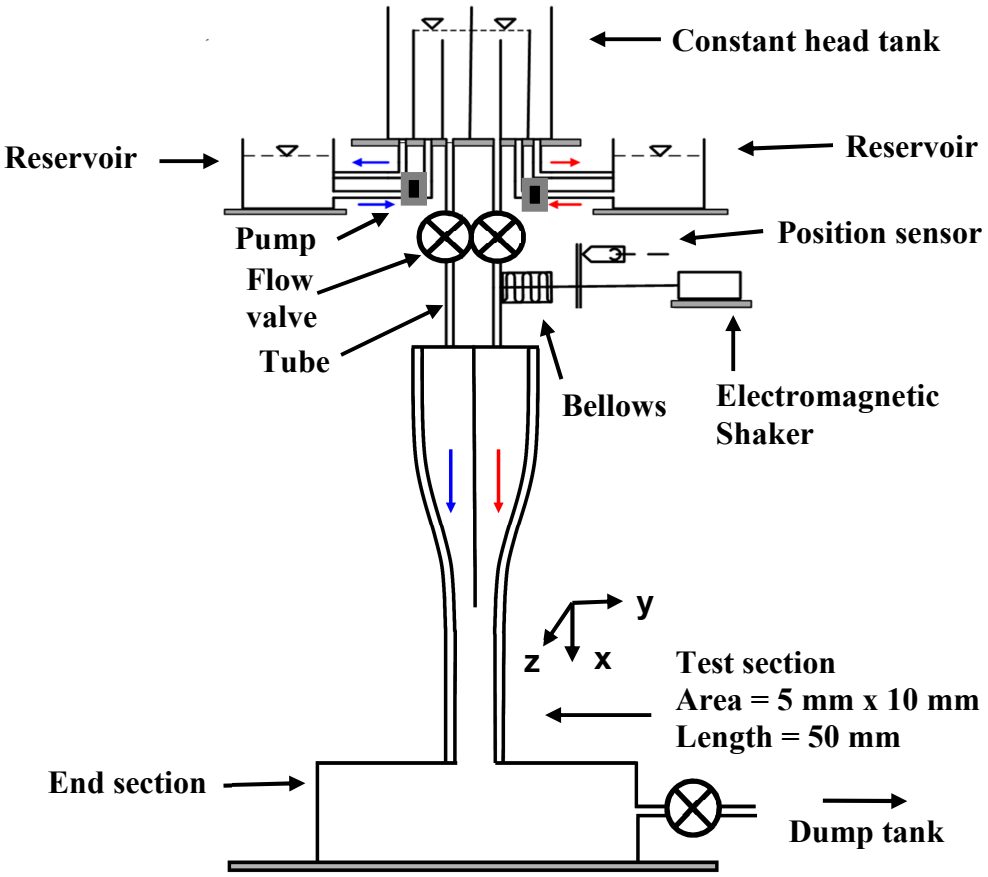

Figure 2-1(a). Schematic of the mixing layer facility (Not drawn to scale)

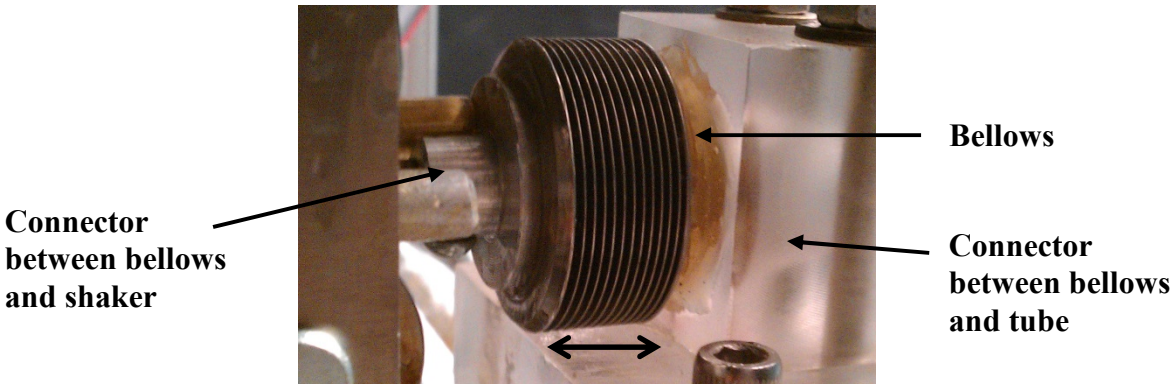

Figure 2-1(b). Forcing mechanism (Bellows)

2.2. FORCING MECHANISM AND CONDITIONS

Perturbations were introduced in one of the flow streams using bellows attached approximately 0.18 m upstream of the test section inlet. The diameter of bellows is 35.6 mm (Figure 2-1b). This mechanism is driven by an electromagnetic shaker (Lab works Inc., ET-132) powered by Haffler power amplifier (P1000) whose command signal originates from a function generator (Stanford Research systems – DS345). A position sensor (Schaevitz sensor, 200 DCD) is used to track the actual motion of the bellows. The signal from the position sensor is digitized by a 16 bit Analog to Digital converter (NI-PCI 6221). The forcing mechanism used in this study provides an active method of control of mixing such that the flow rate of one of the flow stream is continuously modulated at desired frequency and amplitude. For the results described in this dissertation, the forcing amplitude (A) defined is the actual displacement of the bellows. The forcing amplitude in terms of velocity and the relevant analysis for each of the forced cases will be presented in Chapter 4. Sinusoidal perturbation signals were used at three forcing amplitudes A_1 = 25 μm, A_2 = 40 μm and A_3 = 60 μm over the range of frequencies F = 2 Hz to F = 25 Hz. A list of all of the forcing conditions used in this study is tabulated in Table 2-1.

The forced cases described in this dissertation corresponds to the wake velocity U = 20 mm/s. The detail mixedness was measured for two amplitudes (A_2 = 40 μm and A_3 = 60 μm) while the qualitative features of the flow will be presented for the amplitude A_1 = 25 μm. Detail LIF measurements corresponding to A_1 = 25 μm was limited to only few cases since typically a lower amount of mixing was measured at A_1 = 25 μm.

Table 2-1. Forcing conditions for the mixing experiments. The letters ST and SP indicates the streamwise and spanwise LIF imaging.

Forcing frequency (F Hz)	Forcing amplitude		
	$A_1 = 25$ μm	$A_2 = 40$ μm	$A_3 = 60$ μm
2	ST	ST, SP	ST, SP
4	ST	ST, SP	ST, SP
8	ST	ST, SP	ST, SP
10	-	ST, SP	ST, SP
12	ST, SP	ST, SP	ST, SP
15	ST	ST, SP	ST, SP
18	ST, SP	ST, SP	ST, SP
19	-	ST, SP	ST, SP
20	ST	ST, SP	ST, SP
21	-	ST, SP	ST, SP
22	-	ST, SP	-
25	-	ST, SP	ST, SP

2.3. IMAGING SYSTEM

The chemically reacting laser induced fluorescence (LIF) technique is used to measure the mixedness (details about LIF technique is discussed in chapter 3). For these experiments, a Genesis CX488-2000 STM optically pumped semiconductor laser (light mode, λ = 488 nm) was used as the light source. The laser power was typically in the range 0.60 to 0.75 W. The laser beam was transformed into a thin sheet (~ 0.5 mm) using a cylindrical lens (focal length fl = 6.35 mm) and a spherical lens (fl= 200 mm).

Streamwise and spanwise measurements were performed by aligning the laser sheet in the x-y plane (i.e. along the flow direction at midspan) and in a y-z plane (i.e. perpendicular to the flow direction) at different downstream locations. Figure 2-2 illustrates the streamwise imaging and spanwise imaging setup and the coordinate system used in this study.

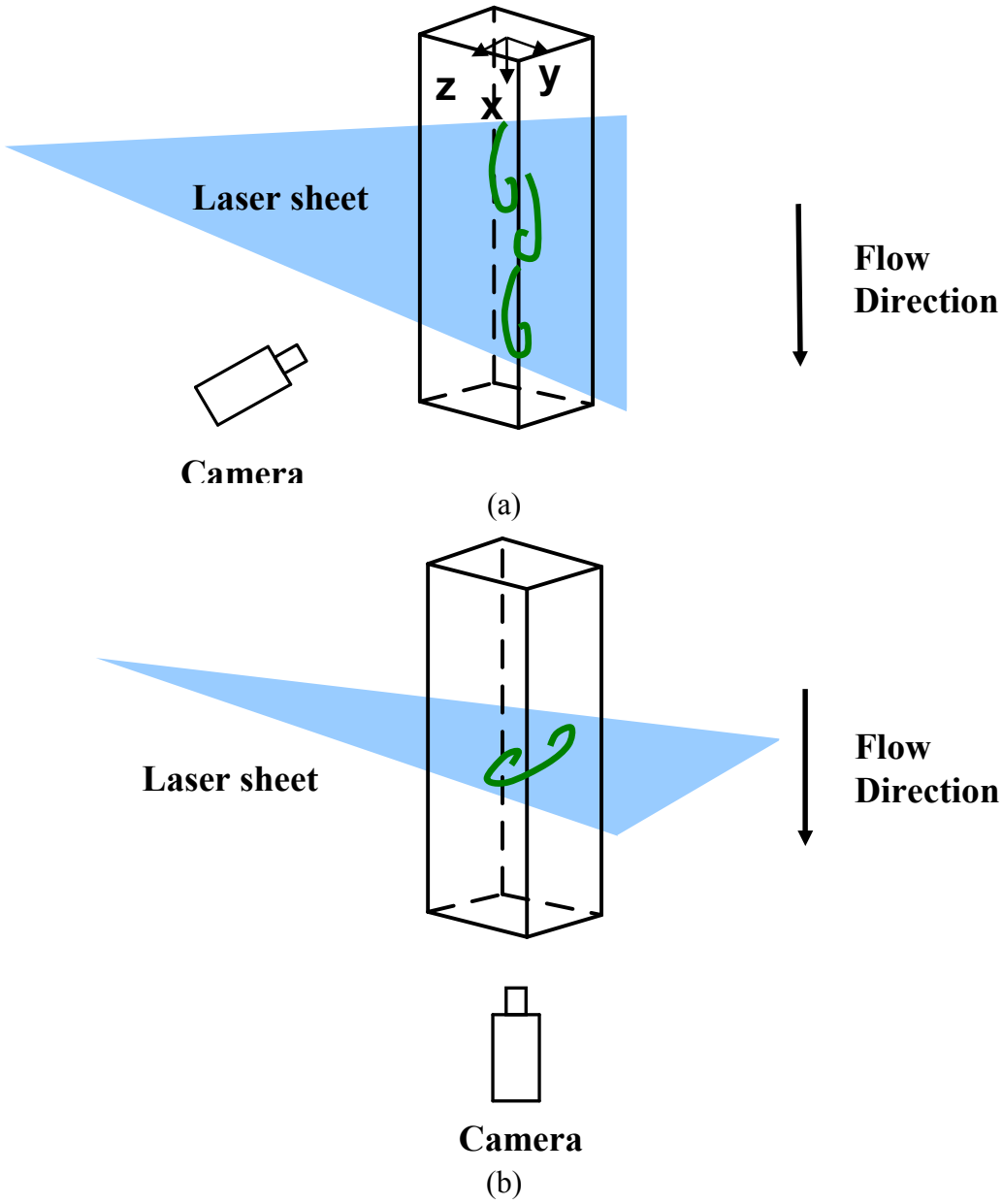

Figure 2-2. Setup for (a) streamwise (x-y plane) and (b) spanwise imaging (y-z plane).

The fluorescence signal was recorded by CCD camera (Pulnix TM-9700) operating at 30 frames per sec (2 ms exposure) and images were digitized to 8 bits. Nikkor 50 mm f/1.2 (streamwise imaging) and Micro-Nikkor 105 mm f/2.8 (spanwise imaging) lenses were used with an orange filter to eliminate the scattered laser light from the test section side walls and from the unwanted impurities in the flow. For each run, 1900 continuous

LIF images were acquired. The in-plane spatial resolution for streamwise imaging (x-y plane) was 65 × 65 μm, and that for spanwise (y-z plane) imaging was about 45 × 45 μm.

Multiple line molecular tagging velocimetry (MTV) was used to measure the streamwise component of velocity in the mixing layer facility. In order to measure the velocity, the laser beam from a Lambda-Physik LPX 220i excimer laser was used to tag the tracer molecules. The laser beam was transformed into thin lines using the necessary optical set up such that the distance between the lines was 0.8 mm (Figure 2-3).

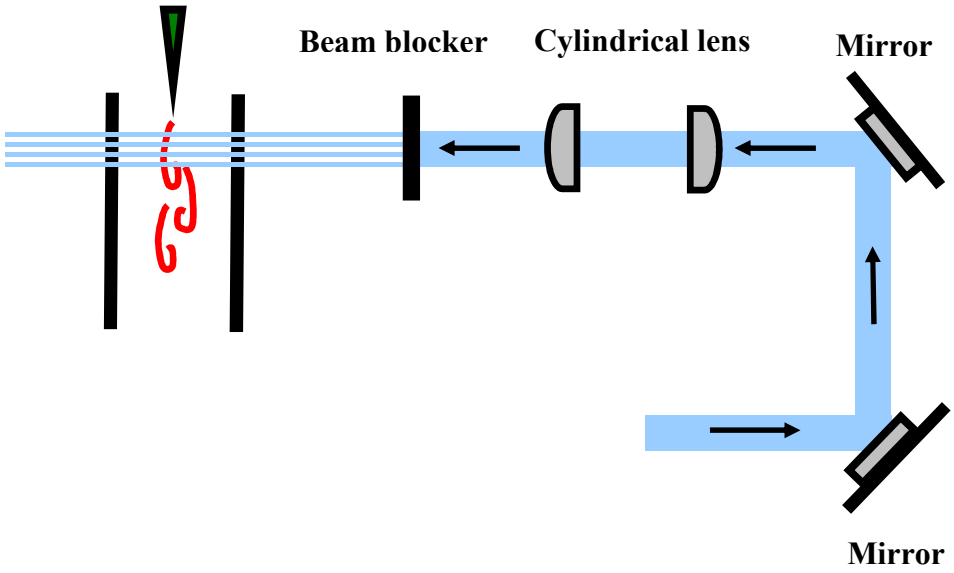

Figure 2-3. Optical experimental configuration for molecular tagging velocimetry (MTV) experiments.

The tagged lines were imaged using an intensified CCD camera (12 bit, DiCam Pro, Cooke Corp.) in a double frame mode at 5 Hz (1950 images) equipped with Nikkor 105 mm f/2.8 lens. In general, the pixel resolution was maintained in the range 17.5 μm to 15.5 μm. The laser and the camera were synchronized using a digital delay generator (Stanford Research Systems -model DDG535). The delay time t_d between undelayed and delayed image was chosen such that maximum pixel displacement as well as high signal

to noise ratio was obtained. Another factor, which puts a constraint on choosing a delay time, is its averaging effect on velocity measurement for high frequency forced cases. Appendix A shows the analysis of the above mentioned problem and also lists the delay and exposure time used for all of the different forcing cases.

3. DIAGNOSTICS: NOTES ON CHEMICALLY REACTING LASER INDUCED FLUORESCENCE

This chapter will describe the working principle of the chemically reacting laser induced fluorescence technique, data reduction procedure and also the definition of some of parameters which are used to define mixedness.

3.1. WORKING PRINCIPLE

A chemically reacting laser induced fluorescence (LIF) technique is used to measure the extent of molecular mixing. This technique is an extension of non-reacting LIF technique. A brief working principle is explained in this section while more details could be found in Koochesfahani (1984) and Koochesfahani and Dimotakis (1986). The chemically reacting LIF technique uses the pH sensitivity of a fluorescent dye, disodium fluorescein, to selectively induce fluorescence only in the mixed region. At low pH the fluorescence is essentially "off" (quenched) while at high pH (pH > 9) the fluorescence is "on" (Figure 3-1). In the mixing layer experiment, one stream is mixed with fluorescein dye (2.4×10^{-7} M, disodium fluorescein) and its fluorescence is turned off by diluting it with sulfuric acid (0.002 M, H_2SO_4). The second stream has no dye but it is buffered to a high pH by adding sodium hydroxide (0.06 M, NaOH) solution. When mixing between the two streams occurs, depending upon the local pH and the dye concentration, a fluorescence signal is seen. The resultant fluorescence intensity is a measure of chemical product which is formed due to a fast acid-base reaction of type $A + B \rightarrow P$. Here, the chemical product is defined as the dye bearing fluid whose local pH is above the fluorescence threshold.

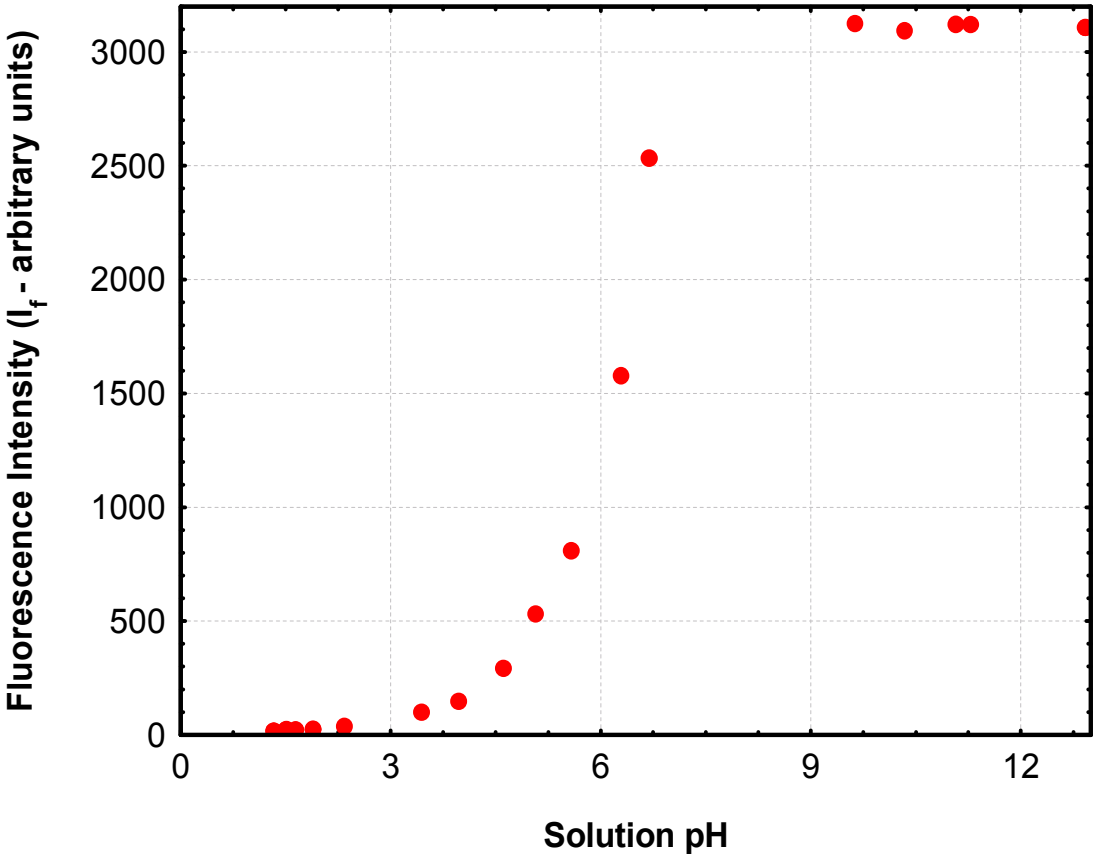

Figure 3-1. Measured pH dependence of fluorescein dye.

Figure 3-2 illustrates the relation between fluorescence intensity (chemical product concentration $C_{p)}$ and the base volume fraction ξ_B in the titration of a fixed volume of acid/dye solution. Initially, fluorescence is off since the pH of the solution is below the threshold. As the base volume fraction is increased beyond a threshold value (stoichiometric base volume fraction ξ_S), the fluorescence intensity sharply rises to maximum value. Here, the stoichiometric base volume fraction ξ_S defines the relative amount of acid and base required for chemical product to form. Beyond ξ_S, any more increase in base volume fraction merely dilutes the dye solution and, as a result, the

fluorescence intensity decreases linearly with base volume fraction. It should be noted that "stoichiometric" base volume fraction can be adjusted by the choice of acid and base concentrations. For the experiments described in this report, stoichiometric base volume fraction was typically measured between 0.06 and 0.07. This base volume fraction defines the maximum possible chemical product concentration $C_{p(max)}$ or the fluorescence intensity $I_{f(max)}$. The instantaneous local chemical product concentration C_p is defined by following relation

$$\frac{C_P}{C_{P(\max)}} = \frac{I_f}{I_{f(\max)}} \tag{1}$$

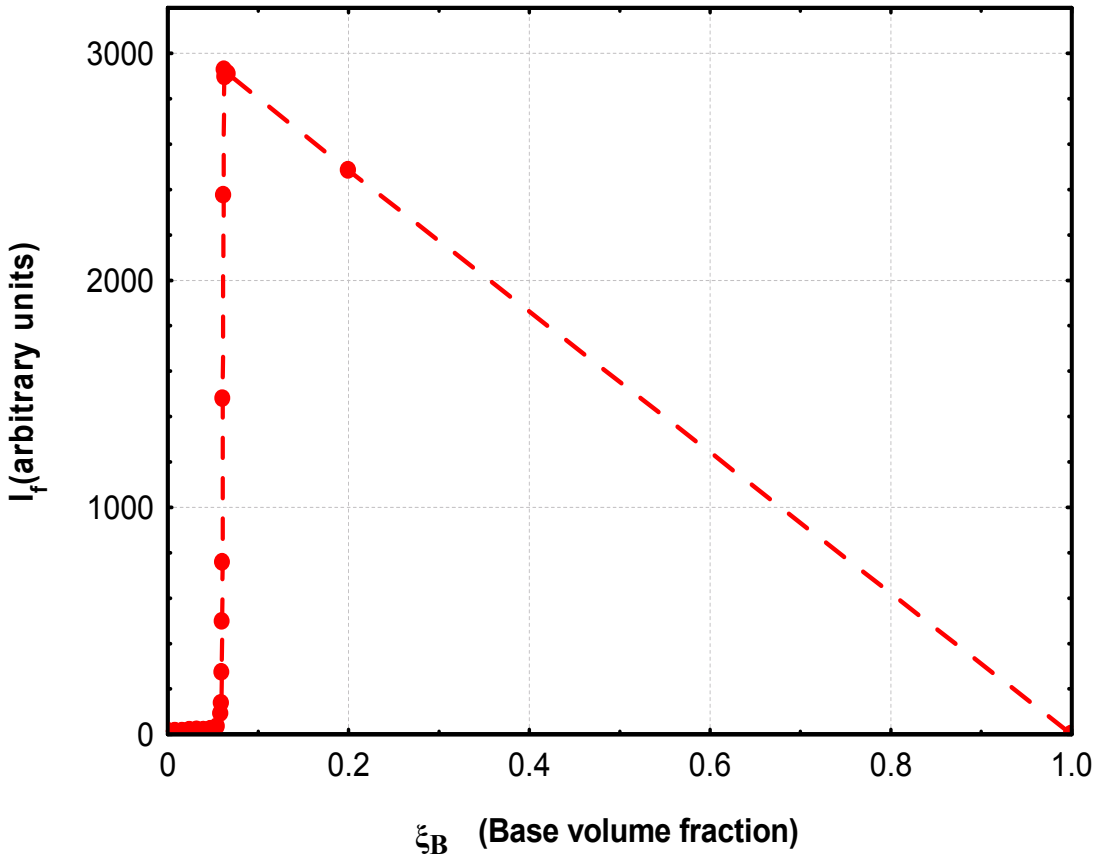

Figure 3-2. Measured fluorescence intensity versus base volume fraction in chemically reacting LIF.

In chemically reacting LIF experiments, due to different concentrations of acid and base a small density mismatch was recorded such that the density of acid and base was measured as 995 kg/m^3 and 1000 kg/m^3 respectively. The densities of the two free streams are matched by adding a sufficient amount of sodium sulfate (Na_2SO_4) to the lighter stream.

Laser beam attenuation by dye molecules forms one of the possible sources of error in LIF experiments. Koochesfahani (1984) measured the absorption coefficient α of the fluorescein dye to be 0.16 cm^{-1} corresponding to dye concentration $C_d = 1 \times 10^{-5}$ M and laser wavelength λ = 514.5 nm. The absorption coefficient scales with the dye concentration and dye molar absorption coefficient (ε_0) as $\alpha = \varepsilon_0 C_d$. Corresponding to the dye concentration and the laser wavelength (λ = 488 nm) used in this experiment, an absorption coefficient of 0.03104 cm^{-1} is calculated. Attenuation of the fluorescent intensity at any distance y is given by $I = I_0 e^{-\alpha y}$. In the worst case scenario, the difference in the intensity between side walls of the test section would be 1.5 %. Thus, laser beam attenuation due to dye molecules was considered negligible.

Continuous excitation of fluorescein dye causes a decrease in its absorption efficiency. As a result, the fluorescence intensity of bleached molecule decreases continuously with respect to time. For the current mixing problem under study, due to the long convective time scale of the flow through the laser sheet, dye molecules are typically seen to be photobleached in streamwise imaging. This effect is typically seen near the walls wherein they are exposed to laser light throughout its travel time within the test section. In case of spanwise images although the flow velocity is small, dye molecules are exposed to laser

light only for small period of time corresponding to passage through the thickness of laser sheet (~ 0.5 mm) (see Appendix B for calibration of photobleaching time constant). Apart from photobleaching time constant characterization, the fluorescence intensity at stoichiometric mixture fraction ξ_s was monitored for two different velocity conditions in the mixing layer facility. The fluorescence intensity was found to be independent of the velocity which showed the absence of photobleaching effect in case of spanwise imaging. Thus, the spanwise measurements will be used for quantifying the mixedness while streamwise measurements will be referred to discuss the qualitative features of the mixed flow.

3.2. DATA REDUCTION PROCEDURE

The data reduction procedure used in this dissertation is discussed in this section. The LIF technique relies on the fact that the ratio of the product concentration C_p at any location to its value at fluorescence turn on, $(C_p)_{max,}$ is the same as the ratio of the fluorescent intensity I_f at that location to its maximum value $(I_f)_{max}$. Because of this, it is necessary to remove the effect of non-uniform laser beam profile and camera pixel response. This was accomplished by dividing all images (1900 images) by a uniform dye concentration reference image. The reference image was generated by using uniform dye solution in both of the streams i.e. flooding the test-section with uniform dye concentration solution. The uniform dye concentration solution was prepared at stoichiometric mixture fraction (ξ_s) which defines the maximum chemical product

$(C_p)_{max}$. This was achieved without altering the positions of the camera, laser sheet and test section.

Each frame in the image sequence was corrected pixel-by-pixel using the formula,

$$I_{corr} = \frac{I - I_B}{I_{ref} - I_B} \tag{2}$$

Where I_{corr} is the corrected pixel intensity, I is the original pixel intensity and I_{ref} is the fluorescent intensity of the same pixel from the reference image. Note, both I and I_{ref} were corrected for background signal I_B . Background signal was obtained by acquiring an image of the flow, wherein water was flooded in the test section in absence of dye solution.

Here, the corrected intensity at each pixel of a spanwise LIF image is actually a normalized chemical product, given as

$$C_P^*(x, y, z, t) = \frac{C_P}{C_{do}} = \frac{I_f}{I_{fo}} \tag{3}$$

Where C_{do} is free stream dye concentration and $I_{fo} = \frac{I_f(\max)}{(1 - \xi_s)}$ (see Figure 3-3).

The time average value of C_P^* defines the normalized average product concentration at each pixel of LIF image. The normalized average product concentration field at any streamwise location is given as,

$$\overline{C_P^*}(x, y, z) = \frac{\sum_{i=1}^{N} (C_P^*)_i}{N}$$

where, N defines the total number of images.

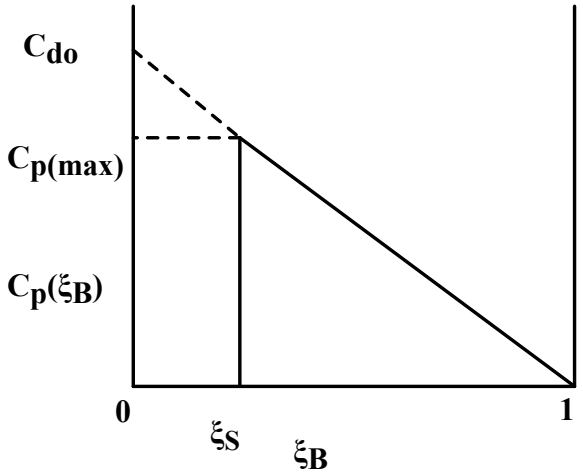

Figure 3-3. Product concentration C_p versus base volume fraction ξ_B in chemically reacting LIF.

It is customary to quantify the amount of mixing product across the wake width using the product thickness δ_p defined as (see Koochesfahani, 1984),

$$\delta_p(x,z) = \int_{-w/2}^{+w/2} \overline{C_P^*}(x,y,z)dy \tag{4}$$

Integrating δ_p across the test section span results in the total amount of product at a downstream distance x. This quantity is called the product area A_p and is defined as

$$A_p(x) = \int_{-d/2}^{+d/2} \delta_p(x,z)dz \tag{5}$$

In this thesis, mixedness will be quantified using product area $A_p(x)$ obtained from spanwise measurements.

4. RESULTS AND DISCUSSION

This chapter provides the results and discussion of the forced flow in the mixing layer facility operated at velocity U = 20 mm/s. Experimental runs were performed at two forcing amplitudes A_2 = 40 μm and A_3 = 60 μm and at a range of forcing frequencies (F = 2, 4, 8, 10, 12, 15, 18, 19, 20, 25 Hz). Mixedness results are obtained from chemically reacting LIF technique. Chemically reacting streamwise LIF imaging was performed at z ≈ 0 while spanwise imaging at x = 4.2, 9, 15 and 25 mm. The chemically reacting streamwise LIF imaging was also performed at A_1 = 25 μm to show the effect of very low forcing amplitude on the mixedness, however the detail mixing measurements are limited to forcing amplitudes A_2 = 40 μm and A_3 = 60 μm. All the mixing results and its discussion will be made based on streamwise and spanwise imaging.

Molecular Tagging Velocimetry (MTV) is used to obtain the streamwise velocity information. Here, U = 20 mm/s represents the maximum streamwise velocity of both of the unforced flow streams measured at x = 3 mm which is the most upstream location where the velocity profile measurements were possible. The streamwise velocity measurements were performed for forced flow at midspan i.e. z ≈ 0 to quantify the velocity perturbation amplitude. The mean streamwise velocity and RMS velocity profile of the forced flow will be utilized to quantify the flow dynamics within one forcing cycle.

4.1. QUALITATIVE FEATURES OF UNFORCED AND FORCED WAKE FLOW FROM STREAMWISE IMAGING (A_3 = 60 µm, F = 0-25 Hz)

A typical instantaneous LIF image of unforced flow is shown in Figure 4-1, illustrating the normalized chemical product field $C_P^*(x,y,t)$ due to mixing of two streams (acid + dye, base) at a given time (t) over the x-y plane at the midspan of the test section. The instantaneous normalized concentration field is pseudo-colored and the color map is shown in Figure 4-1.

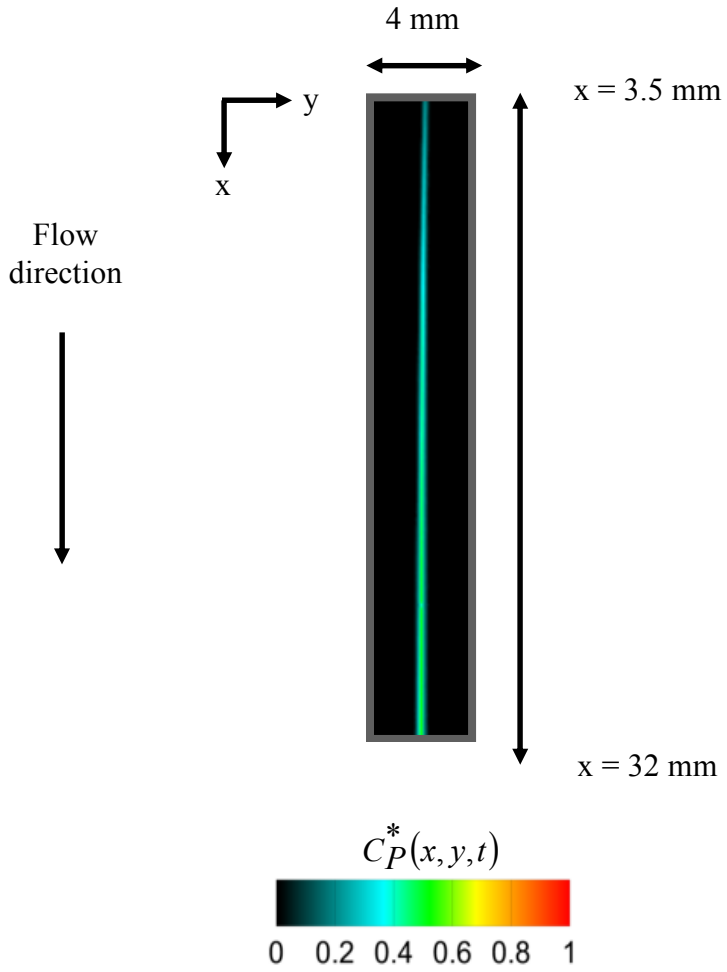

Figure 4-1. Instantaneous normalized product concentration field $C_P^*(x,y,t)$ of unforced flow at midspan (z = 0).

The *unforced flow* shown in Figure 4-1 has such a low velocity that the chemical product appears as a thin straight line at the interface of two co-flowing streams. The chemical product formed at the interface is solely due to the diffusion mechanism. Although the chemical product thickness increases with downstream distance, very little molecular mixing is seen for unforced flow.

Figures 4-2 and 4-3 depict the instantaneous normalized chemical product field of forced flow at midspan for different forcing frequencies. The *forced wake* at forcing frequency 2 Hz shows the interface being stretched and folded along and across the width of channel with the chemical product being formed at the interface. The interfacial structure formed due to forcing appears to maintain its overall shape, with longer tails near the wall region as it progresses downstream. As expected, due to increase in the forcing frequency, the mixed fluid structures formed at 4 Hz forcing frequency are smaller in size compared to 2 Hz, and they appear to be more tightly arranged within the channel. In general, for 2 Hz and 4 Hz forcing cases, the interfacial structures appear to become thicker with more chemical product as the flow moves in the streamwise direction. The mixing structures formed for 8 Hz case are periodic thin striations which spans across the width of the test section. As the flow moves downstream, this thin striation becomes smaller in size. Apart from thin striations of mixed fluid, a dense region of mixed fluid is seen on the side of the flow stream which is being forced.

A dramatic increase in mixed fluid is seen for higher forcing frequencies (10, 12, 18, 19, 20 Hz) except for 15 and 25 Hz. The enhancement in mixedness for these forcing frequencies is so high that the whole height and the width of the test section is filled with mixed fluid and a large amount of chemical product is observed at a very early

streamwise location. Unlike lower forcing frequencies, unmixed fluid region was not seen for the higher forcing frequency forced flow which also indicates the level of molecularly mixed fluid in the test section. Such a complex mixing field is best understood and quantified by spanwise images of the flow taken at various streamwise locations which will be discussed in the Chapter 4.1.2.

Forcing frequencies of 15 and 25 Hz also show an increase in the mixedness compared to low forcing frequencies. Unlike the other higher forced frequency cases it shows regions with low levels of mixed fluid within the test section.

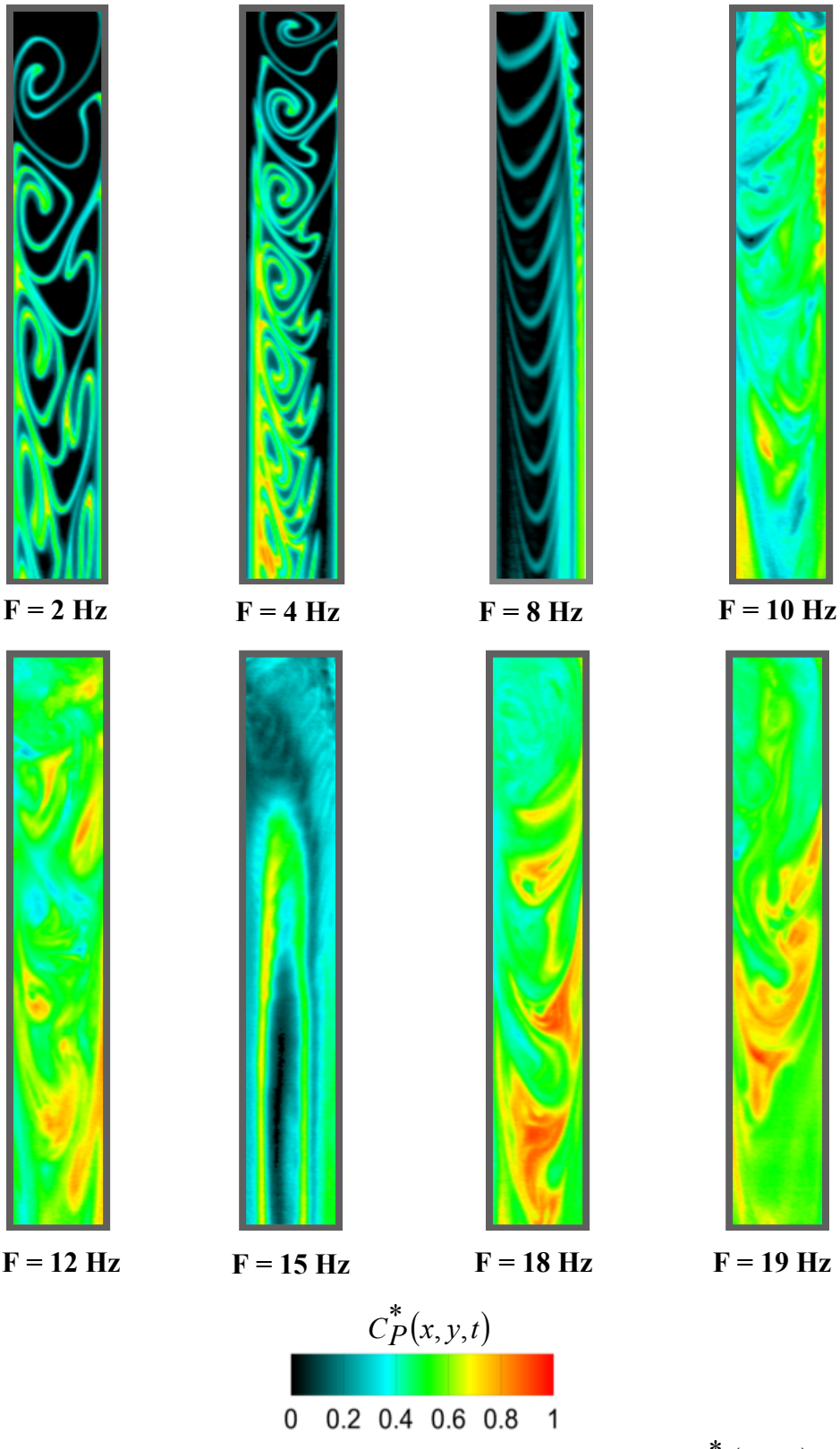

Figure 4-2. Instantaneous normalized product concentration field $C_P^*(x,y,t)$ of forced flow at midspan (U = 20 mm/s and A_3 = 60 μm).

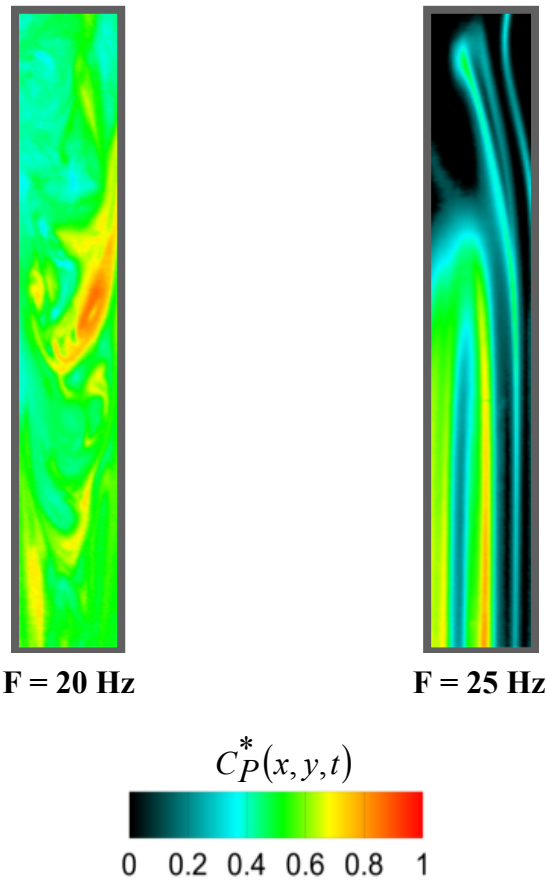

Figure 4-3. Instantaneous normalized product concentration field $C_P^*(x,y,t)$ of forced flow at midspan (U = 20 mm/s and A_3 = 60 μm).

4.1.1. Chemically reacting spanwise LIF measurements

(A_3 = 60 μm, F = 0 - 25 Hz)

In order to quantify the extent of mixedness, the chemical product area is calculated by utilizing the spanwise chemical product concentration field $C_P^*(x,z,y,t)$. Note that, the chemical product referred in this dissertation relates to a chemical reaction described by Figure 3-2 and Figure 3-3. The average chemical product area was calculated at four different streamwise locations (x = 4.2, 9, 15 and 25 mm). The chemical product area at each of the streamwise locations is the span-averaged data obtained from 1900 instantaneous normalized chemical product concentration fields $C_P^*(x,z,y,t)$. If we define A as the measure of the total area at streamwise location x mm (A = 4 mm × 9 mm), then the normalized product area ratio A_P/A represents the measure of the chemical product area per unit cross sectional area (A) of the test section. This can also be interpreted as the mixing efficiency.

Figure 4-4 depicts the normalized chemical product area measured at four different streamwise locations (x = 4.2, 9, 15 and 25 mm) over a range of forcing frequency F = 0 - 25 Hz and for a fixed forcing amplitude A_3 = 60 μm. In the following section, figure 4-4 will be utilized to discuss the amount of chemical product area formed at each forcing frequency and at different streamwise locations. The instantaneous normalized product concentration field $C_P^*(x,y,z,t)$ and average normalized product concentration field $\overline{C_P^*}(x,y,z)$ of unforced and forced cases are shown in Figures 4-5 to 4-15. For each forcing frequency, the instantaneous and average normalized chemical product

concentration field measured at x = 4.2, 9, 15 and 25 mm will be utilized as qualitative and quantitative result.

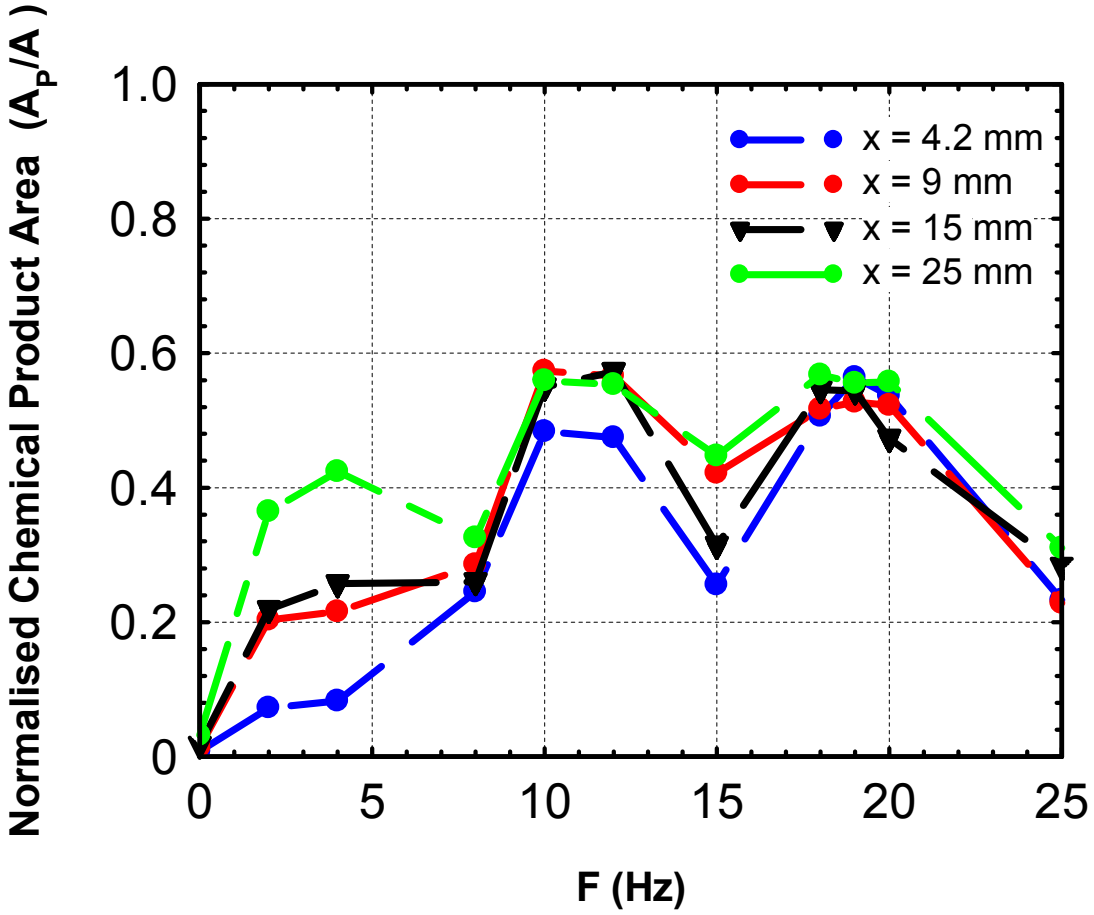

Figure 4-4. Normalized chemical product area for range of forcing frequencies measured at four different streamwise locations (U = 20 mm/s and A_3 = 60 μm).

The effect of forcing on the mixedness is apparent in Figure 4-4 as the normalized chemical product area at any given forcing frequency was found to be greater than that of unforced flow. This is mainly because in case of unforced flow chemical product is limited and found only at the thin interfaces separating the two free stream fluids. This result is seen in both streamwise and spanwise concentration fields shown in Figure 4-1 and 4-5 respectively.

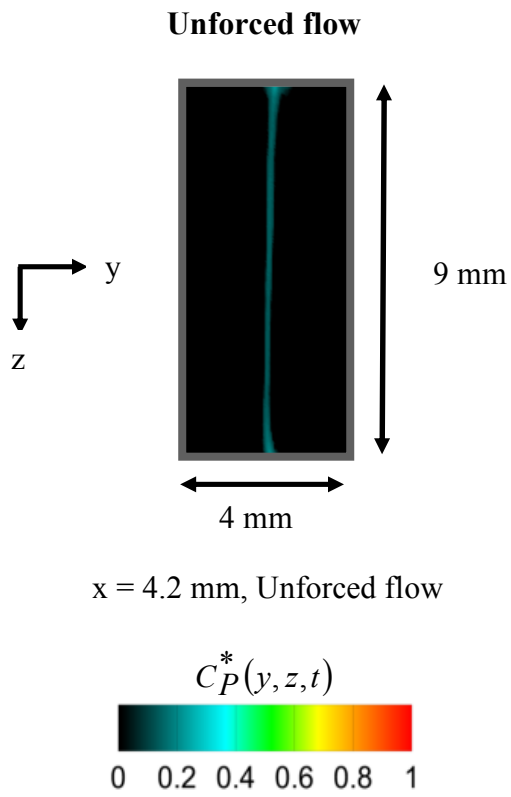

Figure 4-5. Instantaneous normalized chemical product concentration field at x = 4.2 mm of unforced flow.

Figure 4-6, 4-7 and 4-8 highlight the spanwise chemical product concentration field at four different streamwise locations for forcing frequencies 2, 4 and 8 Hz respectively. The visual inspection of the forced flow at frequencies 2 and 4 Hz from streamwise and spanwise concentration fields showed chemical product formed at the interfacial structure, and the amount was seen to increase in the streamwise direction. As a result, the normalized chemical product area for the forcing frequencies 2 and 4 Hz obtained from spanwise concentration fields show an increasing trend with respect to streamwise direction (Figure 4-4). The same conclusion is not applicable to 8 Hz forcing case, since the chemical product area at x = 15 mm is smaller than x = 9 mm, which might be due to change in the mixed fluid composition. However the chemical product area at the farthest location x = 25 mm is greater than that measured at x = 4.2 mm. From the spanwise

concentration field, it can be observed that each forcing frequency creates a unique interfacial structure. These interfacial structures typically maintain their shape, and they become thicker as they travel in the downstream direction. For 8 Hz forcing case, higher amount of chemical product was formed at the very earliest streamwise location compared to 2 and 4 Hz, but as the flow moves downstream, relatively lower chemical product was measured.

F = 2 Hz (Instantaneous normalized concentration field)

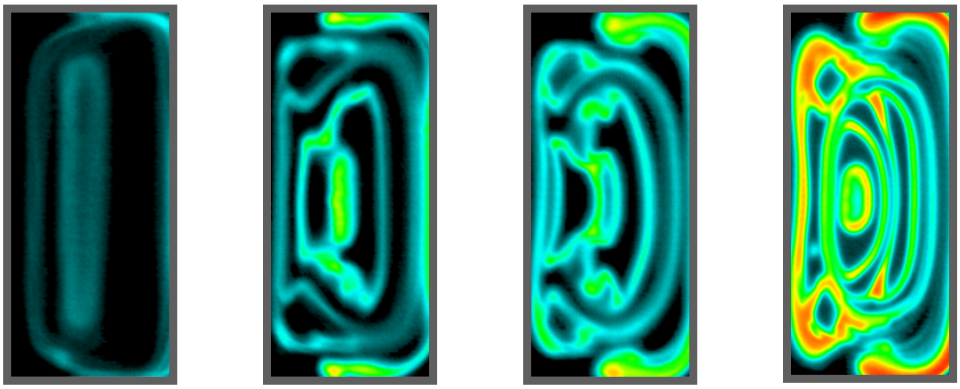

x = 4.2 mm x = 9 mm x = 15 mm x = 25 mm

F = 2 Hz (Average normalized concentration field)

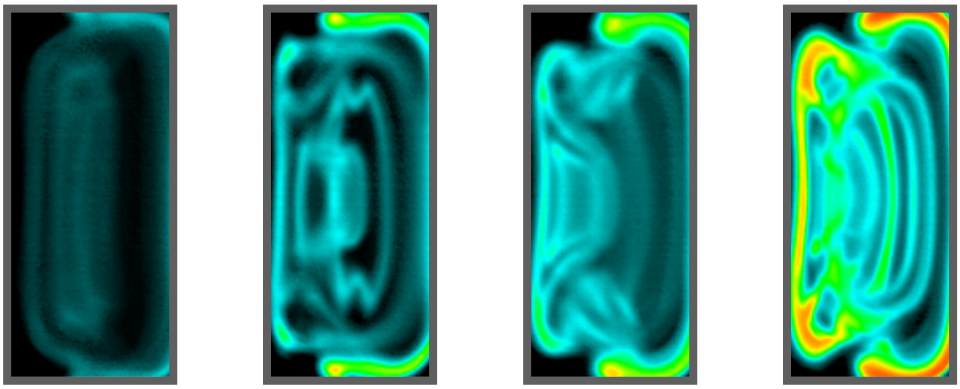

x = 4.2 mm x = 9 mm x = 15 mm x = 25 mm

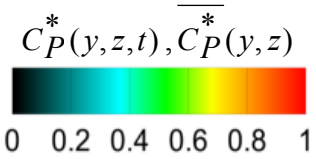

Figure 4-6. Instantaneous and average normalized chemical product concentration field at four different streamwise locations (F = 2 Hz, U = 20 mm/s and A_3 = 60 μm).

F = 4 Hz (Instantaneous normalized concentration field)

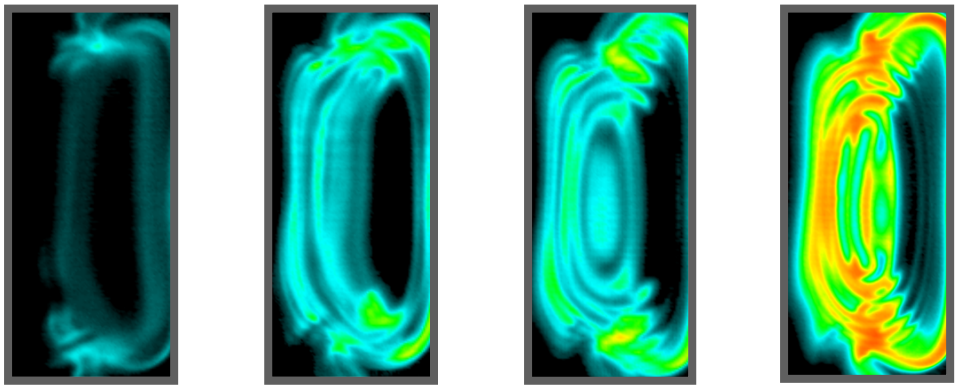

x = 4.2 mm x = 9 mm x = 15 mm x = 25 mm

F = 4 Hz (Average normalized concentration field)

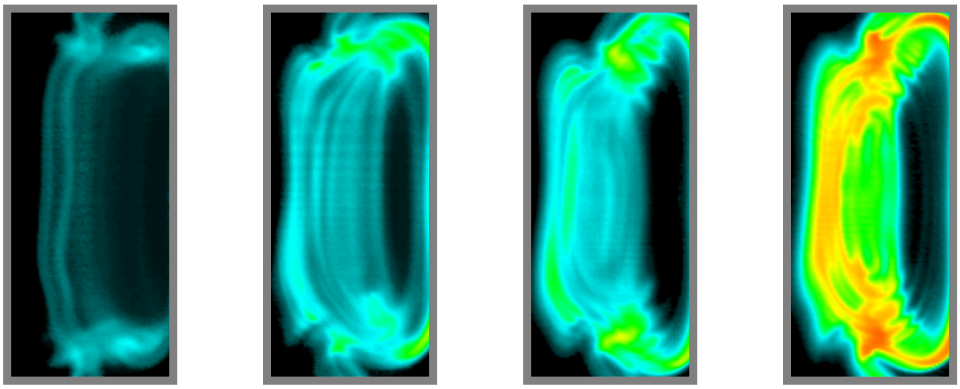

x = 4.2 mm x = 9 mm x = 15 mm x = 25 mm

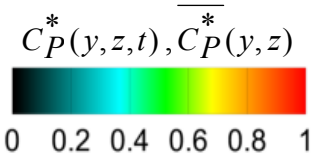

Figure 4-7. Instantaneous and average normalized chemical product concentration field at four different streamwise locations (F = 4 Hz, U = 20 mm/s and A_3 = 60 μm).

F = 8 Hz (Instantaneous normalized concentration field)

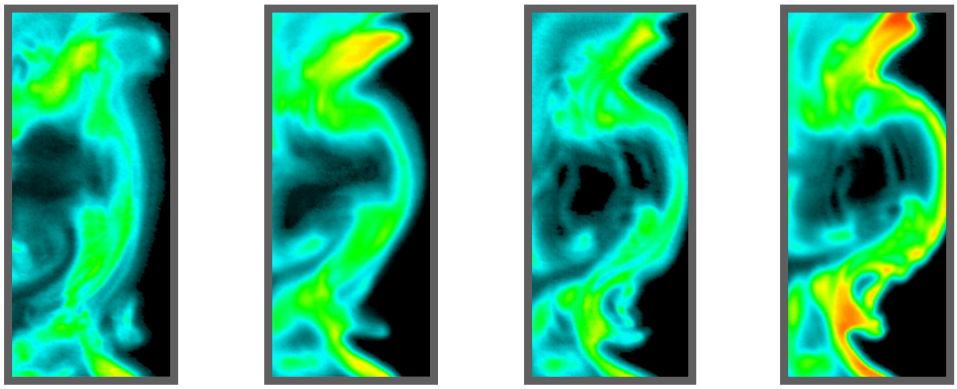

x = 4.2 mm x = 9 mm x = 15 mm x = 25 mm

F = 8 Hz (Average normalized concentration field)

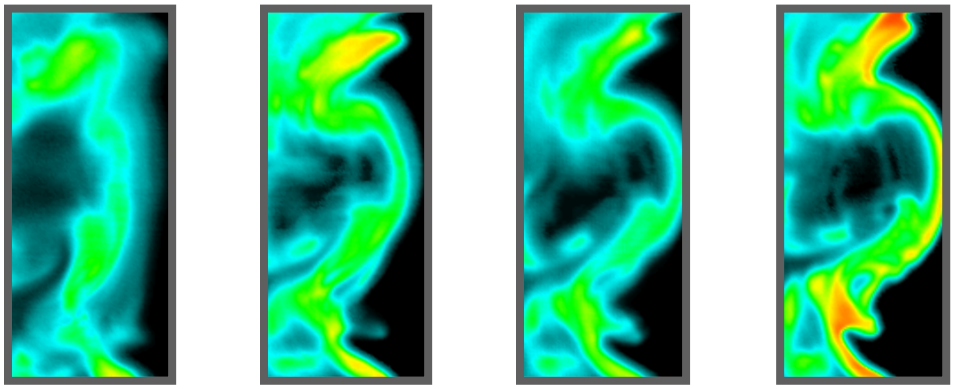

x = 4.2 mm x = 9 mm x = 15 mm x = 25 mm

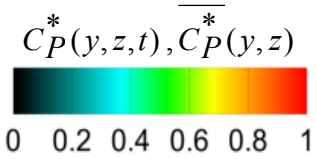

Figure 4-8. Instantaneous and average normalized chemical product concentration field at four different streamwise locations (F = 8 Hz, U = 20 mm/s and A_3 = 60 μm)

Although the forced cases (2, 4 and 8 Hz) produce more chemical product than an unforced flow, they still show the presence of unmixed fluid within the channel. The unmixed fluid information can be obtained through the probability density function (pdf)

of chemical product. The pdf of chemical product is calculated from the entire spanwise concentration field, over the time period corresponding to the data acquisition time (1900 imgaes at 30 Hz). Thus, the pdf is spatially averaged pdf over the cross section area of test section. A pdf of chemical product for all of the forcing frequencies at four different streamwise locations are shown in Appendix C. Each pdf was obtained from spanwise chemical product concentration field with bin size of $C_P^* \approx 0.1$. The pdf shown in Appendix C indicates that there is always an occurrence of unmixed fluid in the channel for 2, 4 and 8 Hz forcing cases. For the 8 Hz forcing case, there is a low probability of unmixed fluid and a larger distribution of mixed fluid probabilities compared to 2 and 4 Hz at the earliest streamwise location (x = 4.2 mm). This highlights the possible local splitter plate tip flow dynamics which increases the contact area between the two streams and thus, as a result, we observe more chemical product at the very early streamwise location (Figures 4-6, 4-7 and 4-8).

The spanwise instantaneous and average normalized product concentration fields corresponding to forcing frequencies in the range 10 to 25 Hz are shown in figures 4-9 to 4-15. The chemical product area for each forcing frequency at four different streamwise locations is depicted in figure 4-4. From figure 4-4, it could be observed that the forcing frequencies 10,12,18,19 and 20 Hz represent the highly mixed fluid cases. The forcing frequencies 15 and 25 Hz show relatively lower amount of chemical product at any streamwise location. This observation is consistent with the streamwise concentration fields shown in figures 4-2 and 4-3.

Although 15 Hz forcing case provides lower chemical product compared to some of the other higher forcing frequencies, it shows an interesting flow feature in the spanwise

images (see Figure 4-11). At x = 4.2 mm, an inverted C-shaped interfacial structure is seen such that chemical product is observed within the region which is bounded by this structure. The mixed fluid found near the wall is connected to this inverted C-shaped structure. The unmixed fluid is found outside of the inverted C-shaped structure which is quantified in the pdf of chemical product shown in Appendix C. As the forced flow moves downstream to x = 9 mm, more amount of chemical product is seen within the inverted C-shaped structure. At this location, the chemical product appears such that the inverted C-shaped structure is not clearly recognized because of the increase in the amount of chemical product as well as the increase in the size of the structure. Also, it should be noted that, the maximum chemical product is seen near the wall region. At x = 15 mm, the inverted C-shaped structure becomes bigger in size, but there is a decrease in the amount of chemical product and thus as a result we measure lower normalized chemical product area (Figure 4-4). The lowering of the chemical product may be because of the change in the mixed fluid composition within the inverted C-shaped structure and the mixed fluid near the wall. Continuing on to x = 25, a large increase in the amount of chemical product is also observed. From the pdf of chemical product corresponding to 15 Hz forcing frequency, it is observed that the amount of unmixed fluid decreases in the streamwise direction.

At the early streamwise location x = 4.2 mm, for 10, 12, 18, 19 and 20 Hz forcing cases (see Figures 4-9 to 4-14), the cross section of the test section is filled with the mixed fluid. As a result, the pdf shown in Appendix C indicates zero probability of finding unmixed fluid. This also defines the level of increase in the molecularly mixed fluid. As the flow moves downstream (x = 9, 15, and 25 mm), an increase in the amount

of chemical product is seen for 10 and 12 Hz forced cases while a small variation is observed for 18, 19 and 20 Hz cases. The three-dimensional nature of the forced flow continues to occupy the whole cross section of the test section, and it remains complex. The pdf of chemical product corresponding to forced cases 10,12,18,19, and 20 Hz show a wide distribution of probabilities of the chemical product. The peak probability of non-zero chemical product is found around $C_P^* \approx 0.5 - 0.55$. The distribution of chemical product greater than 0.5 is due to the mixed fluid which is typically observed away from the center of the channel and near the wall region.

In case of 25 Hz forcing frequency (see figure 4-15), an inverted C-shaped interfacial structure is formed similar to the structure seen for 15 Hz forced case. Compared to 15 Hz case it does not show a significant increase in the amount of chemical product in the streamwise direction.

F = 10 Hz (Instantaneous normalized concentration field)

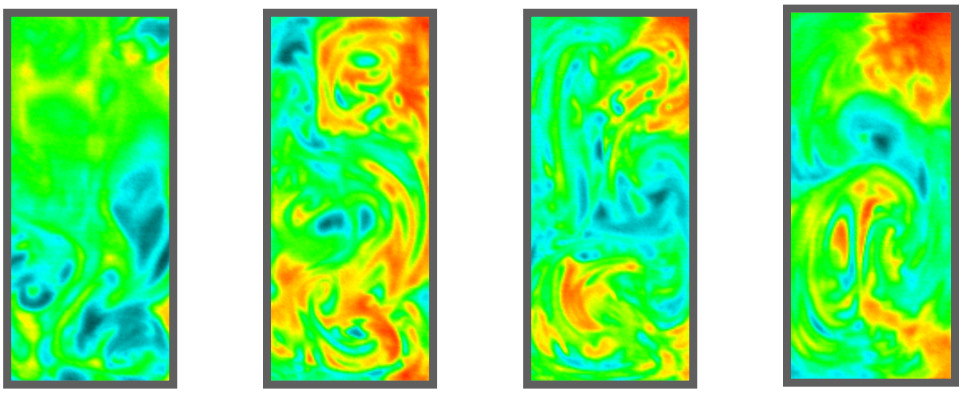

x = 4.2 mm x = 9 mm x = 15 mm x = 25 mm

F = 10 Hz (Average normalized concentration field)

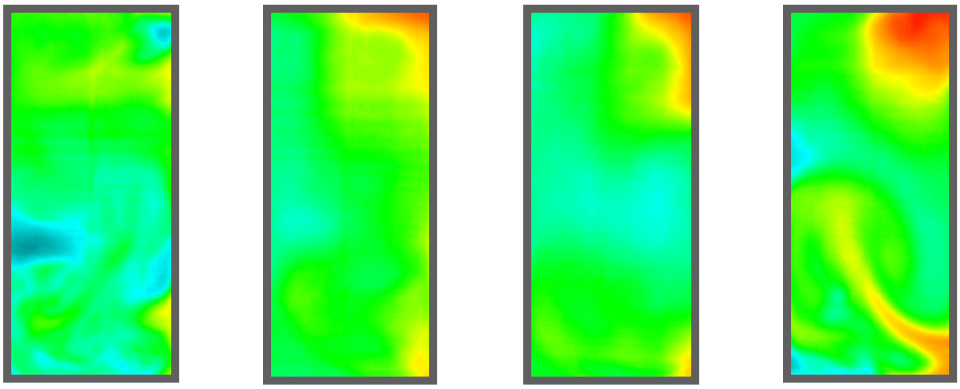

x = 4.2 mm x = 9 mm x = 15 mm x = 25 mm

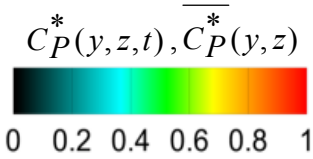

Figure 4-9. Instantaneous and average normalized chemical product concentration field at four different streamwise locations (F = 10 Hz, U = 20 mm/s and A_3 = 60 μm).

F = 12 Hz (Instantaneous normalized concentration field)

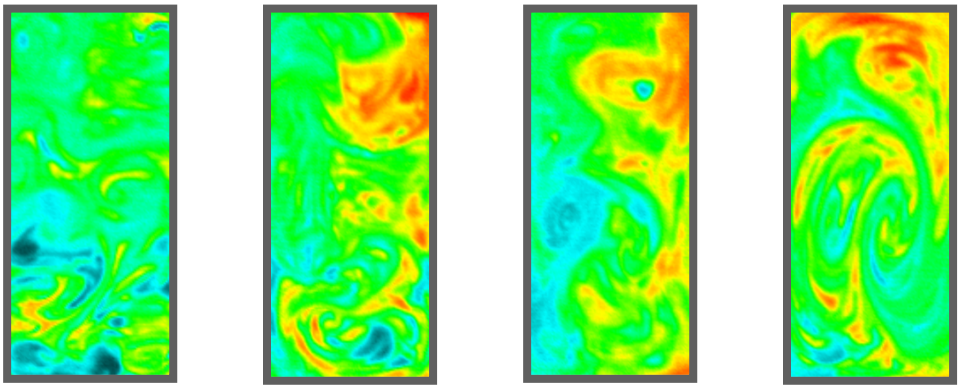

x = 4.2 mm x = 9 mm x = 15 mm x = 25 mm

F = 12 Hz (Average normalized concentration field)

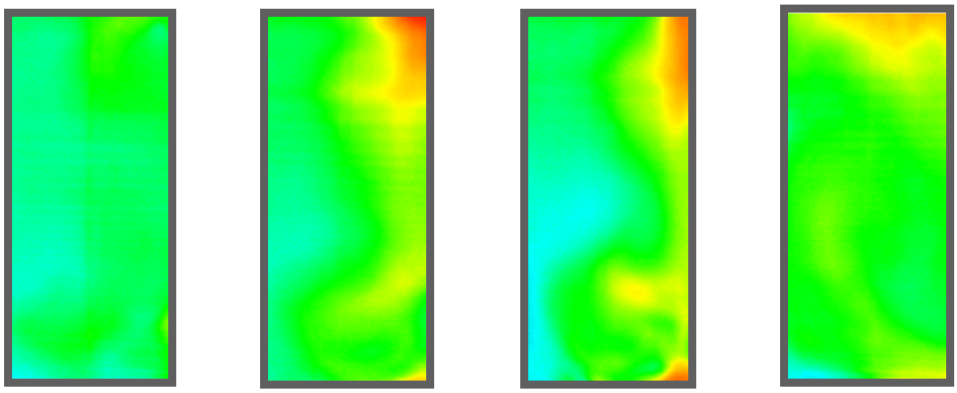

x = 4.2 mm x = 9 mm x = 15 mm x = 25 mm

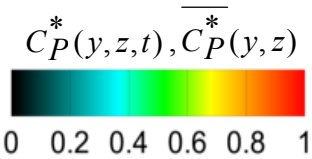

Figure 4-10. Instantaneous and average normalized chemical product concentration field at four different streamwise locations (F = 12 Hz, U = 20 mm/s and A_3 = 60 μm).

F = 15 Hz (Instantaneous normalized concentration field)

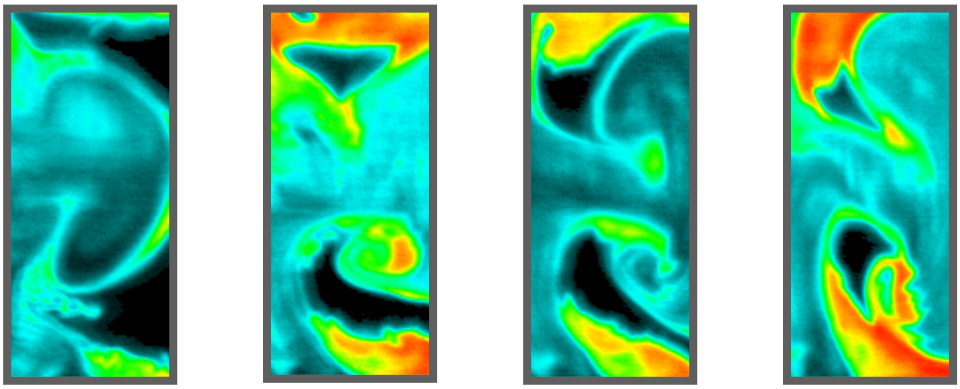

x = 4.2 mm x = 9 mm x = 15 mm x = 25 mm

F = 15 Hz (Average normalized concentration field)

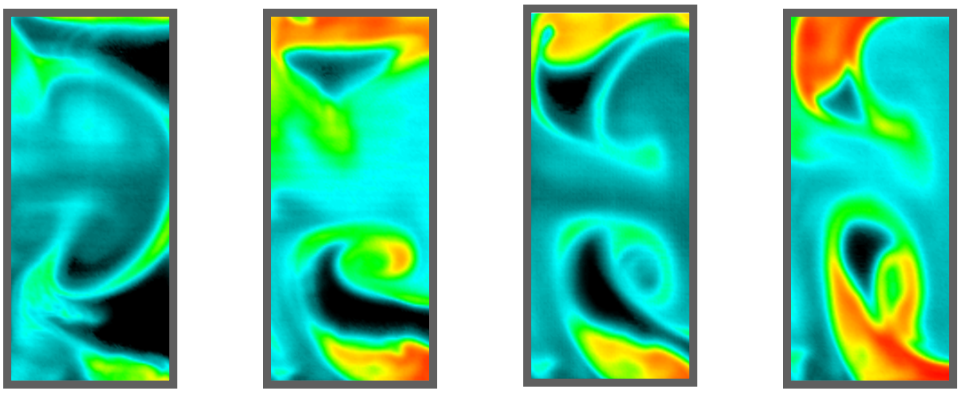

x = 4.2 mm x = 9 mm x = 15 mm x = 25 mm

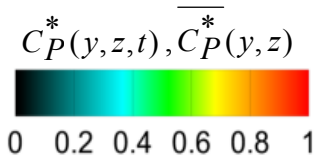

Figure 4-11. Instantaneous and average normalized chemical product concentration field at four different streamwise locations (F = 15 Hz, U = 20 mm/s and A_3 = 60 μm).

F = 18 Hz (Instantaneous normalized concentration field)

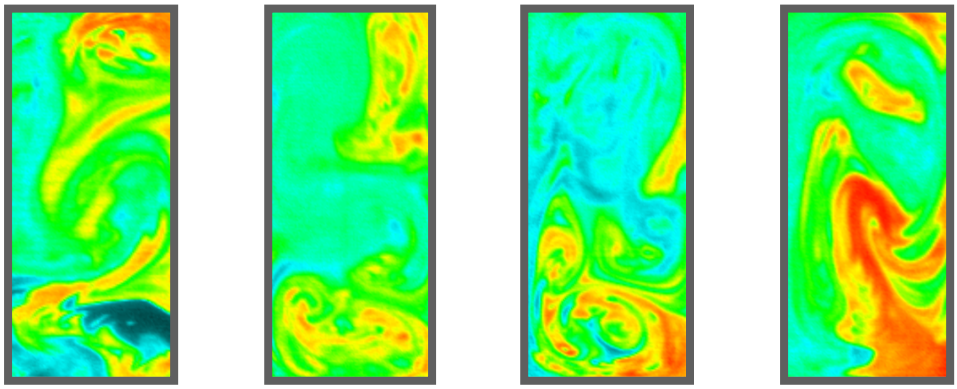

x = 4.2 mm x = 9 mm x = 15 mm x = 25 mm

F = 18 Hz (Average normalized concentration field)

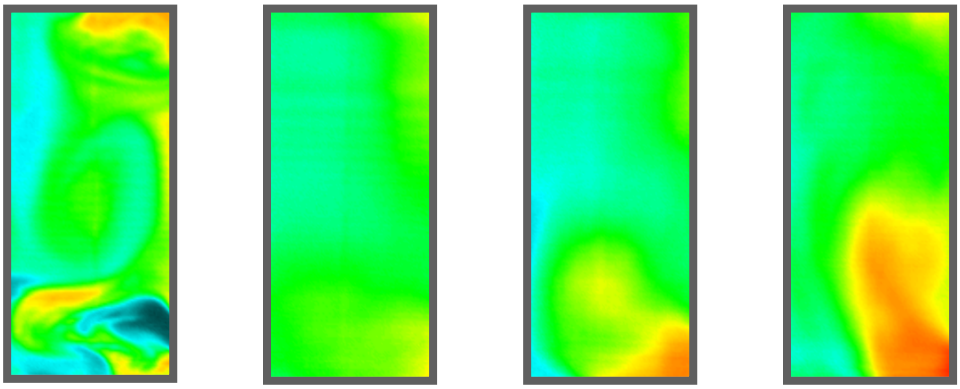

x = 4.2 mm x = 9 mm x = 15 mm x = 25 mm

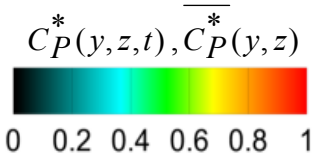

Figure 4-12. Instantaneous and average normalized chemical product concentration field at four different streamwise locations (F = 18 Hz, U = 20 mm/s and A_3 = 60 μm).

F = 19 Hz (Instantaneous normalized concentration field)

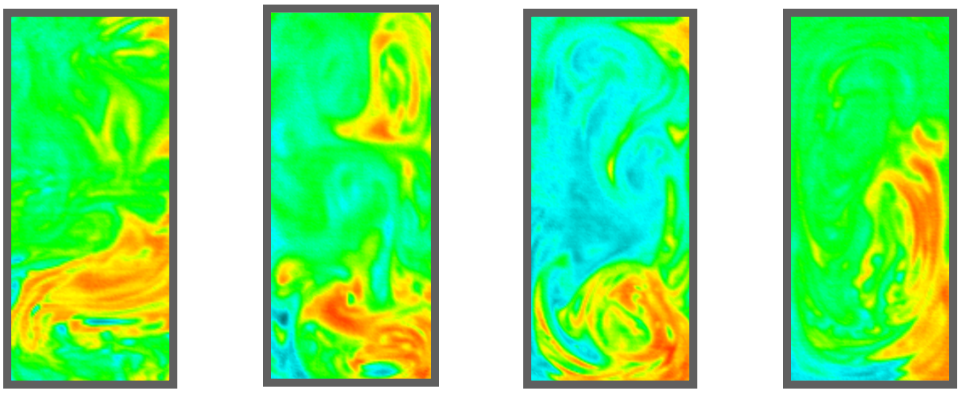

x = 4.2 mm x = 9 mm x = 15 mm x = 25 mm

F = 19 Hz (Average normalized concentration field)

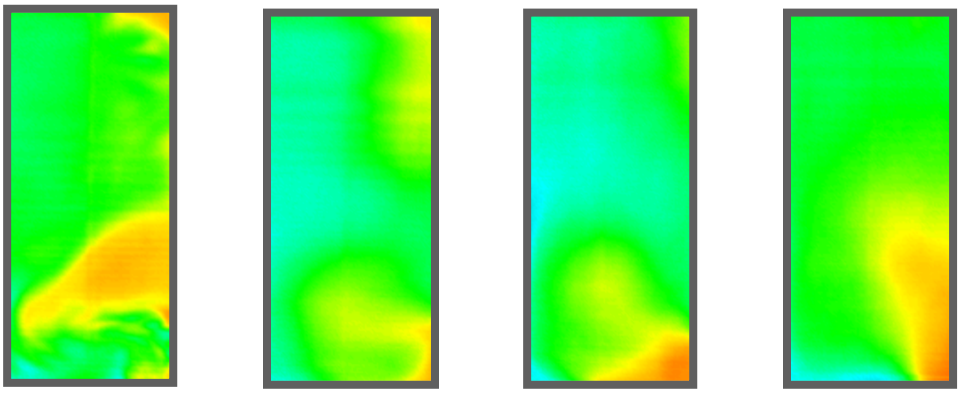

x = 4.2 mm x = 9 mm x = 15 mm x = 25 mm

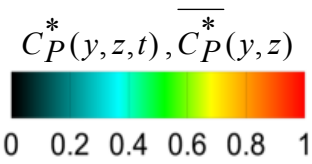

Figure 4-13. Instantaneous and average normalized chemical product concentration field at four different streamwise locations (F = 19 Hz, U = 20 mm/s and A_3 = 60 μm).

F = 20 Hz (Instantaneous normalized concentration field)

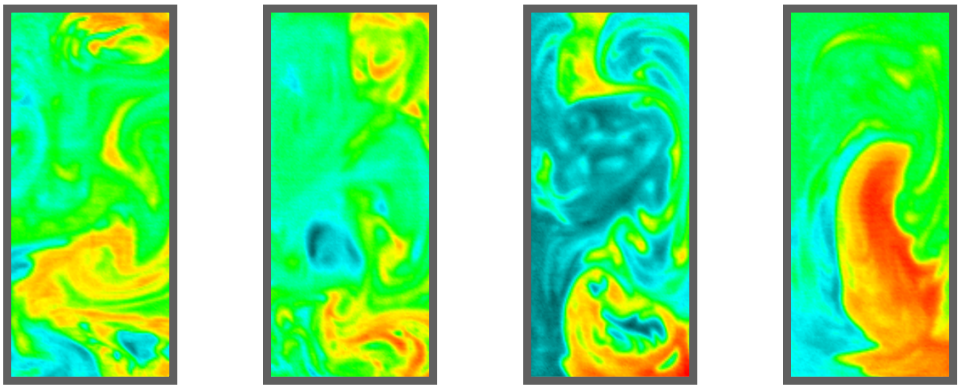

x = 4.2 mm x = 9 mm x = 15 mm x = 25 mm

F = 20 Hz (Average normalized concentration field)

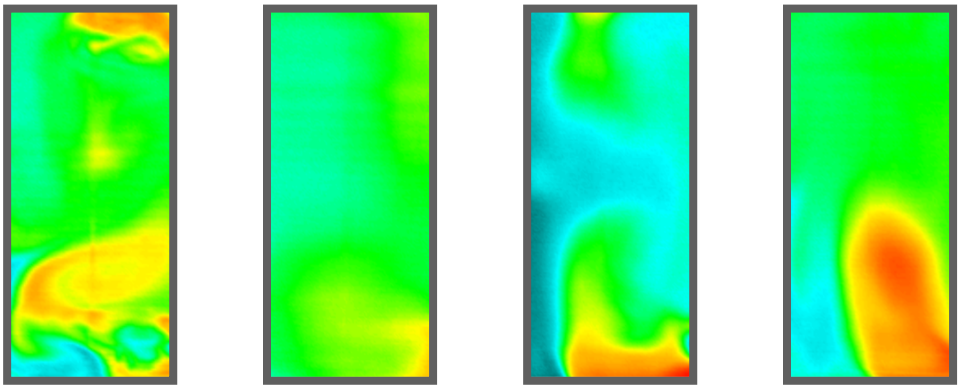

x = 4.2 mm x = 9 mm x = 15 mm x = 25 mm

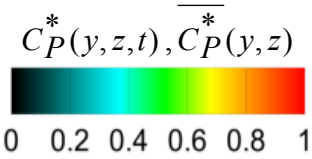

Figure 4-14. Instantaneous and average normalized chemical product concentration field at four different streamwise locations (F = 20 Hz, U = 20 mm/s and A_3 = 60 μm).

F = 25 Hz (Instantaneous normalized concentration field)

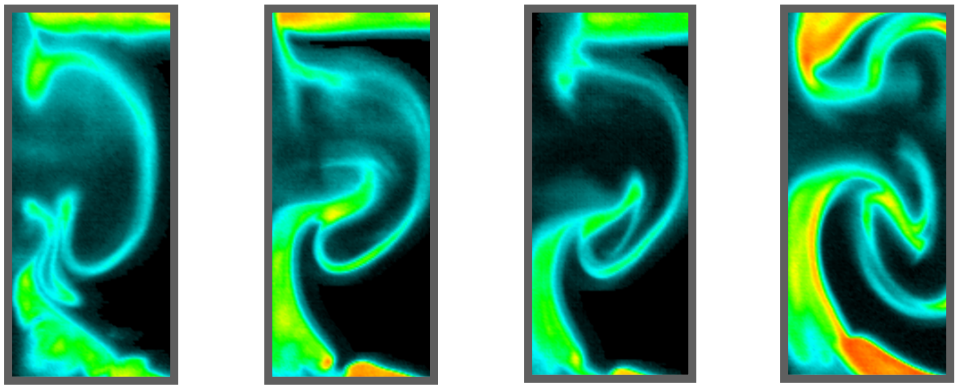

x = 4.2 mm x = 9 mm x = 15 mm x = 25 mm

F = 25 Hz (Average normalized concentration field)

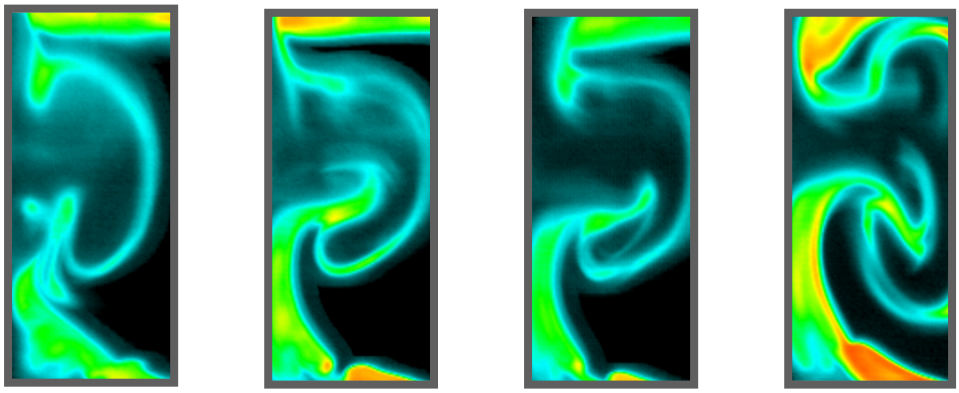

x = 4.2 mm x = 9 mm x = 15 mm x = 25 mm

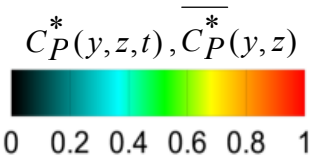

Figure 4-15. Instantaneous and average normalized chemical product concentration field at four different streamwise locations (F = 25 Hz, U = 20 mm/s and A_3 = 60 μm).

4.1.2. Non-reacting spanwise LIF measurement

(A_3 = 60 μm, F = 12 and 19 Hz)

All the results in section 4.1.1 are from chemically reacting LIF experiments performed at *one* fixed value of the reactant stoichiometric ratio ξ_s = 0.065. To obtain information on the entire composition distribution of the mixed fluid, a non-reacting LIF (i.e. standard LIF) experiment was performed. In non-reacting LIF experiment, fluorescein dye molecules were seeded in one of the two flow streams and the mixed fluid composition was quantified by examining the concentration of the dye molecules. Although non-reacting LIF is known to provide an upper bound to the actual amount of molecular mixing (See Breidenthal 1981 and Koochesfahani and Dimotakis 1986), it still remains the simplest diagnostic technique to estimate the entire mixture composition in a single experiment. Thus, a non-reacting LIF experiment was performed for 12 and 19 Hz forcing cases in the spanwise direction at x = 25 mm to quantify mixed fluid composition. For non-reacting LIF, the experimental facility and instruments were same as used for chemically reacting LIF experiments. For the forcing frequencies 12 and 19 Hz, 1900 images were acquired to monitor the spatio-temporal evolution of the mixed fluid concentration field. The steps for processing the fluorescence intensity data are described in detail by Koochesfahani and Dimotakis (1986) and thus they are not repeated here. The normalized concentration ξ is related to local instantaneous dye concentration C_d and the free stream dye concentration C_0 as

$$\xi = \frac{C_d}{C_0} \tag{1}$$

Here, the normalized concentration is defined such that $\xi = 1$ indicates the unmixed fluid from the right-side stream seen in the image which was premixed with the dye while $\xi = 0$ indicates the unmixed fluid from the other stream (the one which had pure fluid). Thus, the normalized concentration in the range $0 < \xi < 1$ indicates the mixed fluid concentration.

Figure 4-16 depicts the instantaneous normalized concentration field $\xi(y,z)$ obtained from non-reacting LIF experiment for 12 Hz and 19 Hz forcing frequency. The mixing field is obtained at x = 25 mm over the y-z plane. Pseudo colors are assigned to the different mixed fluid concentration levels in order to aid the interpretation of data. The concentration $\xi = 0$ and $\xi = 1$ are assigned black color which indicates the unmixed fluid from the two different flow streams. From 1900 normalized concentration

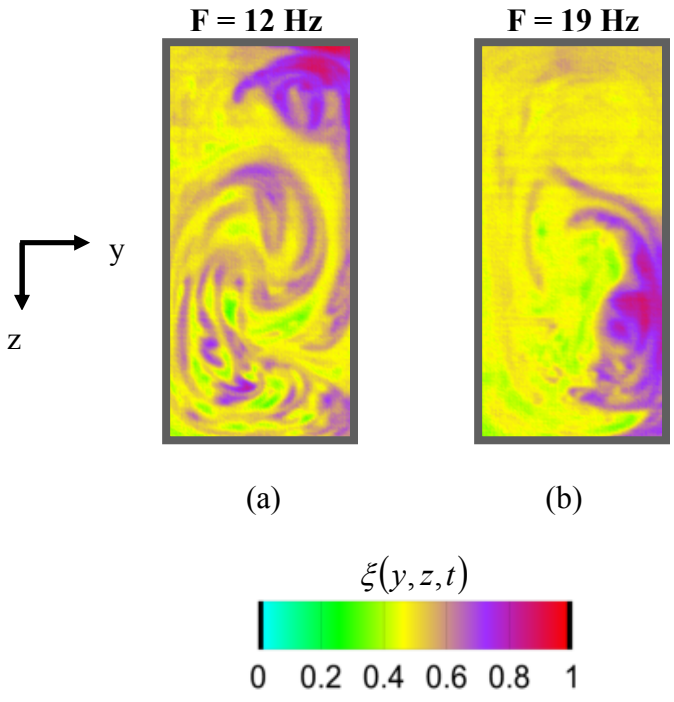

Figure 4-16. Instantaneous normalized concentration field $\xi(y,z)$ from non-reacting LIF experiment corresponding to 12 and 19 Hz forcing frequency at x = 25 mm. (U = 20 mm/s, A_3 = 60 μm, spanwise imaging)

fields $\xi(y,z)$, a total probability density function (pdf) is constructed using the entire y-z plane data at x = 25 mm for 12 and 19 Hz forcing frequency (see Figure 4-17a and b). Each pdf is calculated with the bin size as ε = 0.05. It is observed from figure 4-17a and b that the maximum probability corresponds to mixed fluid concentration $\xi = 0.5$ i.e. there is maximum occurrence of symmetric mixed fluid composition. The total pdf of the mixed fluid composition is asymmetric as it is biased towards the dye bearing stream i.e. the right-side fluid stream which is being forced. This indicates that the mixing field for the highly mixed fluid cases has asymmetric mixing characteristics.

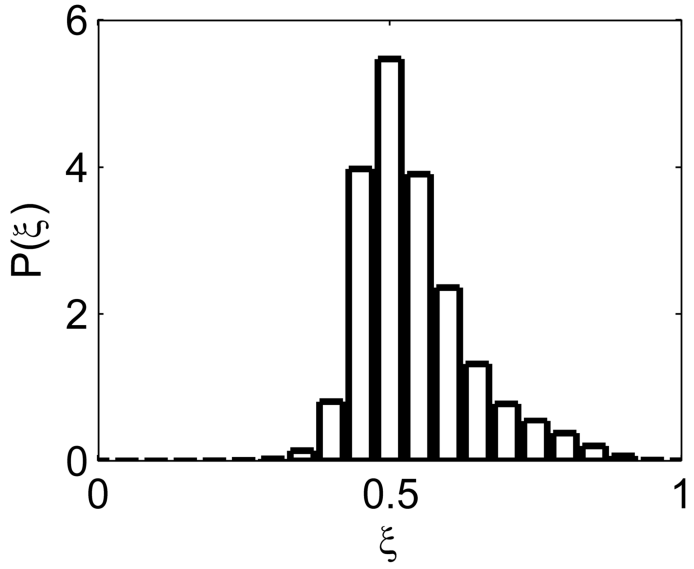

Figure 4-17(a). Total pdf of mixed fluid concentration from non-reacting LIF experiment (F = 12 Hz, A_3 = 60 μm, x = 25 mm, Spanwise imaging)

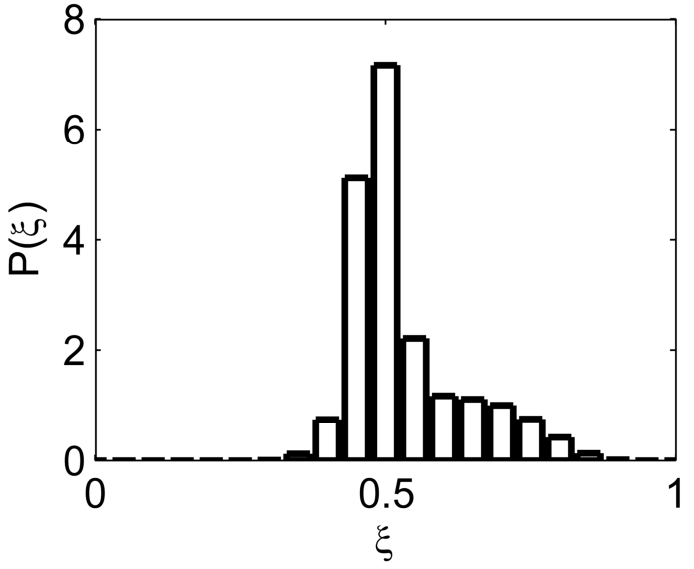

Figure 4-17(b). Total pdf of mixed fluid concentration from non-reacting LIF experiment (F = 19 Hz, A_3 = 60 μm, x = 25 mm, Spanwise imaging)

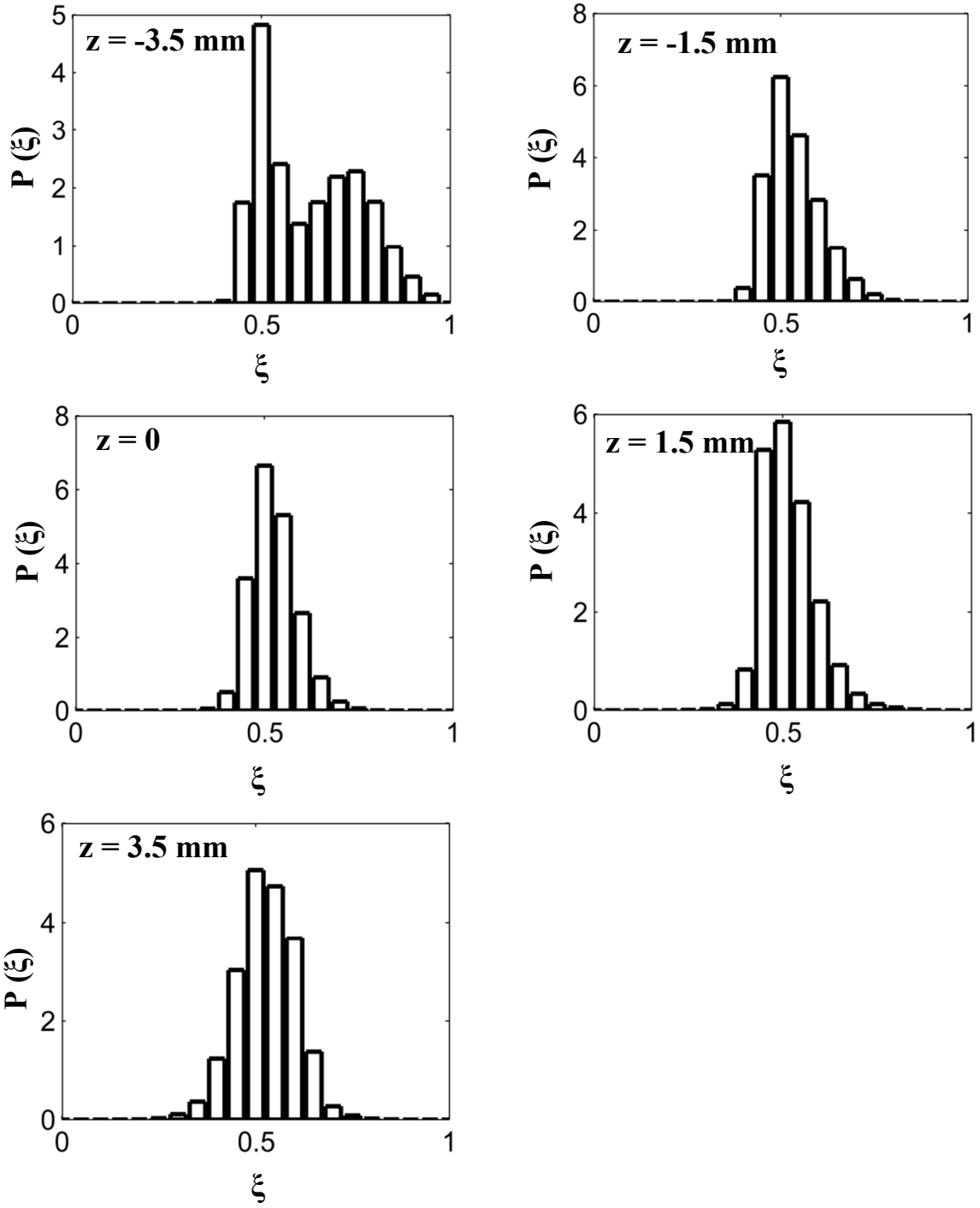

Figure 4-18. Pdf of mixed fluid concentration from standard LIF experiment at various span locations and fixed streamwise location x = 25 mm.
(F = 12 Hz, A_3 = 60 μm, x = 25 mm, Spanwise imaging)

Unlike the pdf of concentration field shown in Figure 4-17(a), Figure 4-18 shows the pdf at five different span locations (z = 0, 1.5, 3.5,-1.5 and 3.5 mm) and a fixed

streamwise location x = 25 for 12 Hz forcing frequency. It is observed that the functional form of the pdf of concentration field along the span is same except at location z = -3.5 mm. At z = -3.5 mm, there is a more occurrence of mixed fluid with concentration in the range $0.5 < \xi < 0.95$ compared to other span locations. This means that along the span, at position z = -3.5 mm, the mixed fluid composition is more asymmetrically mixed and is in favor of dye bearing fluid stream.

Figure 4-19 shows the pdf at five different span locations and a fixed streamwise location x = 25 mm for 19 Hz forcing frequency. The 19 Hz forced case has non-uniform mixed fluid composition as the functional form as well as the width of pdf distribution show noticeable difference at all of the five span locations. For the 19 Hz forced case, the biased nature of the mixed fluid composition is towards the dye bearing fluid which is seen on the positive side of the z-axis unlike to 12 Hz case. This means that, although the highly mixed forced cases (12 and 19 Hz) provide the same amount of maximum normalized chemical product area, its lateral uniformity of mixed fluid composition varies.

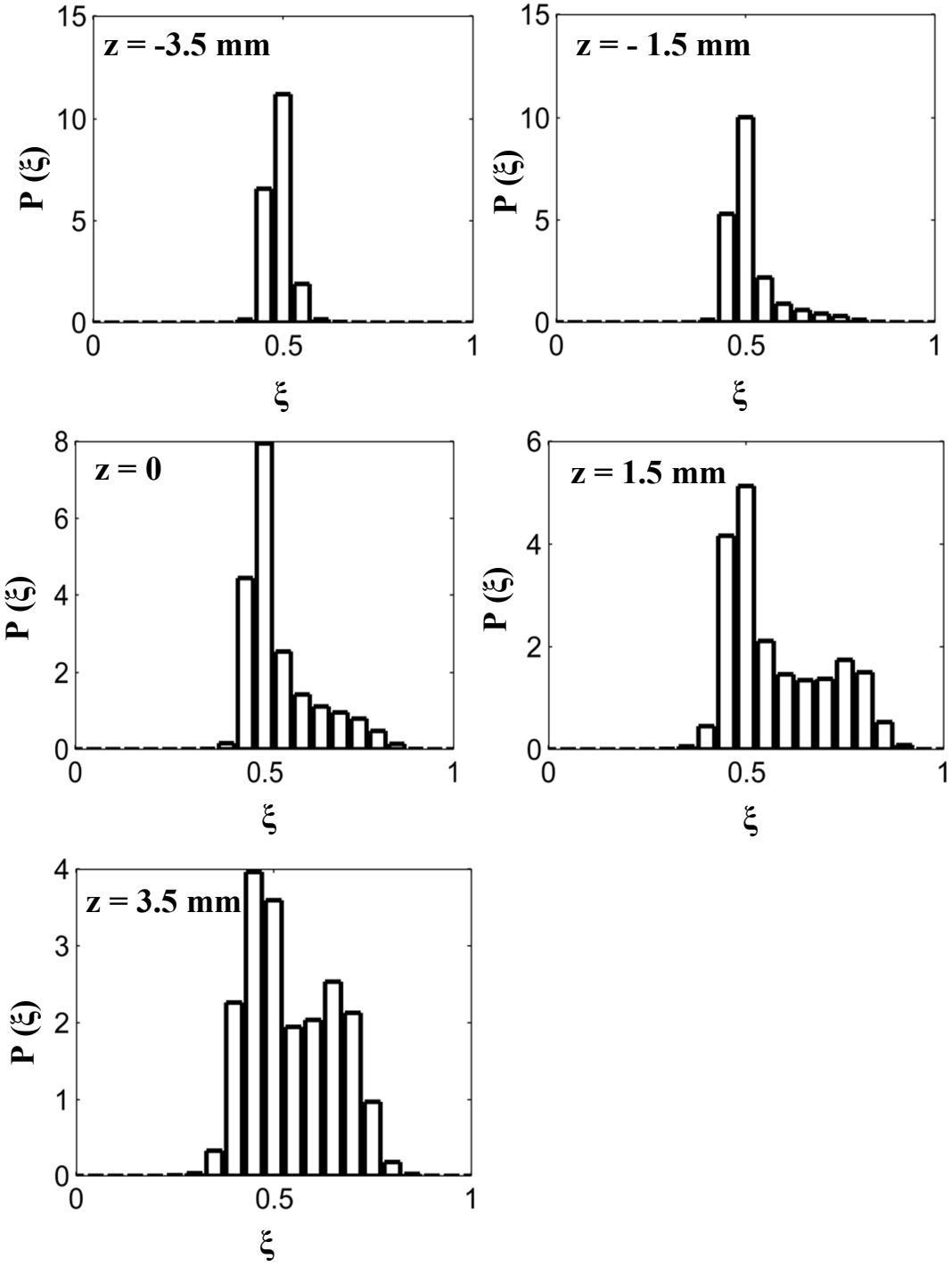

Figure 4-19. Pdf of mixed fluid concentration from standard LIF experiment at various span locations and fixed streamwise location x = 25 mm.

(F = 19 Hz, A_3 = 60 μm, x = 25, Spanwise imaging)

4.1.3. Streamwise velocity measurement of the unforced and forced flow

(A_3 = 60 µm, F = 0 - 25 Hz)

Molecular Tagging Velocimetry (MTV) technique was used to measure the streamwise velocity at the mid-span of the mixing layer facility. MTV experiments were performed for unforced and forced flow. A typical undelayed and delayed image obtained from an MTV experiment is shown in Figure 4-20. The results obtained from the MTV experiments are discussed in the following section of this chapter while the details of the MTV experiment are provided in chapter 2.

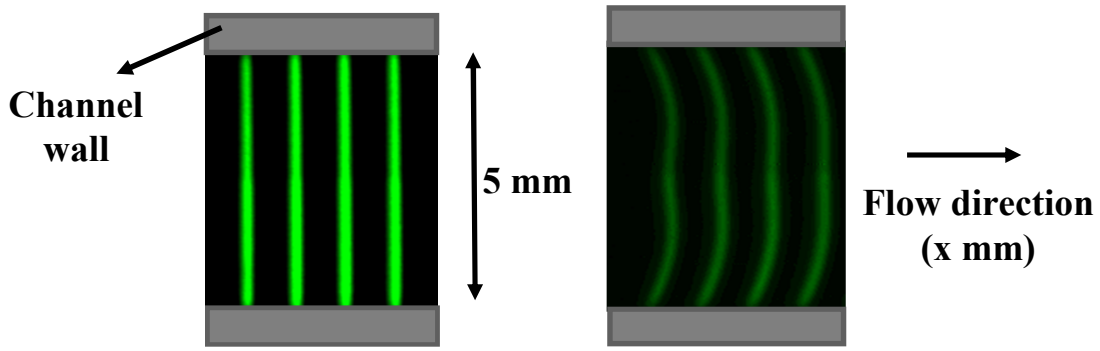

(a) Undelayed image (b) Delayed image (Δt = 10.25 ms)

Figure 4-20.Undelayed and delayed MTV image of an unforced flow.

UNFORCED FLOW CHARACTERISTICS

Figure 4-21 shows the measured streamwise velocity profile across the test section at three downstream locations (x = 3, 4.55, 6.86 mm). The flow valves (upstream and end section valves) were adjusted such that the maximum mean streamwise velocity of both of the flow stream was $U_1 = U_2$ = 20 mm/s at x = 3 mm. Unlike the typical velocity profile of a wake flow, it can be observed from Figure 4-21 that there is no region across the channel width with uniform streamwise velocity.

The velocity defect, which is caused due to presence of the splitter plate wake, is apparent in Figure 4-21. The strength of this defect at x = 3 mm is such that the minimum velocity of the wake U_{min} is 15% less than U_{max} = 20 mm/s. As the flow progresses downstream, decay in the velocity defect is observed such that at x = 6.86 mm zero velocity defect is measured (Figure 4-22). The Reynolds number for the experiments discussed in this dissertation is defined based on the width (w) of the channel.

$$\mathrm{Re} = \frac{\rho U_M w}{\mu} \tag{2}$$

The value of U_M at the midspan is chosen to be the average velocity across the width of the test section at x = 3 mm. Based on this definition the Reynolds number is Re ≈ 75.

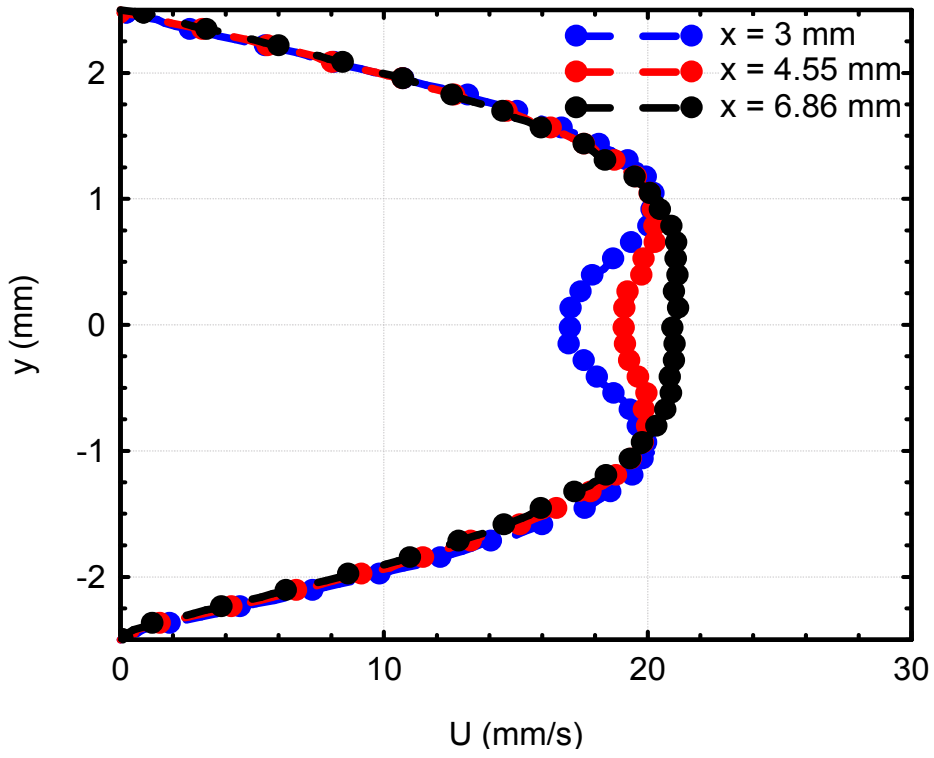

Figure 4-21. Mean streamwise velocity profile of unforced wake flow at midspan.

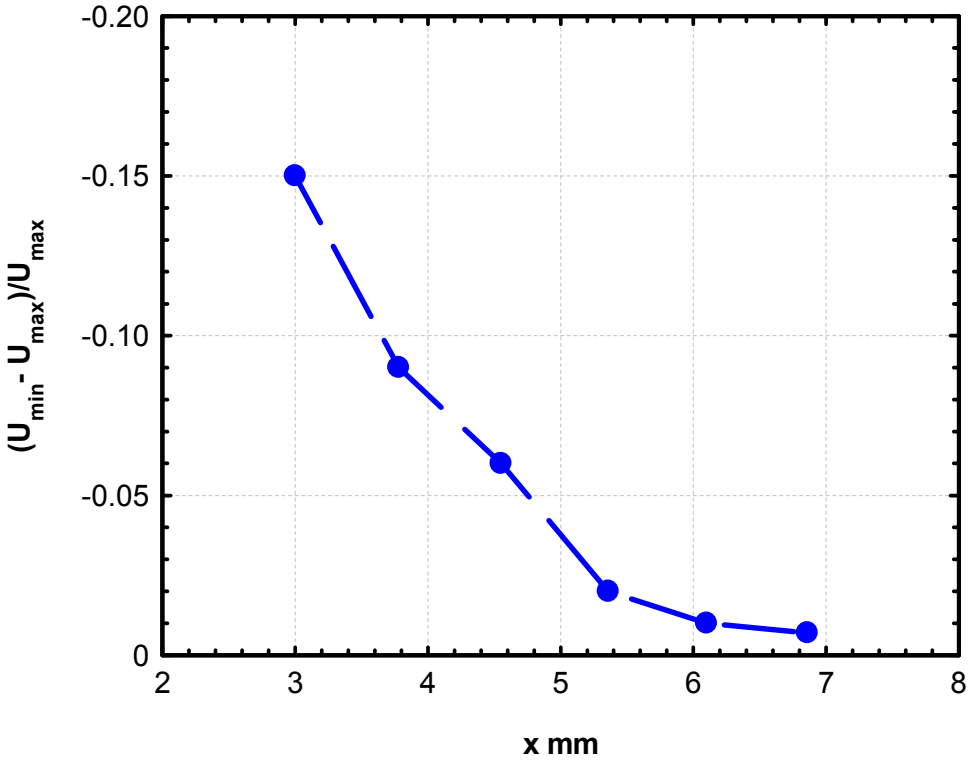

Figure 4-22. Evolution of the wake velocity deficit of unforced wake flow in the streamwise direction at midspan.

FORCED FLOW CHARACTERISTICS

As shown in the Figure 4-21, due to the small size of the test section no "free stream" region exists in the unforced wake flow. Thus, the normalized average RMS streamwise velocity magnitude for each forcing frequency is calculated by spatially averaging the RMS velocity over the width of the test section and normalizing it with respect to the spatially averaged streamwise velocity. Normalized average RMS streamwise velocity is calculated to provide label for each forcing frequency in terms of perturbation velocity amplitude.

The normalized average RMS streamwise velocity can be written as,

$$\frac{U_{RMS}}{U_M} = \frac{\left(\frac{\int U_{RMS}(y)dy}{w} \right)}{U_M} \quad , \tag{3}$$

where U_M is the spatially average streamwise velocity across the width of the channel at the midspan and w is the width of the channel. Figure 4-23 shows the normalized average RMS streamwise velocity calculated for various forcing frequencies. Figure 4-23 will be utilized in the following section while discussing the RMS velocity magnitude for each forcing frequency.

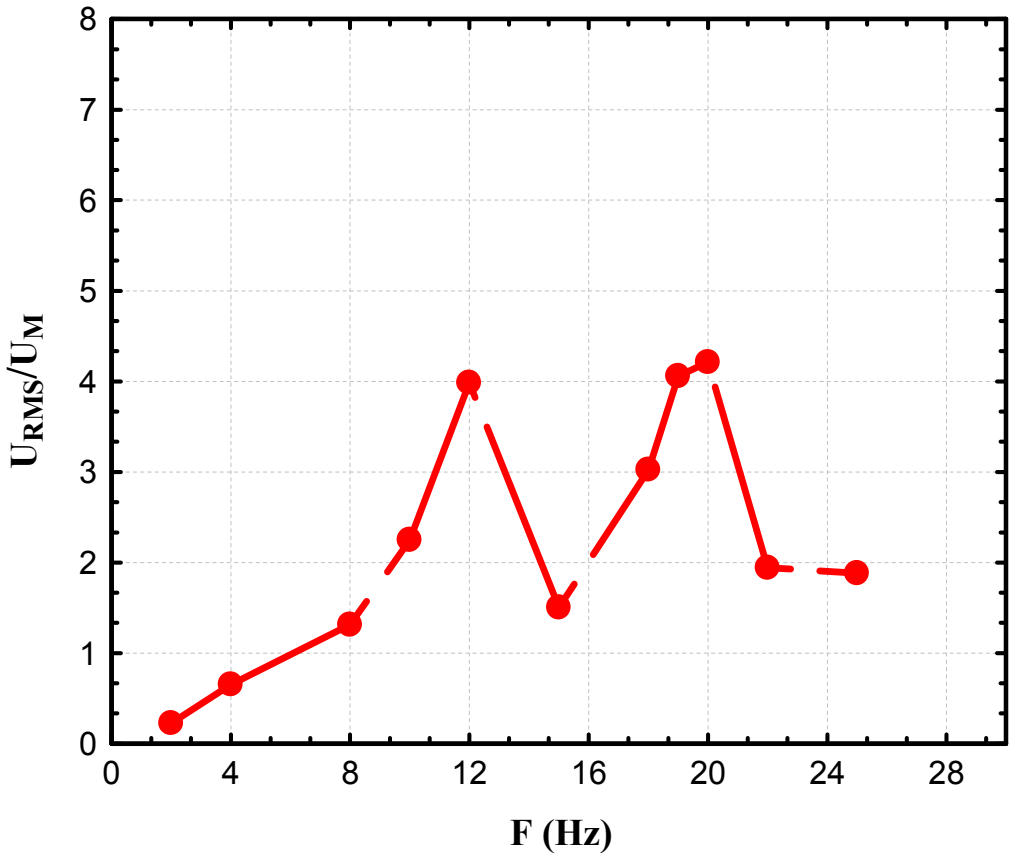

Figure 4-23. Normalized average RMS streamwise velocity for various forcing frequencies and for a fixed perturbation amplitude A_3 = 60 μm measured at x = 3 mm**.**

Figures 4-24 to 4-29 depicts the streamwise velocity measured at x = 3 mm and z = 0 (midspan) for various forcing frequencies (F = 0 to 25 Hz). For each forcing frequency, mean, phase resolved ($\phi_1 = 0, \phi_2 = 0.25, \phi_3 = 0.50, \phi_4 = 0.75$) and the RMS streamwise velocity are highlighted. It is observed that 2 Hz and 4 Hz forcing frequencies have similar mean streamwise velocity profile showing a parabolic functional form with the maximum velocity near the center of the channel (see Figure 4-24). One important aspect of this forced flow is that the signature of the wake flow (velocity deficit) which is seen in the unforced flow (Figure 4-21) is completely absent. Although both the frequencies have similar looking mean streamwise velocity profile, 4 Hz forcing case has higher

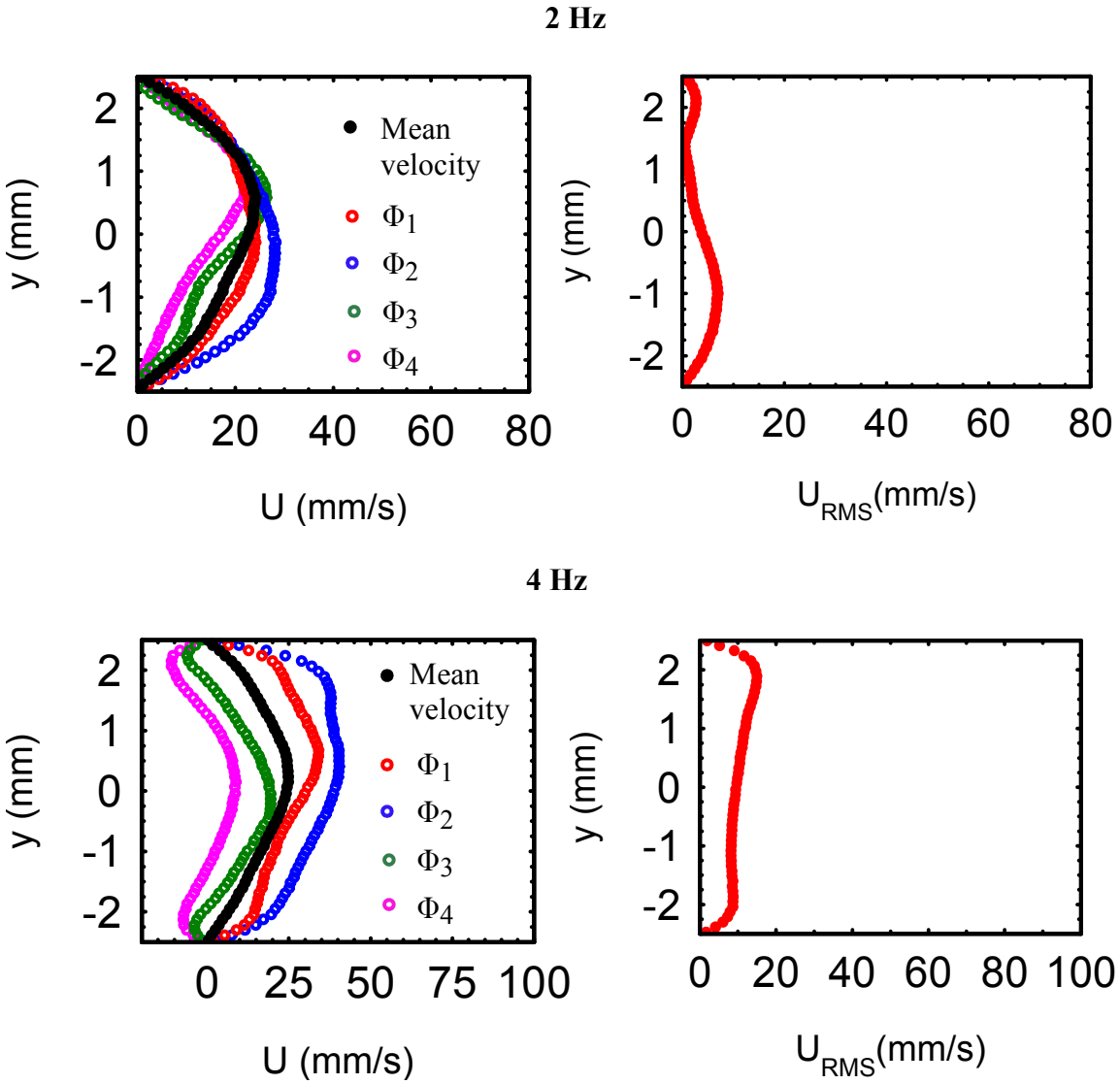

Figure 4-24. Mean, phase resolved and RMS streamwise velocity profile corresponding to 2 and 4 Hz forcing frequency at midspan (U = 20 mm/s, A_3 = 60 μm).

RMS velocity compare to 2 Hz forcing frequency. Also it could be observed that for 4 Hz case, a negative velocity is seen in one of the phase resolved velocity profiles near the wall of the channel. This indicates that during the time period of perturbation, forced flow has reverse flow near the wall. The reverse flow characteristic is absent in 2 Hz forcing case. The mean streamwise velocity profile for 8 Hz forcing case has a lateral variation and also its shape is much different from the 2 Hz and 4 Hz case (see Figure 4-24 and 4-

25). Unlike 2 and 4 Hz cases, the phase resolved velocity profiles for 8 Hz case shows the reverse flow behavior near the center as well as near the wall. The RMS velocity for 8 Hz case is also larger than 4 and 2 Hz forcing frequencies.

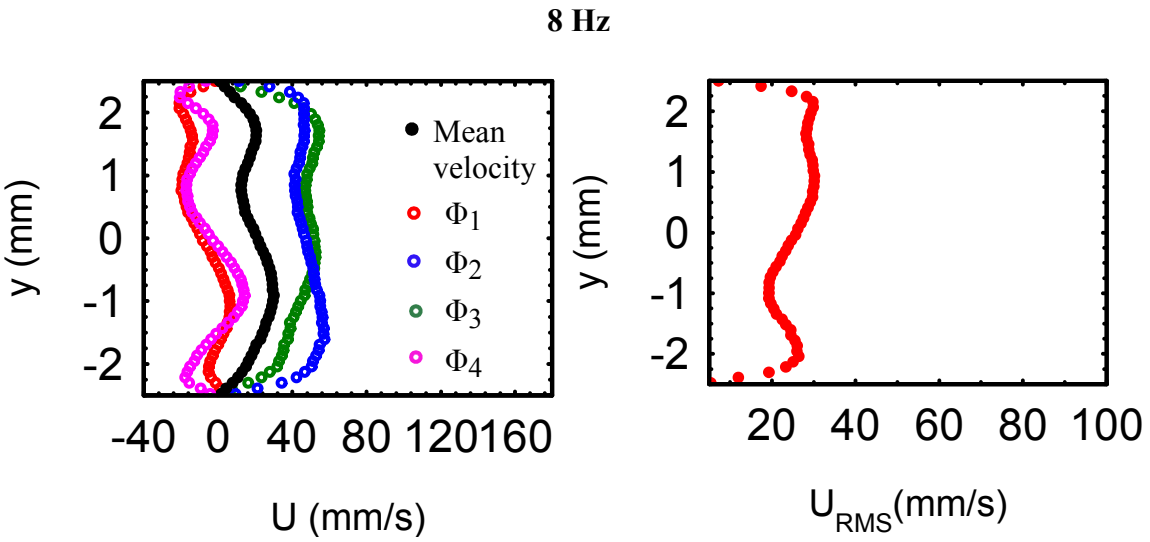

Figure 4-25. Mean, phase resolved and RMS streamwise velocity profile of 8 Hz forcing frequency at midspan (U = 20 mm/s, A_3 = 60 μm).

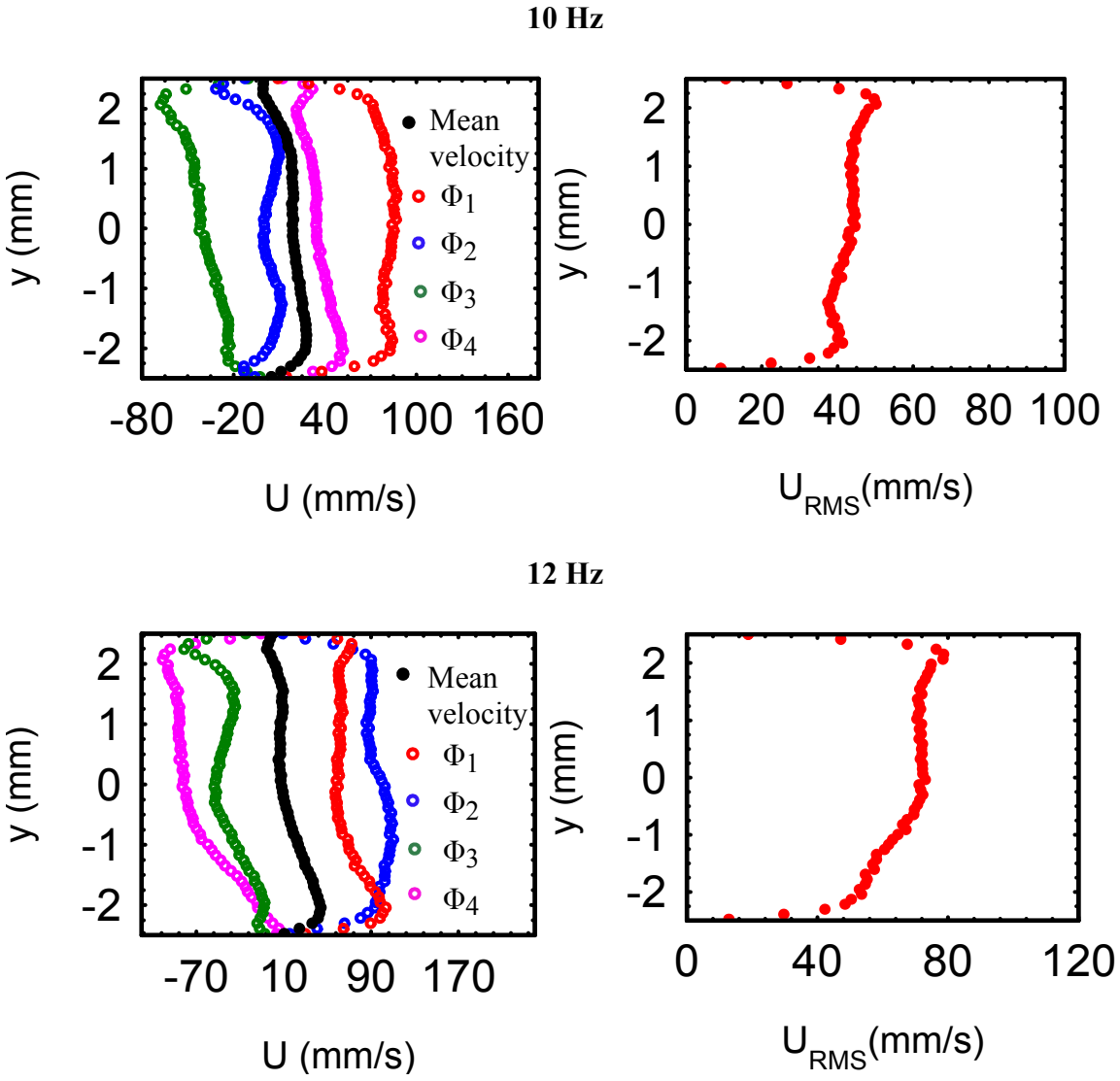

Figure 4-26. Mean, phase resolved and RMS streamwise velocity profile of 10 and 12 Hz forcing frequency at midspan (U = 20 mm/s, A_3 = 60 μm).

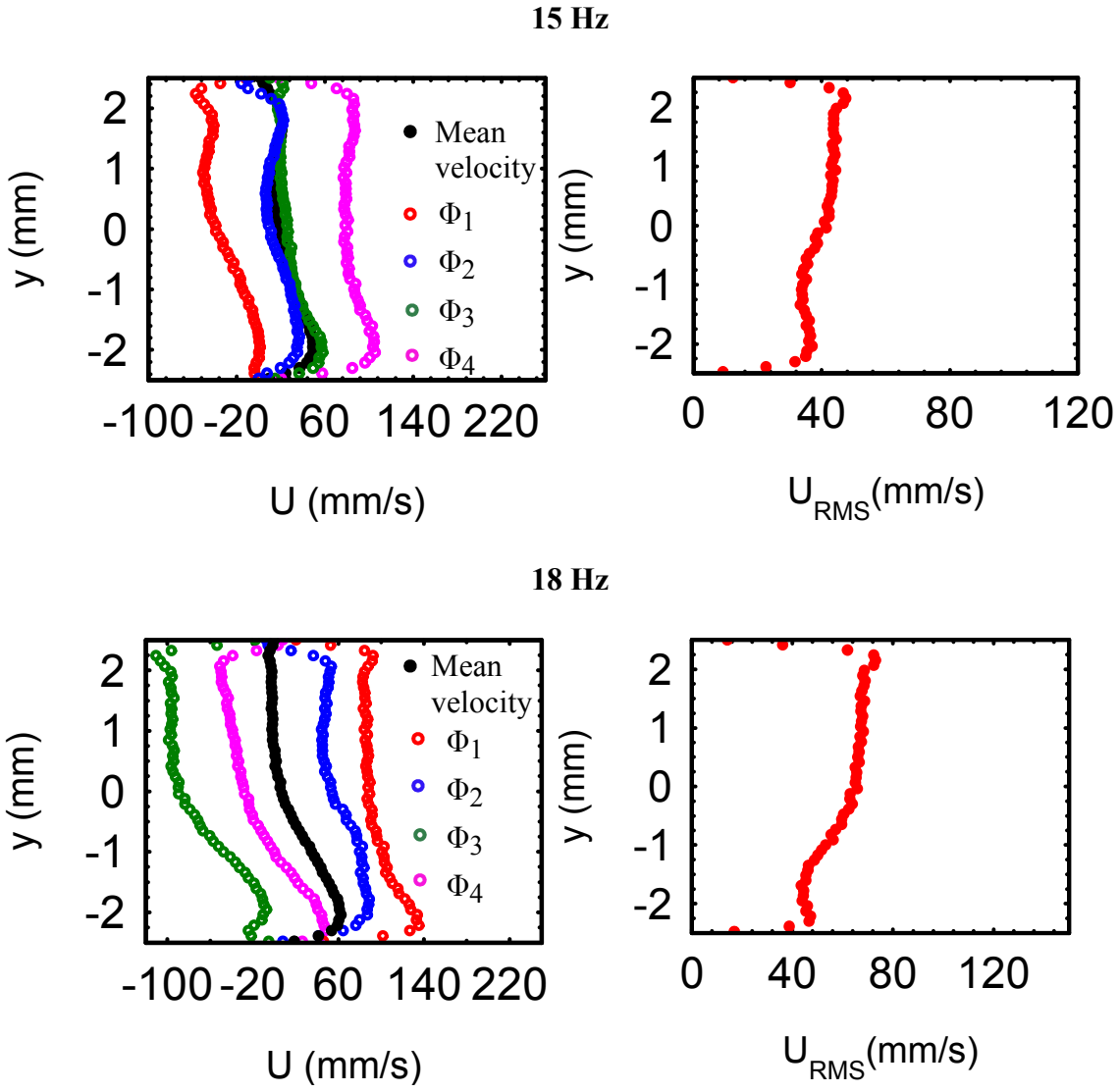

Figure 4-27. Mean, phase resolved and RMS streamwise velocity profile of 15 and 18 Hz forcing frequency at midspan (U = 20 mm/s, A_3 = 60 μm).

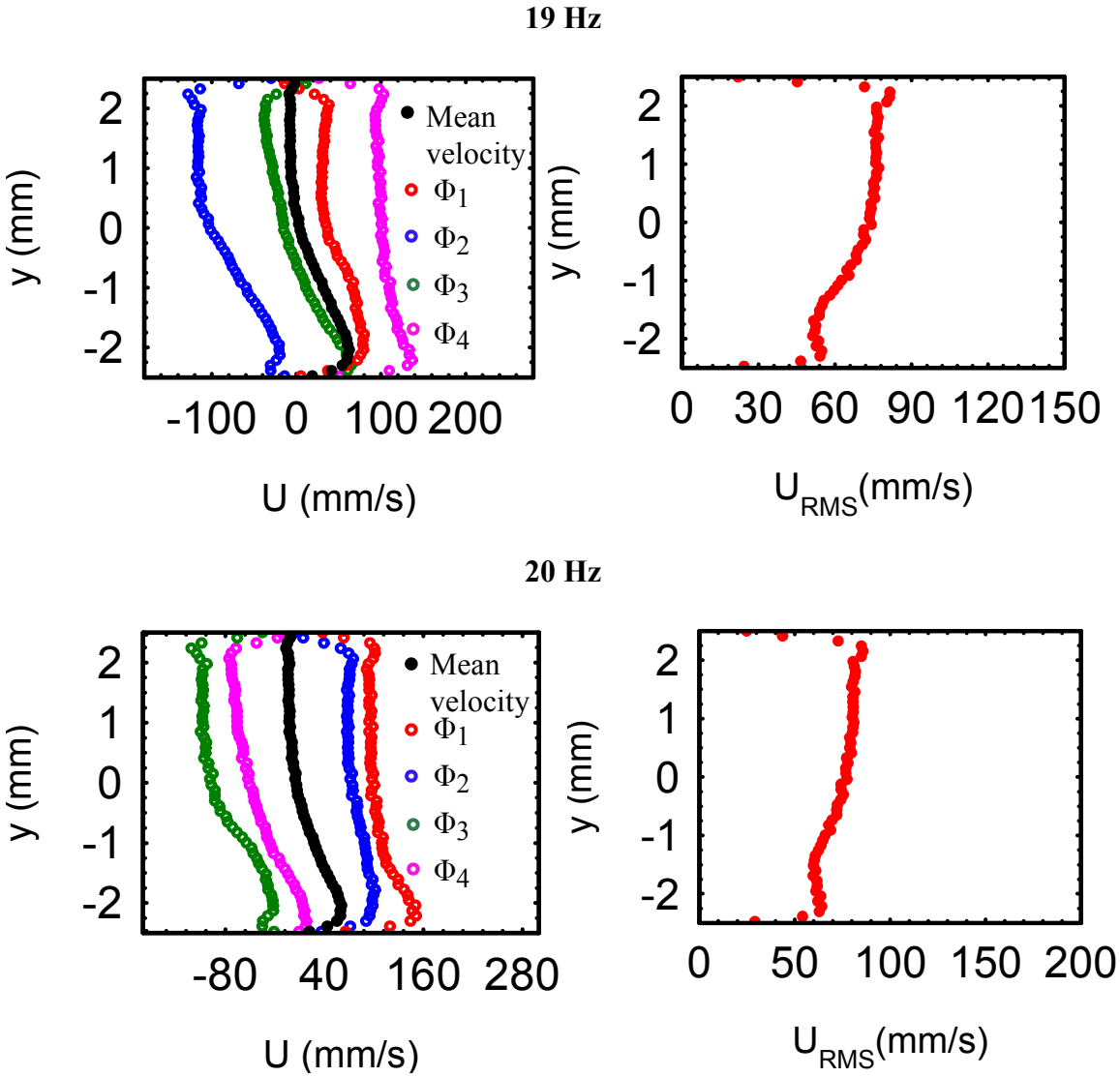

Figure 4-28. Mean, phase resolved and RMS streamwise velocity profile of 19 and 20 Hz forcing frequency at midspan (U = 20 mm/s, A_3 = 60 μm).

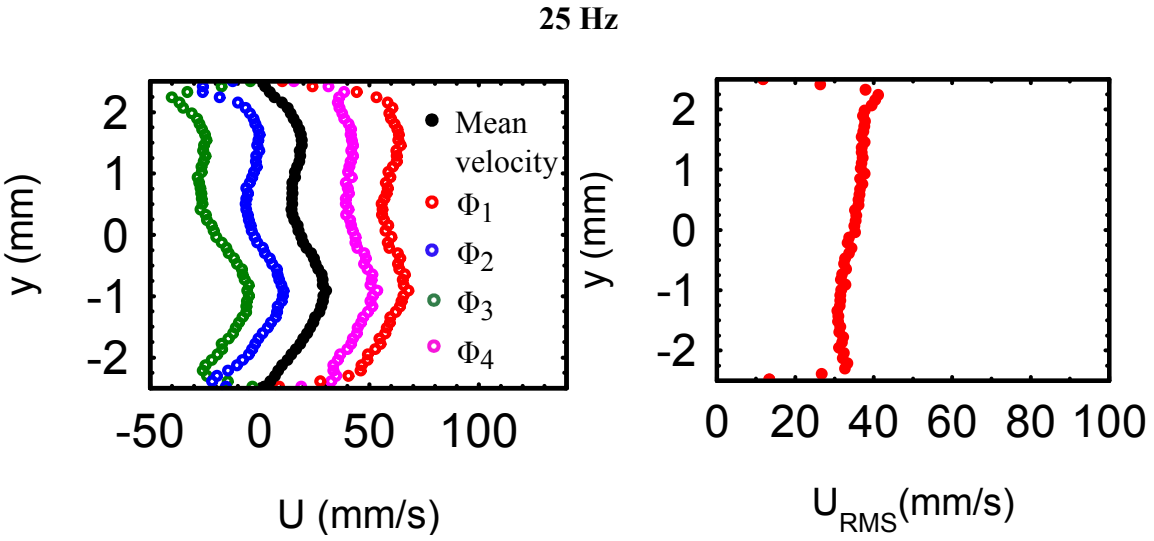

Figure 4-29. Mean, phase resolved and RMS streamwise velocity profile of 25 Hz forcing frequency at midspan (U = 20 mm/s, A_3 = 60 μm).

The forcing frequency cases in the range 10 Hz to 25 Hz exhibit a very large velocity dynamics (Figure 4-26 to 4-29). A reverse flow and a forward flow behavior is observed for the high forcing frequency cases within a single cycle of forcing. The reverse flow is seen across the whole width of the channel unlike the low forcing frequency cases. The phase resolved velocity profiles of all of the high forcing frequency cases highlight that the stream which was forced (y > 0) has always a large negative velocity compare to the other co-flowing stream.

The maximum normalized average RMS streamwise velocity was measured for 12, 19 and 20 Hz, while among the high forcing frequency cases, 15 and 25 Hz are the forcing frequencies with lower RMS velocity (see Figure 4-23). This also explains the reason for 15 and 25 Hz cases showing lower chemical product. It should be noted that although a fixed bellows amplitude was used, depending upon the frequency different level of RMS velocity is measured for each forcing frequency.

4.2. CHEMICALLY REACTING STREAMWISE AND SPANWISE LIF MEASUREMENTS (U = 20 mm/s, A_2 = 40 μm, F = 2 – 25 Hz)

Instantaneous normalized concentration fields shown in Figure 4-30 and 4-31 correspond to the forced flow at lower forcing amplitude A_2 = 40 μm and over the range of forcing frequencies 2 to 25 Hz. The streamwise LIF measurements are performed at midspan over the x-y plane (along the flow direction). To quantify the chemical product across the cross section of the channel (y-z plane), spanwise LIF measurements are performed at four different streamwise locations (x = 4.2, 9, 15 and 25 mm).

Figure 4-32 to 4-41 represents the collage of normalized product concentration fields of forced flow obtained from spanwise LIF measurements. For each forcing frequency instantaneous and average normalized concentration field is highlighted. Average spanwise normalized concentration field is calculated from 1900 LIF images. The average spanwise normalized concentration field is utilized to calculate the chemical product area (A_p). Figure 4-42 depicts the chemical product area for each forcing frequency at four different streamwise locations. To find the probability of unmixed fluid, a spatio-temporal probability density function (pdf) is calculated from 1900 LIF images. The pdf for each forcing frequencies at four different streamwise locations is shown in Appendix D. Figures 4-30 to 4-42 will be utilized in the following section to discuss the effect of lower forcing amplitude A_2 = 40 μm on mixedness over the range of forcing frequencies (2 to 25 Hz).

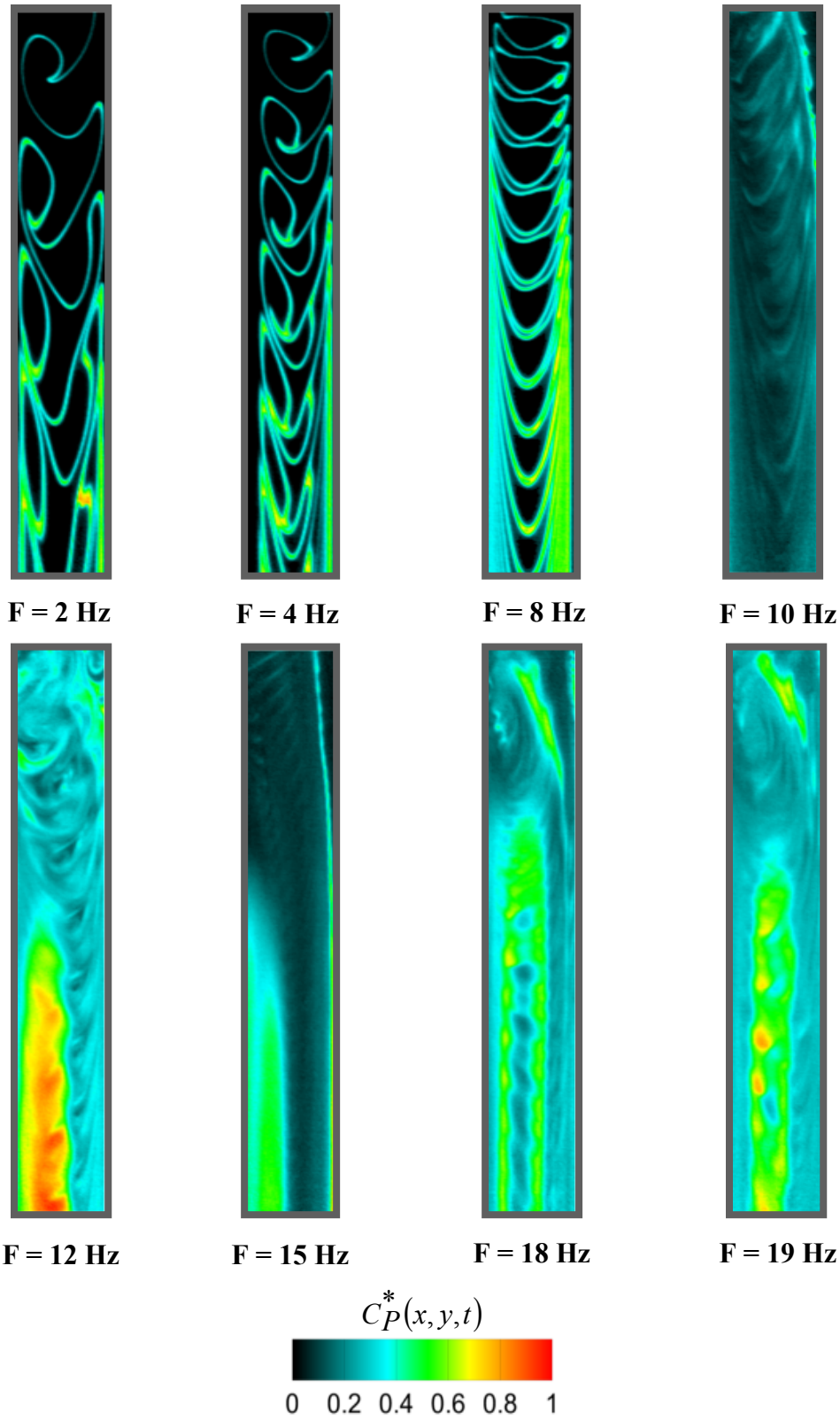

Figure 4-30. Instantaneous normalized product concentration field $C_P^*(x,y,t)$ of forced flow at midspan (U = 20 mm/s and A_2= 40 μm).

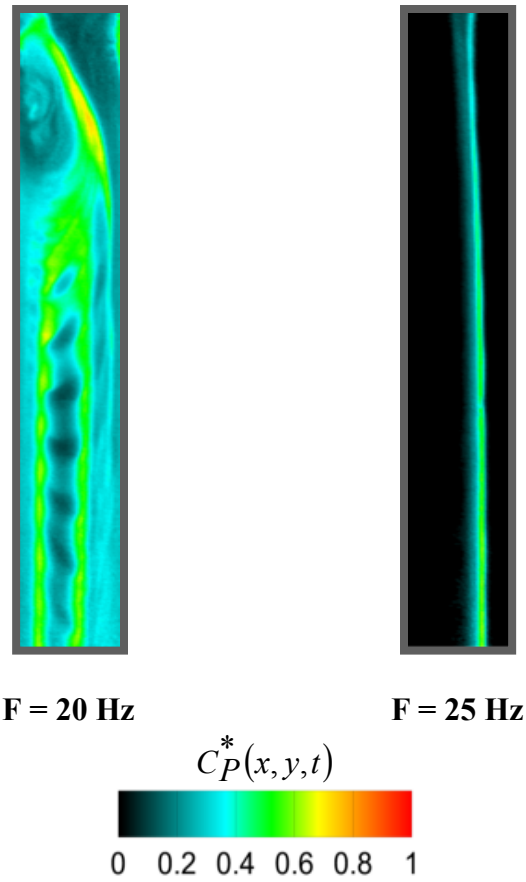

Figure 4-31. Instantaneous normalized product concentration field $C_P^*(x,y,t)$ of forced flow at midspan (U = 20 mm/s and A_2= 40 μm).

The low forcing frequency cases 2, 4 and 8 Hz show a unique interfacial flow structure formed in the channel which is observed in both streamwise and spanwise LIF measurements (Figures 4-30, 4-32, 4-33 and 4-34). The interfacial structures are formed such that the chemical product is found on these structures. As the forced flow moves in the downstream direction, the chemical product found on the interfacial structures increases, which is also depicted in the normalized product area versus forcing frequency plot (Figure 4-42). It is interesting to note that, the maximum chemical product is typically observed near the wall region. The forced flow has a very high shear near the wall. Thus, due to the shear in the velocity and large residence time for the diffusion near

the wall, maximum chemical product is typically seen on the interfaces which are closer to the channel wall (see Figure 4-32, 4-33 and 4-34).

Although an increasing trend in the chemical product is seen in the streamwise direction, unmixed fluid is always found in the channel which is quantified in the pdf plots shown in Appendix D (Figures D-1, D-2 and D-3). Unlike the higher forcing amplitude A_3, the interfacial structures seen for 2, 4 and 8 Hz at lower forcing amplitude A_2 = 40 μm are less tightly wound. Thus, as a result due to a lesser interfacial contact area for A_2 = 40 μm, a lower amount of chemical product is seen compared to A_3 = 60 μm.

F = 2 Hz (Instantaneous normalized concentration field)

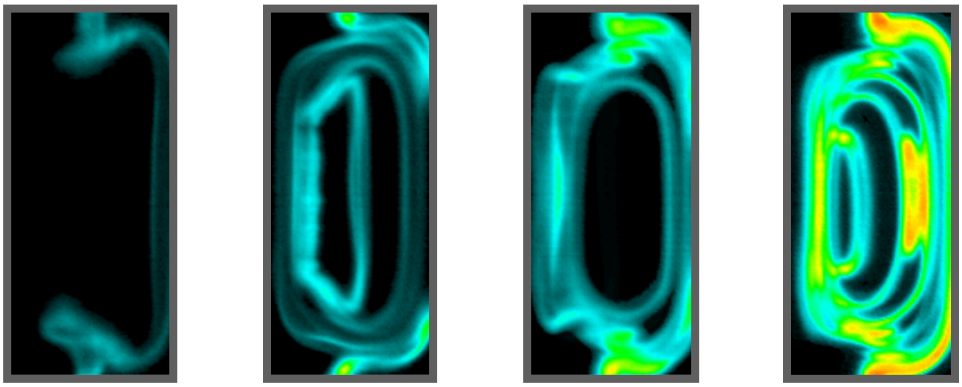

x = 4.2 mm x = 9 mm x = 15 mm x = 25 mm

F = 2 Hz (Average normalized concentration field)

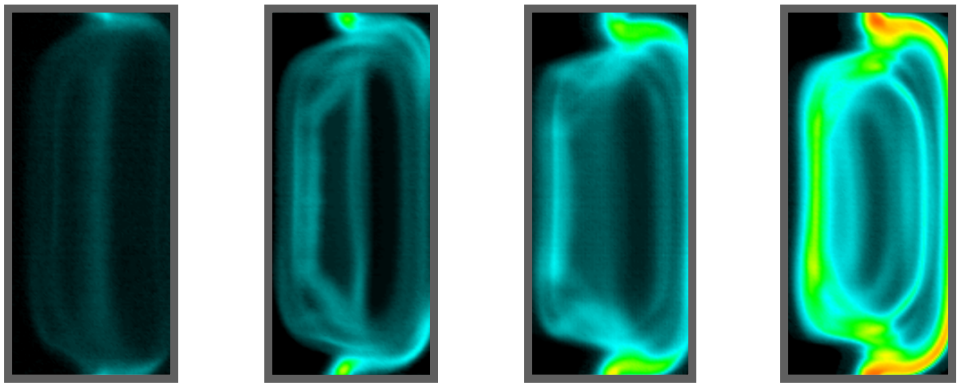

x = 4.2 mm x = 9 mm x = 15 mm x = 25 mm

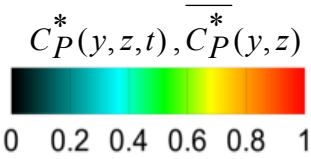

Figure 4-32. Instantaneous and average normalized chemical product concentration field at four different streamwise locations (F = 2 Hz, U = 20 mm/s and A_2 = 40 μm).

F = 4 Hz (Instantaneous normalized concentration field)

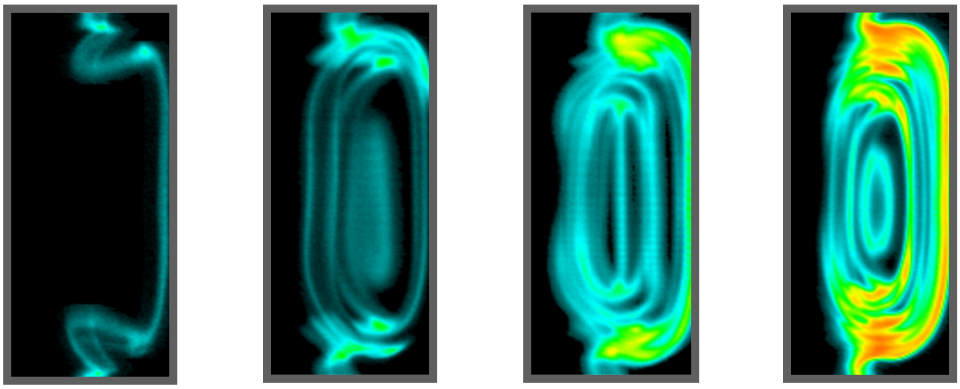

x = 4.2 mm x = 9 mm x = 15 mm x = 25 mm

F = 4 Hz (Average normalized concentration field)

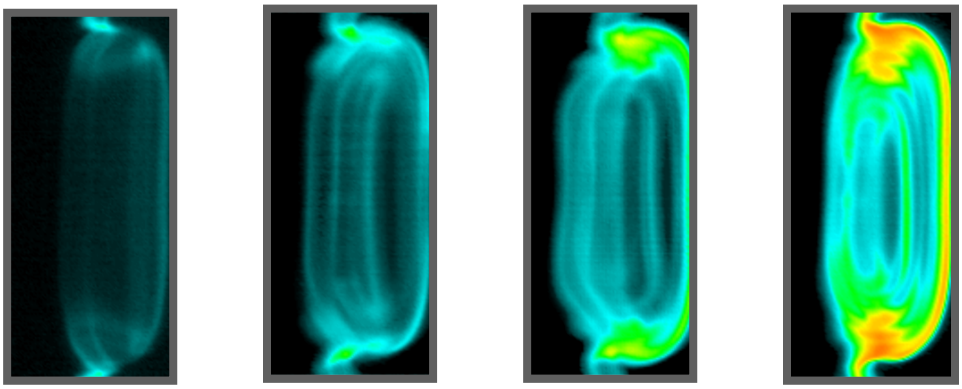

x = 4.2 mm x = 9 mm x = 15 mm x = 25 mm

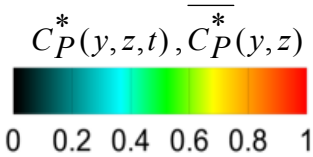

Figure 4-33. Instantaneous and average normalized chemical product concentration field at four different streamwise locations (F = 4 Hz, U = 20 mm/s and A_2 = 40 μm).

F = 8 Hz (Instantaneous normalized concentration field)

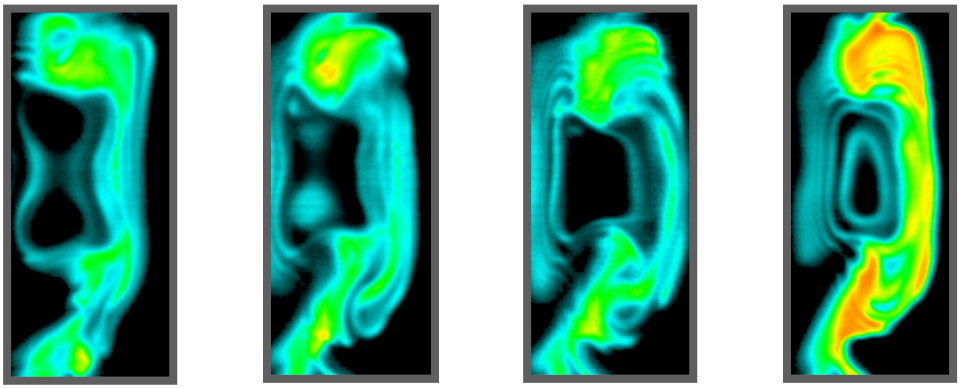

x = 4.2 mm x = 9 mm x = 15 mm x = 25 mm

F = 8 Hz (Average normalized concentration field)

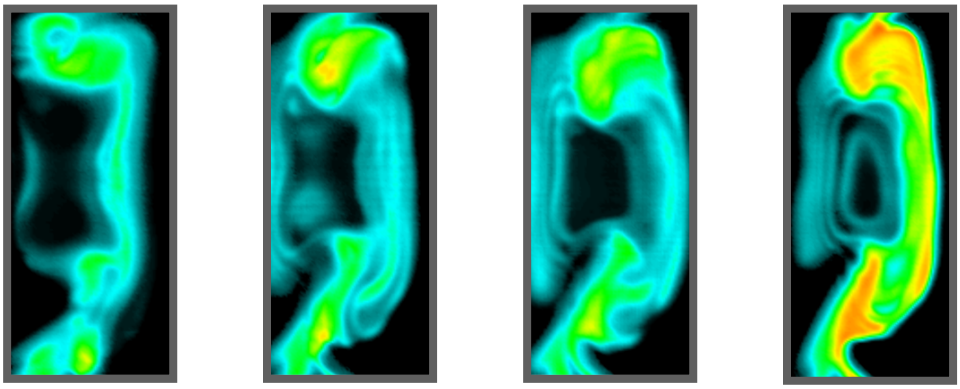

x = 4.2 mm x = 9 mm x = 15 mm x = 25 mm

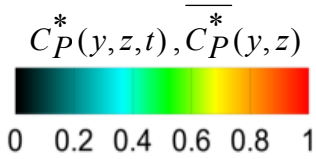

Figure 4-34. Instantaneous and average normalized chemical product concentration field at four different streamwise locations (F = 8 Hz, U = 20 mm/s and A_2 = 40 μm).

F = 10 Hz (Instantaneous normalized concentration field)

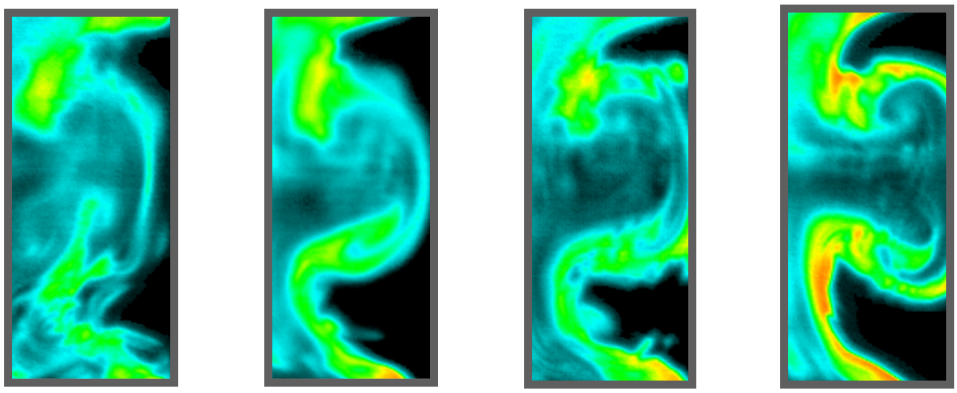

x = 4.2 mm x = 9 mm x = 15 mm x = 25 mm

F = 10 Hz (Average normalized concentration field)

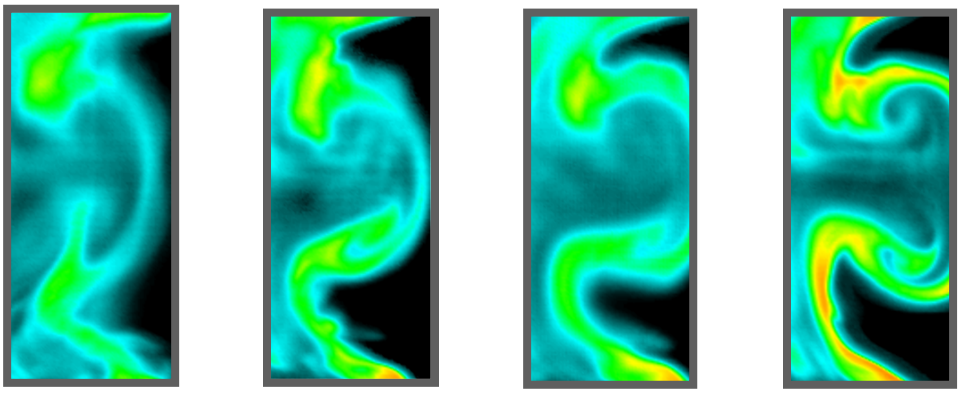

x = 4.2 mm x = 9 mm x = 15 mm x = 25 mm

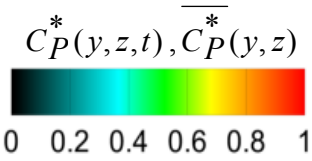

Figure 4-35. Instantaneous and average normalized chemical product concentration field at four different streamwise locations (F = 10 Hz, U = 20 mm/s and A_2 = 40 μm).

F = 12 Hz (Instantaneous normalized concentration field)

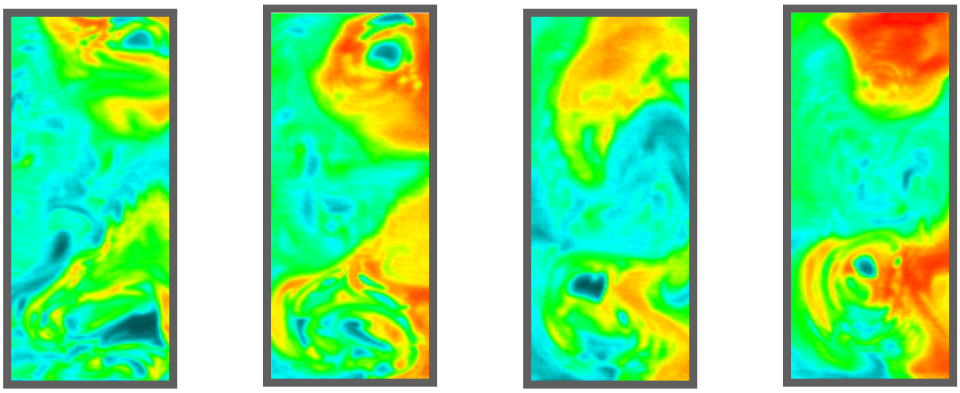

x = 4.2 mm x = 9 mm x = 15 mm x = 25 mm

F = 12 Hz (Average normalized concentration field)

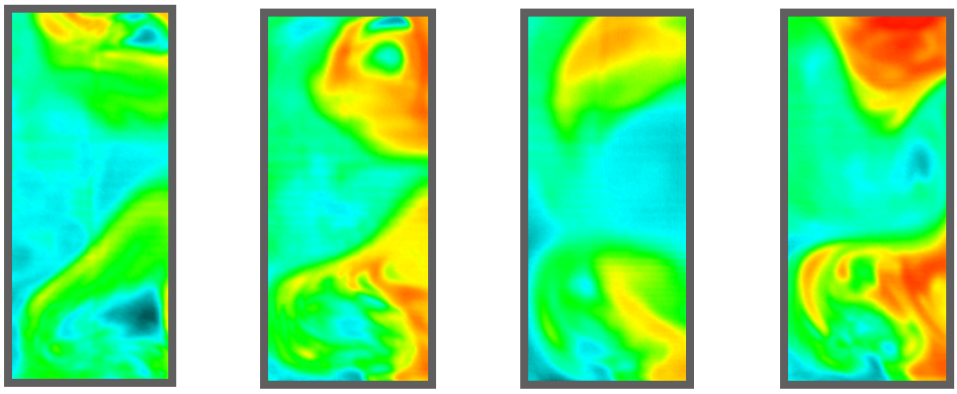

x = 4.2 mm x = 9 mm x = 15 mm x = 25 mm

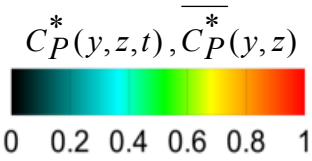

Figure 4-36. Instantaneous and average normalized chemical product concentration field at four different streamwise locations (F = 12 Hz, U = 20 mm/s and A_2 = 40 μm).

F = 15 Hz (Instantaneous normalized concentration field)

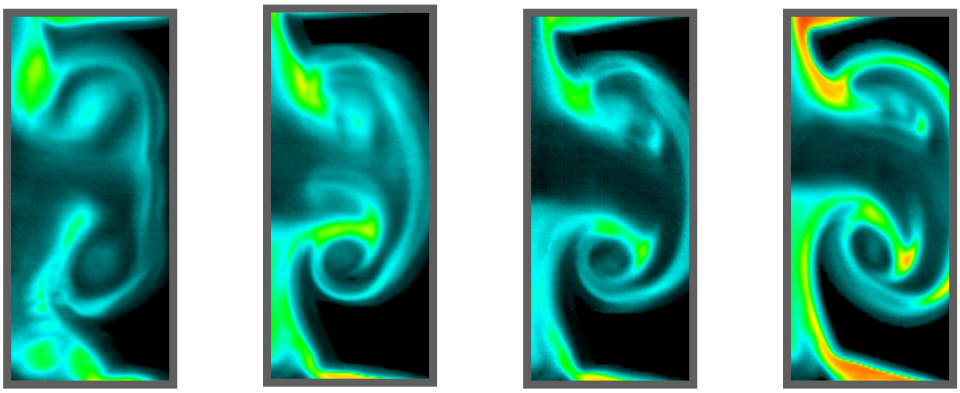

x = 4.2 mm x = 9 mm x = 15 mm x = 25 mm

F = 15 Hz (Average normalized concentration field)

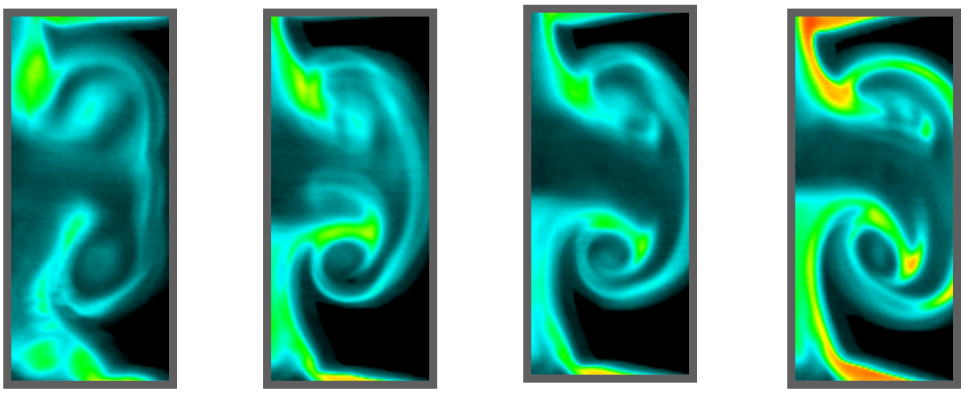

x = 4.2 mm x = 9 mm x = 15 mm x = 25 mm

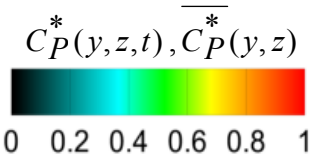

Figure 4-37. Instantaneous and average normalized chemical product concentration field at four different streamwise locations (F = 15 Hz, U = 20 mm/s and A_2 = 40 μm).

F = 18 Hz (Instantaneous normalized concentration field)

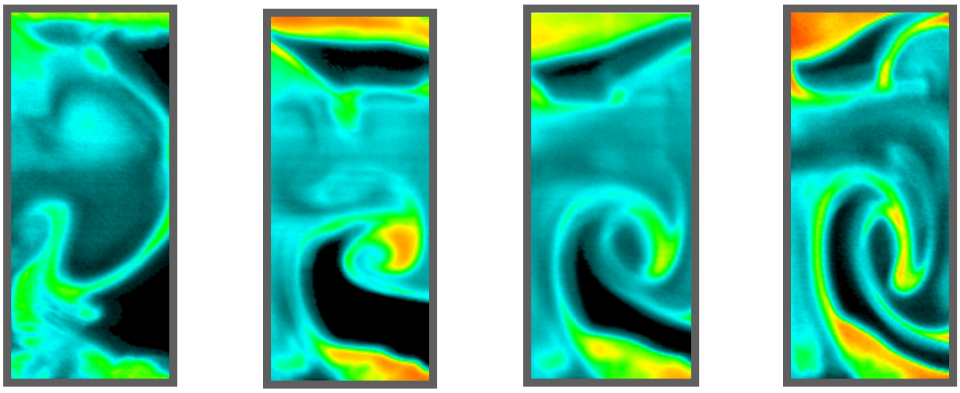

x = 4.2 mm x = 9 mm x = 15 mm x = 25 mm

F = 18 Hz (Average normalized concentration field)

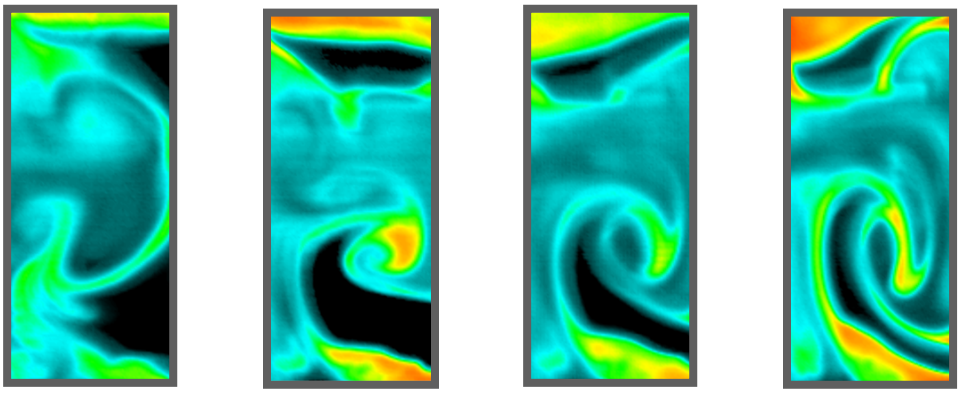

x = 4.2 mm x = 9 mm x = 15 mm x = 25 mm

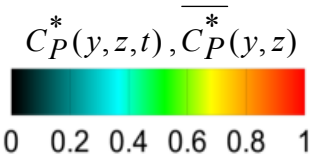

Figure 4-38. Instantaneous and average normalized chemical product concentration field at four different streamwise locations (F = 18 Hz, U = 20 mm/s and A_2 = 40 μm).

F = 19 Hz (Instantaneous normalized concentration field)

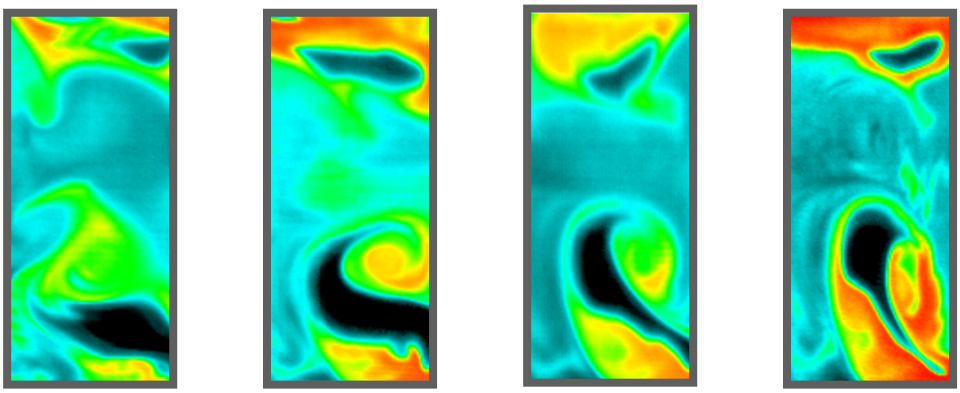

x = 4.2 mm x = 9 mm x = 15 mm x = 25 mm

F = 19 Hz (Average normalized concentration field)

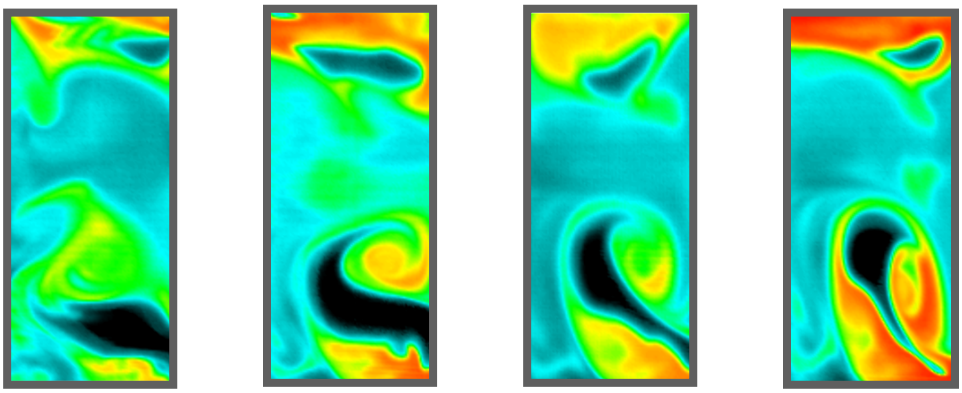

x = 4.2 mm x = 9 mm x = 15 mm x = 25 mm

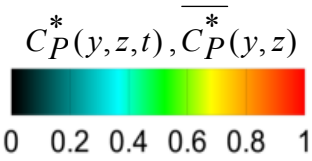

Figure 4-39. Instantaneous and average normalized chemical product concentration field at four different streamwise locations (F = 19 Hz, U = 20 mm/s and A_2 = 40 μm).

F = 20 Hz (Instantaneous normalized concentration field)

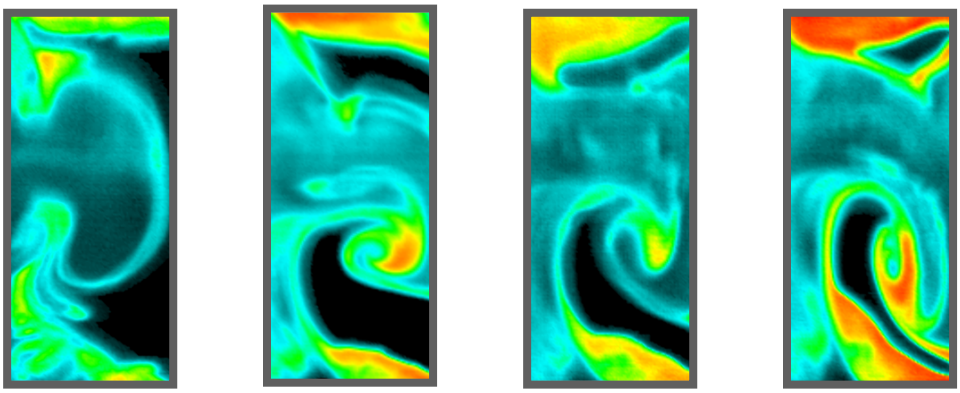

x = 4.2 mm x = 9 mm x = 15 mm x = 25 mm

F = 20 Hz (Average normalized concentration field)

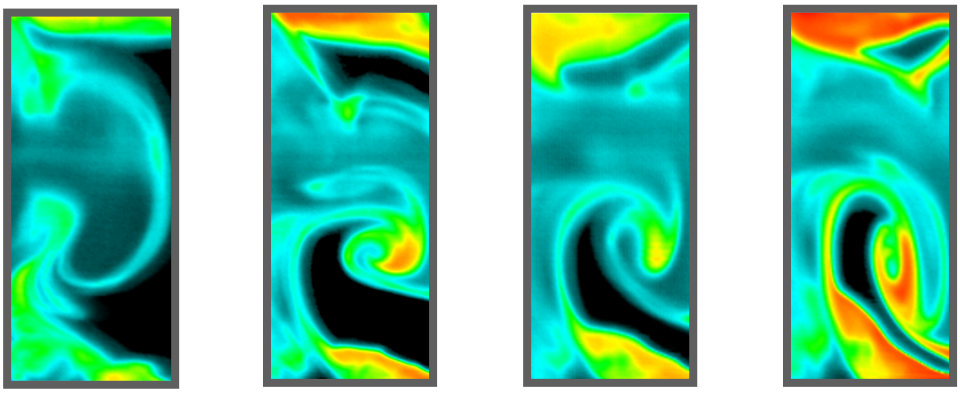

x = 4.2 mm x = 9 mm x = 15 mm x = 25 mm

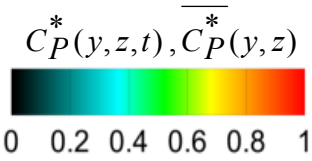

Figure 4-40. Instantaneous and average normalized chemical product concentration field at four different streamwise locations (F = 20 Hz, U = 20 mm/s and A_2 = 40 μm).

F = 25 Hz (Instantaneous normalized concentration field)

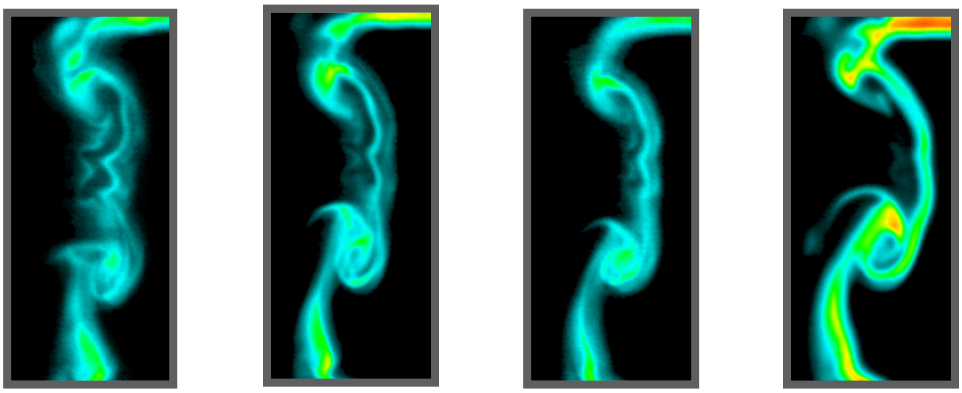

x = 4.2 mm x = 9 mm x = 15 mm x = 25 mm

F = 25 Hz (Average normalized concentration field)

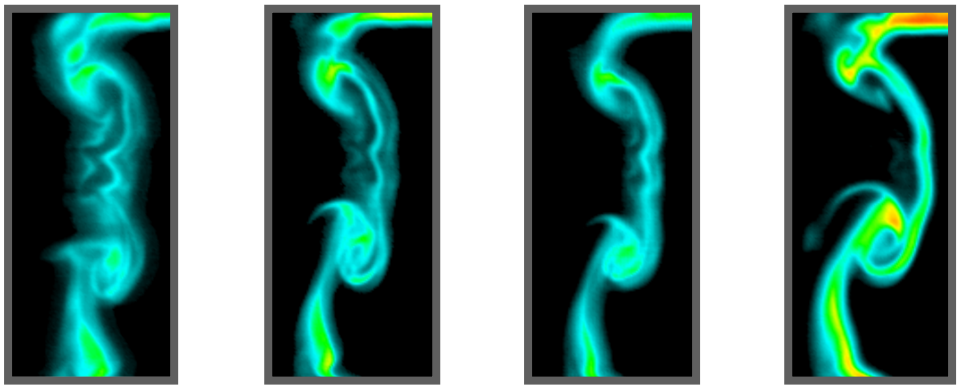

x = 4.2 mm x = 9 mm x = 15 mm x = 25 mm

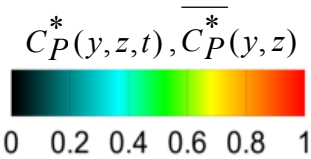

Figure 4-41. Instantaneous and average normalized chemical product concentration field at four different streamwise locations (F = 25 Hz, U = 20 mm/s and A_2 = 40 μm).

Among the high forcing frequency cases between 10 to 25 Hz, 12 Hz forcing case shows the maximum amount of chemical product formed in the channel (see Figure 4-42). The level of mixedness for 12 Hz forcing case is so high such that chemical product occupies the whole width and the height of channel as observed in streamwise and spanwise concentration fields. Thus, for the 12 Hz forcing case a zero probability of unmixed fluid is measured (see Appendix D, Figure D-5). This means that within one forcing cycle there is always a passage of mixed fluid in the channel. From the spanwise concentration field it can be observed that at any streamwise location the maximum chemical product is typically seen near the wall. Similar observation was also made for higher forcing amplitude.

The forcing frequency cases 10,15,18,19 and 20 Hz, show different levels of chemical product but they have similar looking mixed fluid structure. At the earliest streamwise location x = 4.2 mm, an inverted C–shaped structure is observed in the channel (Figures 4-35, 4-37, 4-38, 4-39 and 4-40). The arms of the inverted C-shaped structure are connected to the mixed fluid appearing near the wall. The thickness of the inverted C-shaped structure i.e. the amount of chemical product varies depending upon the forcing frequency. The maximum chemical product is found in the mixed fluid region which connects the arm of the inverted C-shaped structure with the wall. Unlike 12 Hz forcing case, 10,15,18,19 and 20 Hz forcing cases show the presence of unmixed fluid (see the pdf of chemical product in Appendix D; Figures D-4 to D-9). The unmixed fluid region is generally found outside of the inverted C-shaped structure. As the flow moves downstream in the channel, by x = 25 mm, an increase in the chemical product area is measured with maximum chemical product appearing near the wall.

For 25 Hz forcing case a '*mini*' inverted C-shaped interfacial structure is observed at any streamwise location (Figure 4-41). A very small amount of chemical product is measured as the chemical product is limited to the 'mini' inverted C-shaped structure which occupies a small area within the test section.

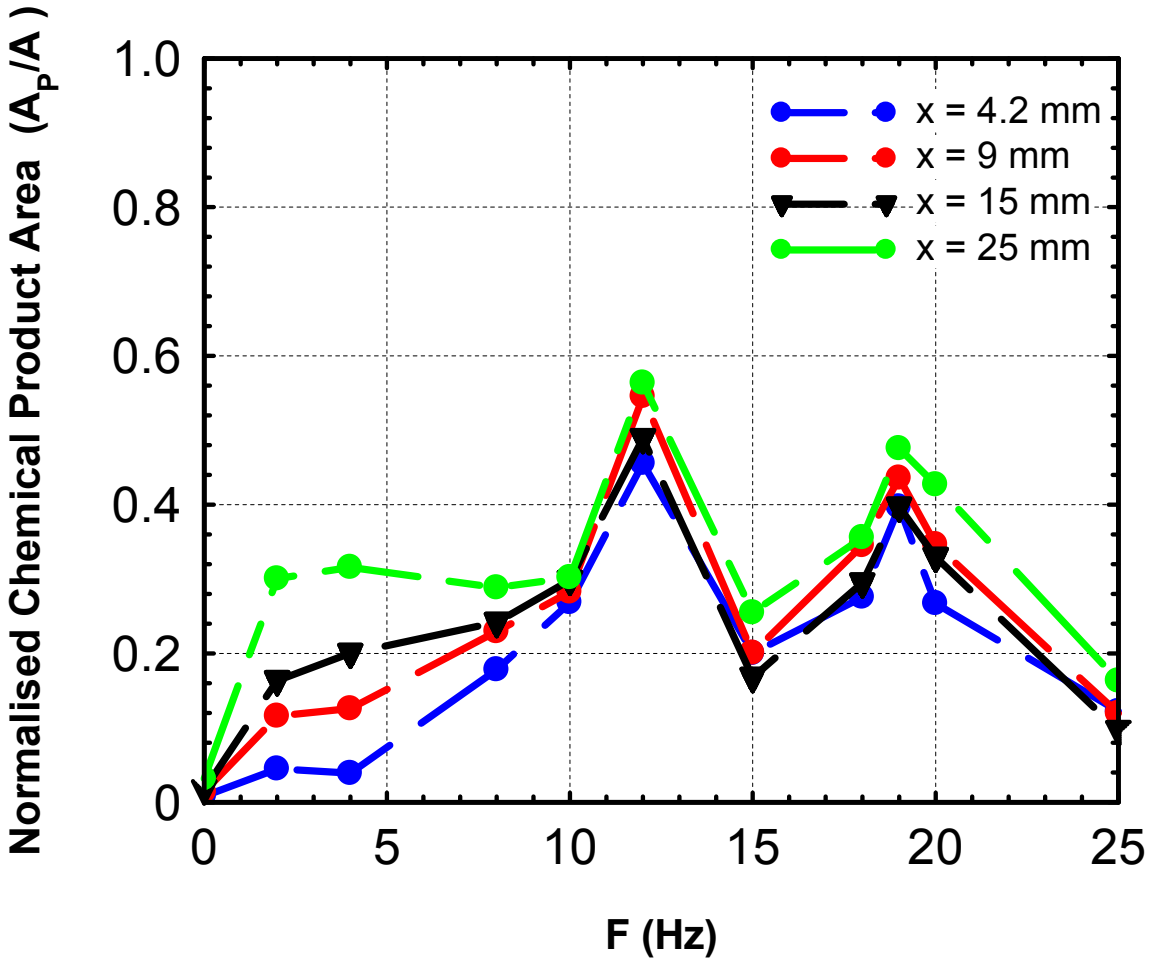

Figure 4-42. Normalized chemical product area for range of forcing frequencies measured at four different streamwise locations (U = 20 mm/s and A_2 = 40 μm).

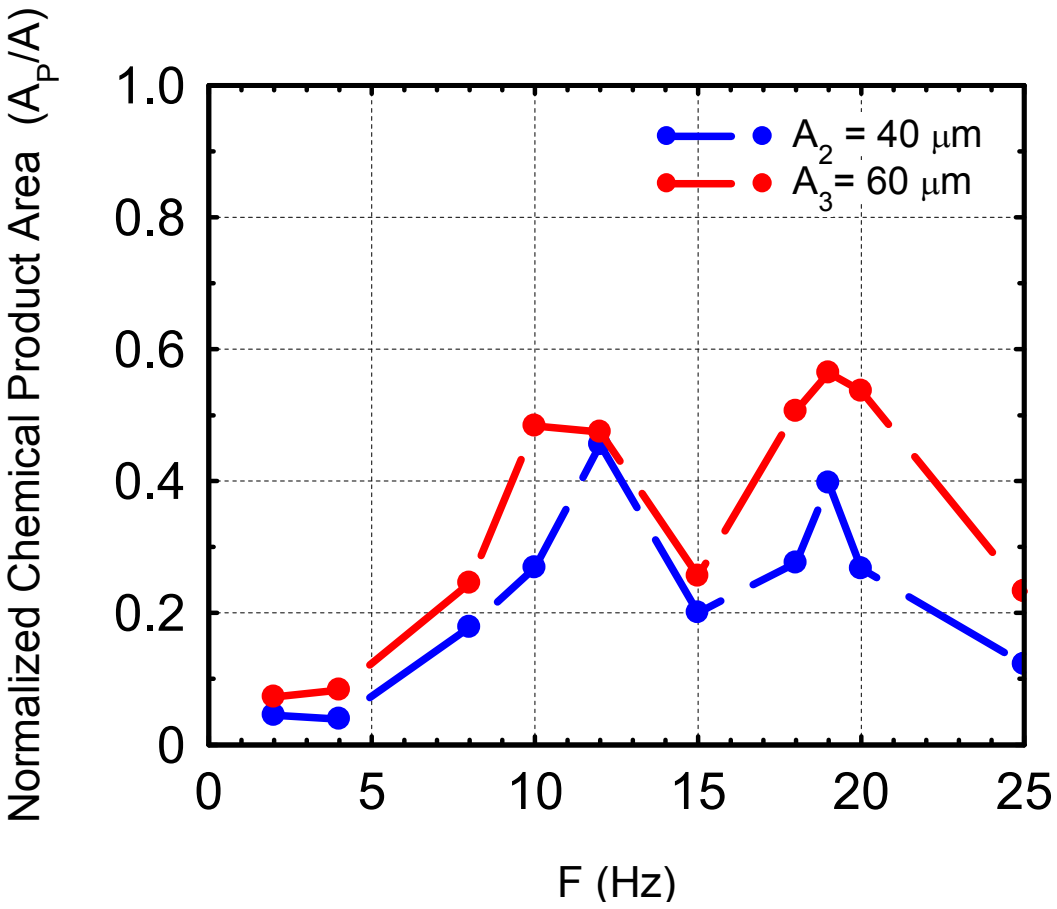

Figure 4-43. Normalized chemical product area for range of forcing frequencies measured at x = 4.2 mm for two different forcing amplitudes.

Figure 4-43 depicts the normalized chemical product area versus forcing frequency for two different forcing amplitudes (A_2 = 40 μm and A_3 = 60 μm) measured at earliest streamwise location x = 4.2 mm. It is interesting to note that for both of the forcing amplitudes A_2 and A_3, the forcing frequencies 12 Hz and 19 Hz provides the maximum amount of chemical product area. The direct relation between the normalized chemical product area and the forcing amplitude is also apparent from Figure 4-43. For any given forcing frequency in the range 2 - 25 Hz, the maximum chemical product area is always found for the highest forcing amplitude. Thus, as we lower the forcing amplitude, lower chemical product area is measured in the channel at any forcing frequency.

4.2.1. Streamwise velocity measurement of the forced flow

(A_2 = 40 µm, F = 2 - 25 Hz)

In this section, streamwise velocity results will be discussed corresponding to forced flow of forcing amplitude A_2 = 40 µm and over a range of forcing frequencies (2 - 25 Hz). To measure the streamwise velocity, MTV experiments were performed at x = 3 mm and z = 0 (midspan). As mentioned in section 4.1.3, the main motivation of velocity measurement is to find the forcing amplitude in terms of velocity. A spatially averaged

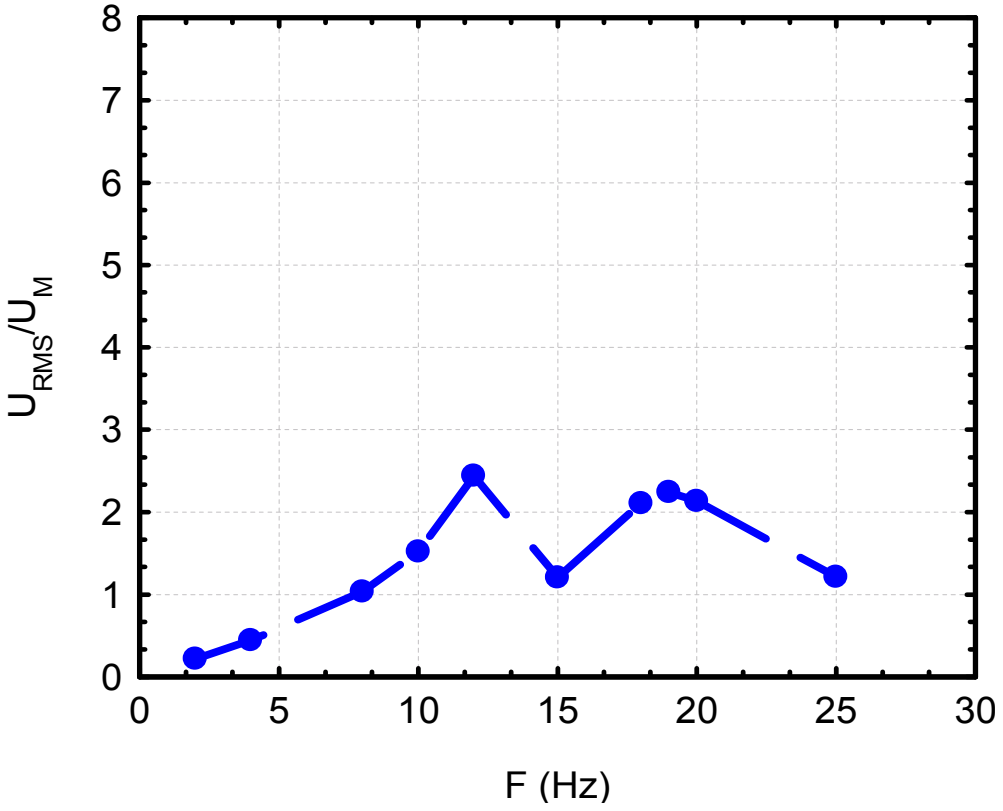

Figure 4-44. Normalized spatially averaged RMS streamwise velocity for various forcing frequencies and for a fixed perturbation amplitude A_2 = 40 µm measured at x = 3 mm and z = 0**.**

RMS streamwise velocity (U_{RMS}) is normalized by spatially-averaged streamwise velocity (U_M) to define the forcing amplitude in terms of velocity. Figure 4-44 shows

the normalized streamwise RMS velocity for each forcing frequency measured at x = 3 mm corresponding to forcing amplitude A_2 = 40 μm. The normalized streamwise RMS velocity results shown in figure 4-44 will be utilized in discussing the streamwise velocity measurements of each forcing frequency in the following section.

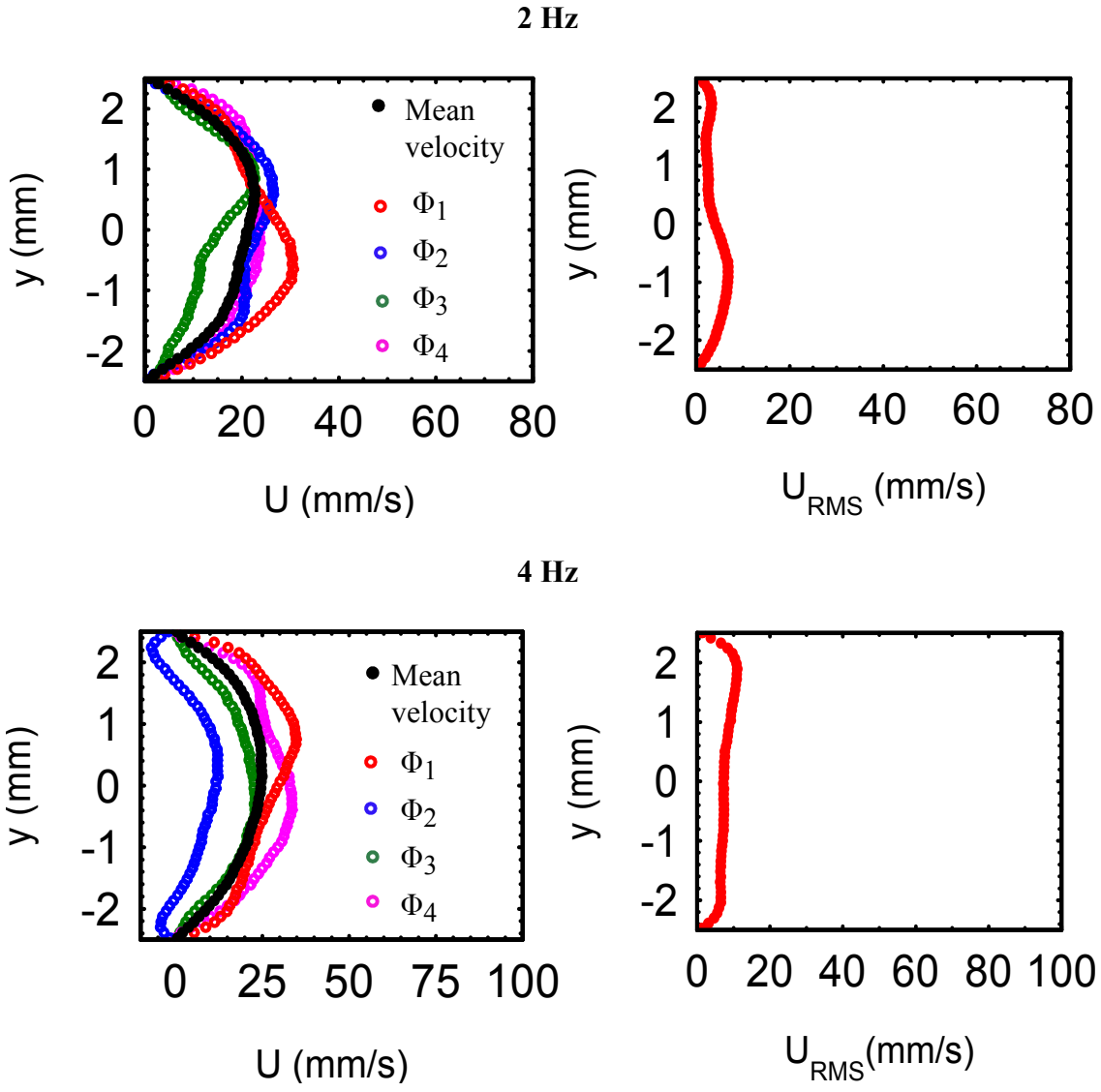

Figure 4-45. Mean, phase resolved and RMS streamwise velocity profile corresponding to 2 and 4 Hz forcing frequency at midspan (U = 20 mm/s, A_2 = 40 μm).

8 Hz

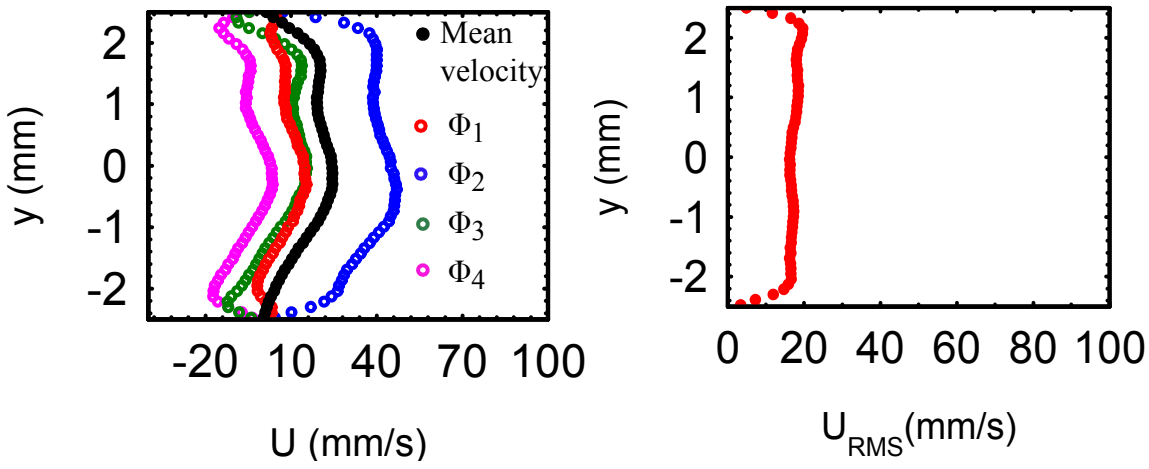

Figure 4-46. Mean, phase resolved and RMS streamwise velocity profile corresponding to 8 Hz forcing frequency at midspan (U = 20 mm/s, A_2 = 40 μm).

Figure 4-45 and 4-46 depicts the mean, phase resolved ($\phi_1, \phi_2, \phi_3, \phi_4$) and RMS streamwise velocity for 2, 4 and 8 Hz forcing frequency at x = 3 mm. The mean streamwise velocity profile of 2 Hz and 4 Hz forcing case has a parabolic functional form while 8 Hz forcing case has a unique profile which was also observed for forcing amplitude A_3 = 60 μm (see Figures 4-25). From the phase resolved velocity profiles it can be observed that the reverse flow behavior is absent for 2 Hz forcing case while 4 and 8 Hz case highlights the reverse flow characteristics away from the center and near the wall region. Among 2, 4 and 8 Hz forcing cases, the maximum normalized spatially averaged RMS velocity is measured for 8 Hz which is depicted in Figure 4-44. As expected, the RMS velocity of 2, 4 and 8 Hz forcing frequencies in case of forcing amplitude A_2 is smaller than the corresponding cases of forcing amplitude A_3. It is interesting to note that, the RMS velocity profiles of 2, 4 and 8 Hz cases have same functional form for forcing amplitudes A_2 and A_3 (see Figures 4-24,4-25,4-45 and 4-46).

10 Hz

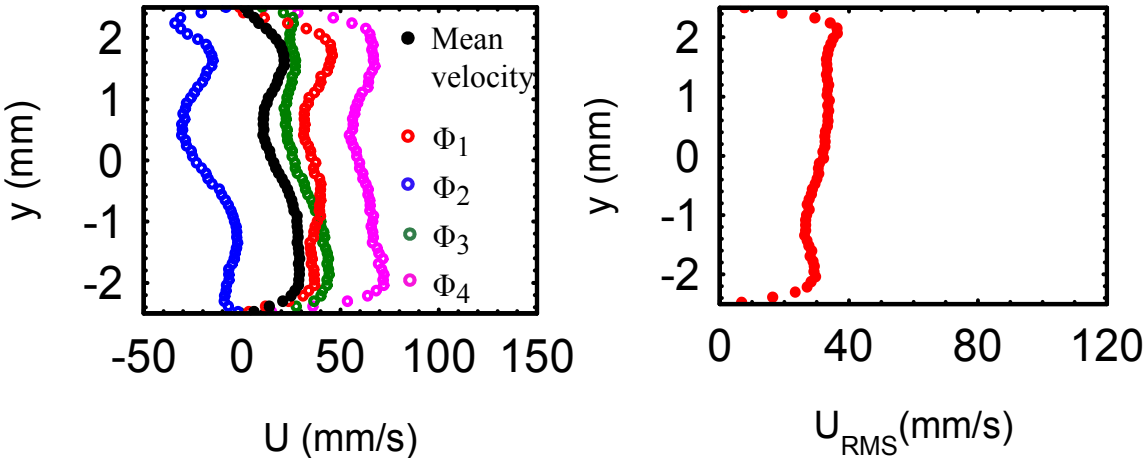

12 Hz

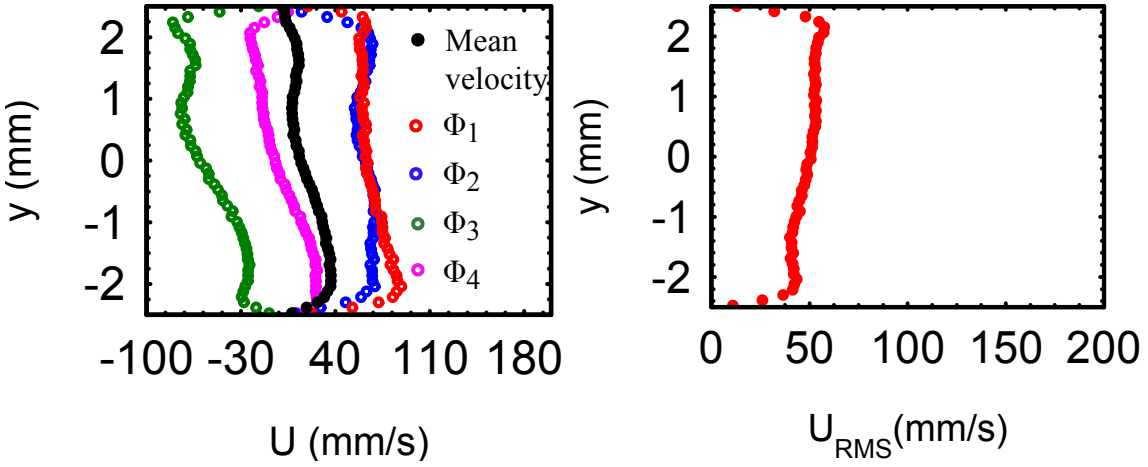

Figure 4-47. Mean, phase resolved and RMS streamwise velocity profile corresponding to 10 and 12 Hz forcing frequency at midspan (U = 20 mm/s, A_2 = 40 μm).

15 Hz

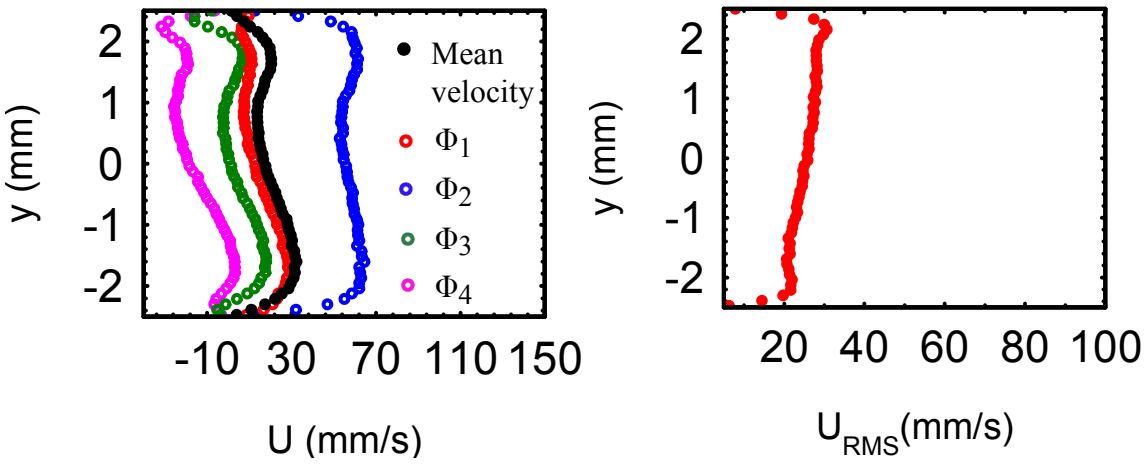

18 Hz

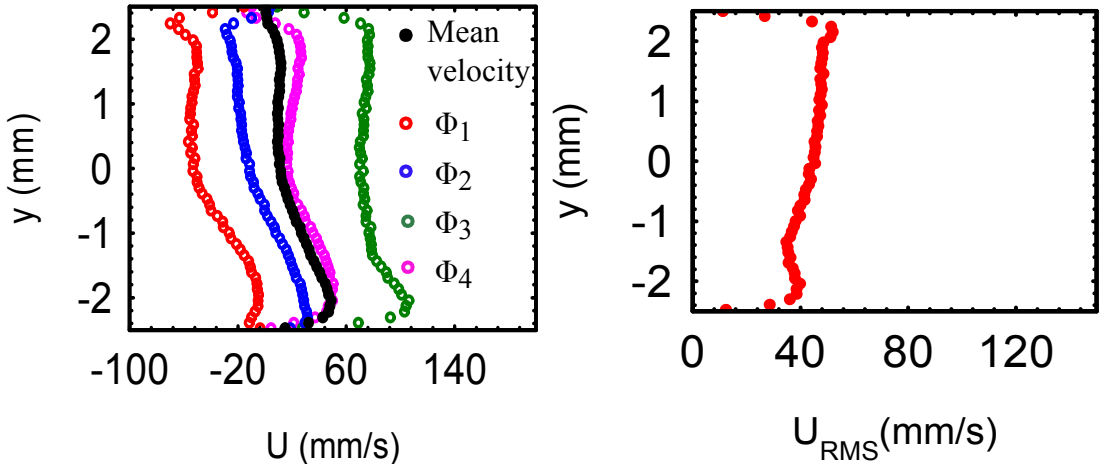

Figure 4-48. Mean, phase resolved and RMS streamwise velocity profile corresponding to 15 and 18 Hz forcing frequency at midspan (U = 20 mm/s, A_2 = 40 μm).

19 Hz

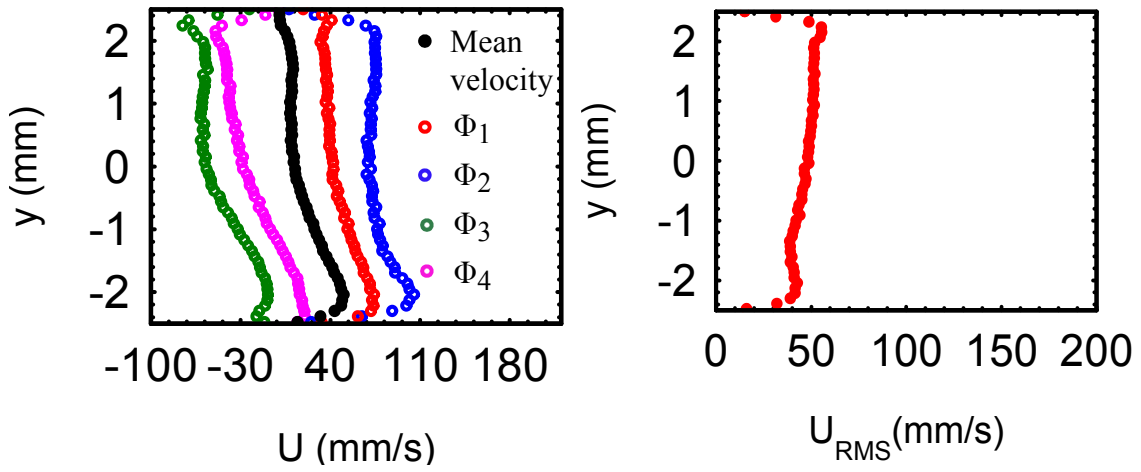

20 Hz

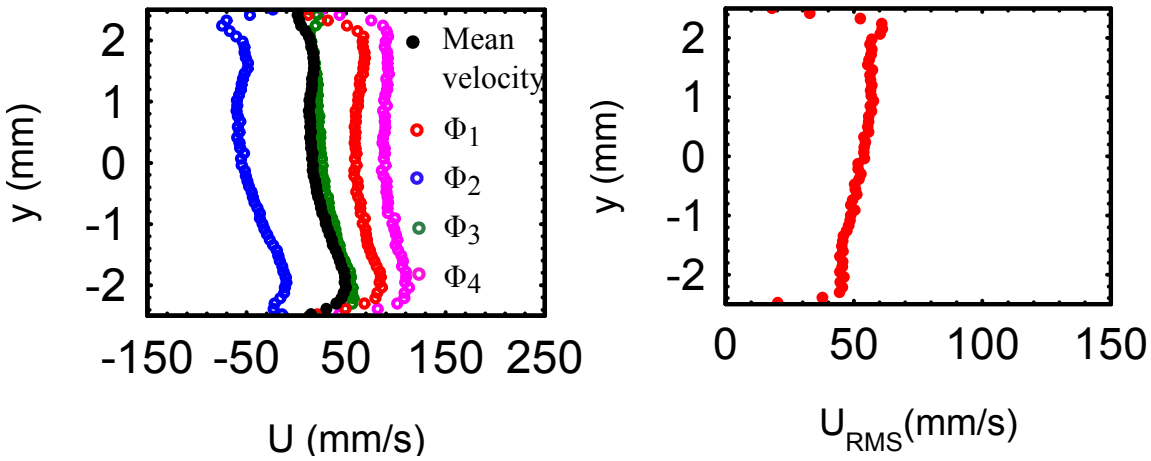

Figure 4-49. Mean, phase resolved and RMS streamwise velocity profile corresponding to 19 and 20 Hz forcing frequency at midspan (U = 20 mm/s, A_2 = 40 μm).

25 Hz

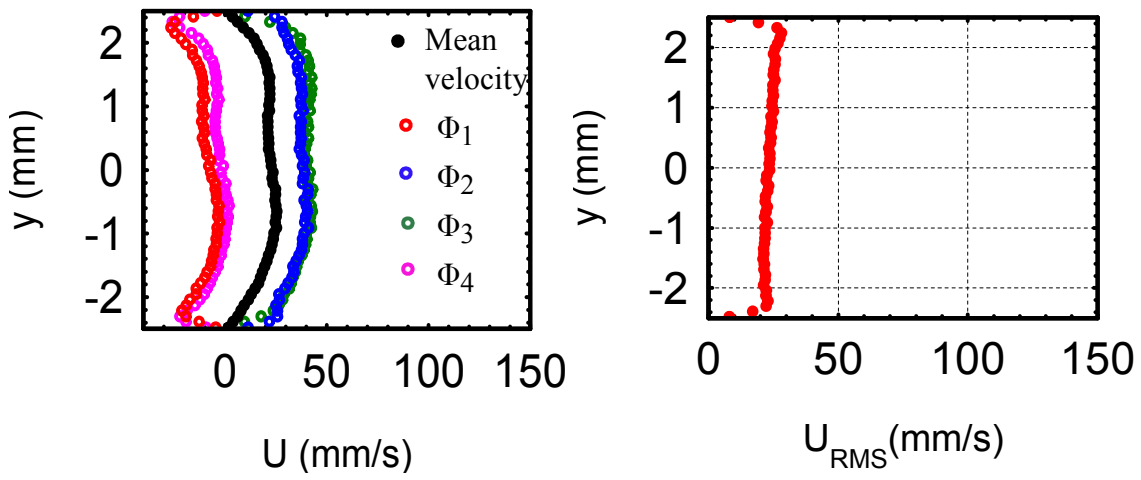

Figure 4-50. Mean, phase resolved and RMS streamwise velocity profile corresponding to 25 Hz forcing frequency at midspan (U = 20 mm/s, A_2 = 40 μm).

Figures 4-47 to 4-50 depicts the mean, phase resolved ($\phi_1, \phi_2, \phi_3, \phi_4$) and RMS velocity of a forced flow corresponding to forcing frequencies 10, 12, 15, 18, 19, 20 and 25 Hz and forcing amplitude A_2 measured at x = 3 mm. Similar to higher forcing amplitude A_3, a large velocity dynamics is also seen for lower forcing amplitude A_2 in case of each forcing frequencies within one forcing cycle. For each forcing frequency, the phase resolved streamwise velocity profiles show forward and reverse flow behavior in the channel. It is interesting to note that, although the forced flow in case of higher forcing frequencies show a large velocity dynamics, the functional form of the phase resolved streamwise velocity profiles ($\phi_1, \phi_2, \phi_3, \phi_4$) remains same with respect to the mean streamwise velocity profile.

Among the high forcing frequency cases, 12 and 19 Hz case depict the maximum normalized spatially average RMS streamwise velocity (see figure 4-44). The RMS

streamwise velocity profile of high forcing frequency cases has same functional form. Similar result was also seen in case of higher forcing amplitude A_3. As expected, the normalized spatially averaged RMS streamwise velocity for each forcing frequency corresponding to forcing amplitude A_2 is always smaller than that of forcing amplitude A_3 (see figure 4-23 and 4-44).

4.3. CHEMICALLY REACTING STREAMWISE LIF MEASUREMENTS AT LOW FORCING AMPLITUDE (A_1 = 25 μm, F = 2 - 25 Hz)

A streamwise chemically reacting LIF measurement was perform at forcing amplitude A_1 = 25 μm to qualitatively study the effect of a very low forcing amplitude on mixedness. Figure 4-51 and 4-52 shows the instantaneous normalized streamwise concentration field $C_P^*(x,y,t)$ at midspan for a forcing amplitude A_1 = 25 μm and for few selected forcing frequencies in the range F = 0 - 25 Hz. The effect of lower forcing amplitude is such that, no forcing case is observed with the large increase in the mixedness which was typically observed for forcing amplitudes A_2 = 40 μm and A_3 = 60 μm. Since a very small amount of chemical product was observed for forcing amplitude A_1 = 25 μm in the streamwise LIF measurements, the detail spanwise chemically reacting LIF and MTV measurements were performed only for A_2 = 40 μm and A_3 = 60 μm forcing amplitudes.

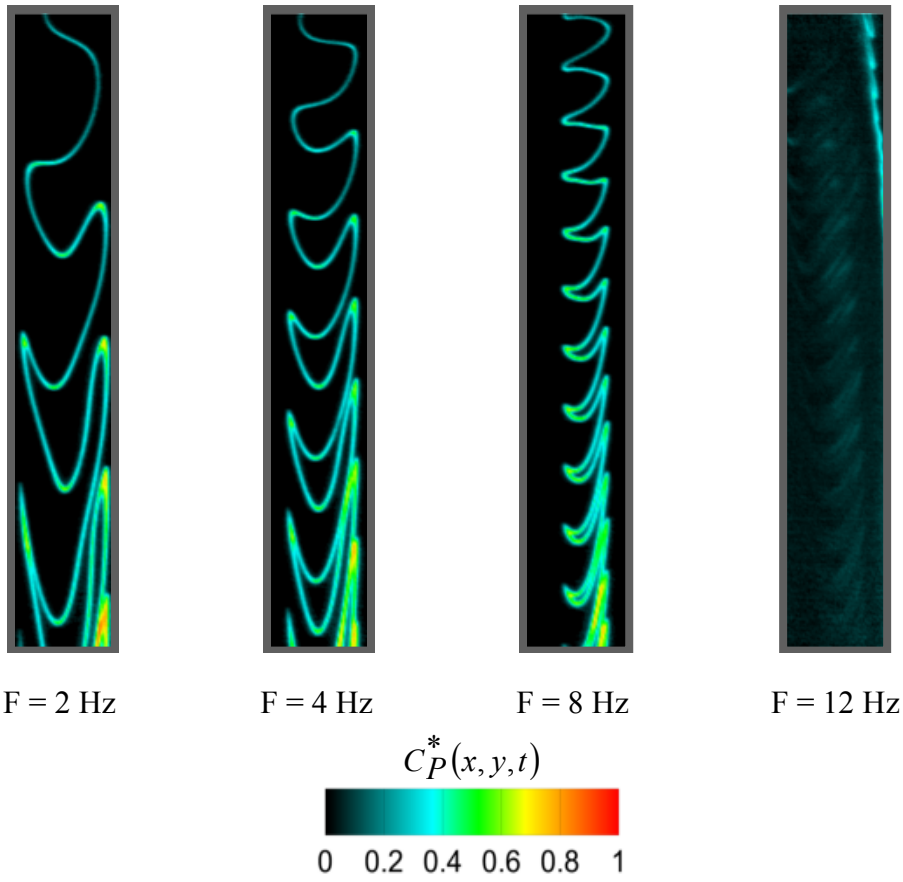

Figure 4-51. Instantaneous normalized product concentration field $C_P^*(x,y,t)$ of forced flow at midspan (U = 20 mm/s and A_1 = 25 μm).

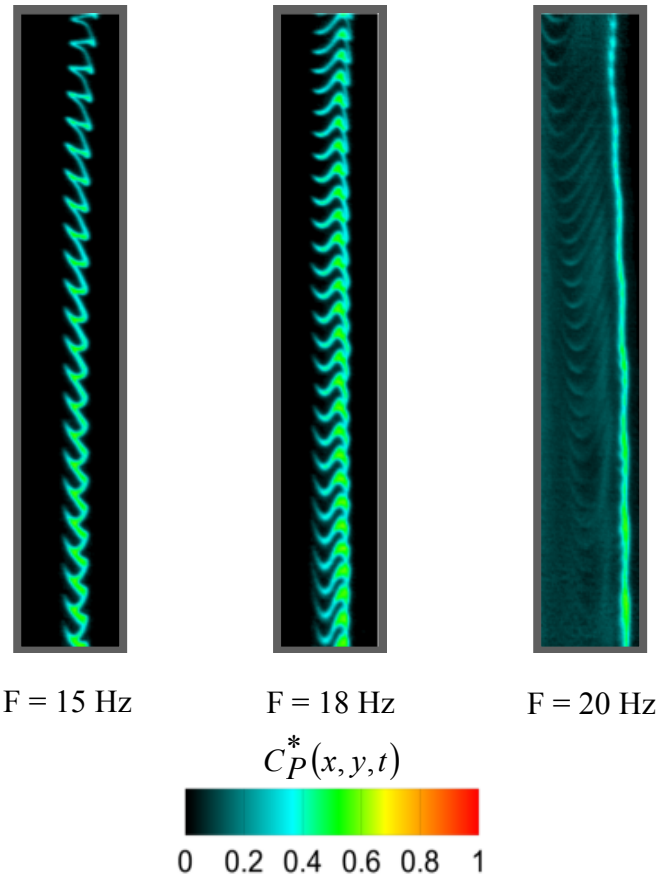

Figure 4-52. Instantaneous normalized product concentration field $C_P^*(x,y,t)$ of forced flow at midspan (U = 20 mm/s and A_1 = 25 μm).

4.4. STATIONARY FLOW BEHAVIOR OF MIXED FLUID

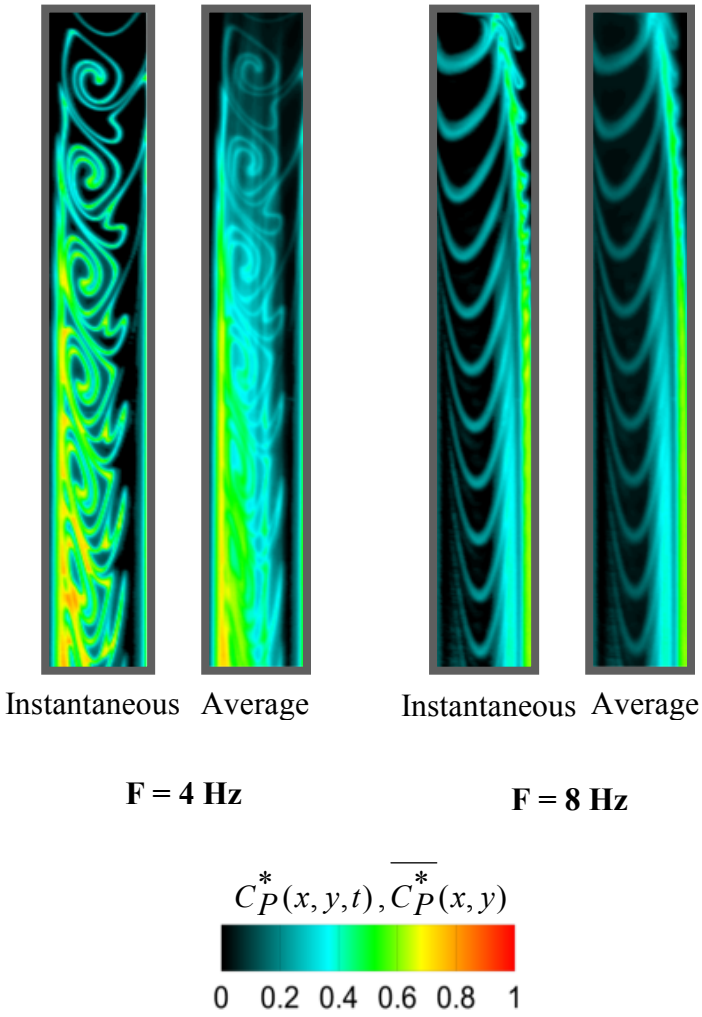

Figure 4-53. Instantaneous and average normalized product concentration field of forced flow at midspan (U = 20 mm/s and A_3 = 60 μm).

Figure 4-53 depicts the instantaneous and average normalized product concentration field of forced flow at midspan corresponding to forcing amplitude A_3 = 60 μm and forcing frequencies 4 and 8 Hz. In general, the averaging of the instantaneous normalized concentration field provides a smoothing effect on the flow structure. In other words, this means that the mixed fluid structures observed in the instantaneous normalized product concentration field are smeared out in the average normalized product concentration field.

It is interesting to note that, the average normalized concentration field of 4 and 8 Hz forcing case does have a smoothing effect but it also shows a presence of a well-defined mixed fluid structure which is observed in the instantaneous normalized concentration field. This phenomenon is also noticed in the spanwise LIF measurements highlighted in figures 4-7 and 4-8. To better understand this effect, the streamwise instantaneous normalized concentration fields (1900 LIF images) were phase ordered such that it described the flow structure behavior for one complete forcing cycle. The instantaneous normalized concentration fields obtained from streamwise LIF measurements were phase ordered such that 95 phase ordered normalized concentration fields represented one complete cycle of forcing. Each concentration field out of 95 phase ordered concentration fields is an average of 20 instantaneous normalized concentration fields.

From the phase-ordered streamwise images, it was found that, within the time period of one forcing cycle the flow structures showed stationary and reverse flow behavior for a certain fraction of a forcing cycle. As a result, the averaging of the instantaneous normalized concentration field showed both, a smoothing effect as well as a well-defined pattern of mixed fluid structure wherein the well-defined mixed fluid structure corresponds to the phases where the flow exhibits stationary flow behavior. To find the phase duration for which the flow exhibits stationary behavior within one complete forcing cycle, an in-house correlation program was used made by D. Olson. This program calculates the phase resolved displacement and the velocity of a mixed fluid structure utilizing the phase ordered streamwise LIF images. For each forcing frequency, the location of the structure whose displacement is measured is shown by its respective x and y co-ordinates (see figure 4-54). Although the displacement of the mixed fluid structure

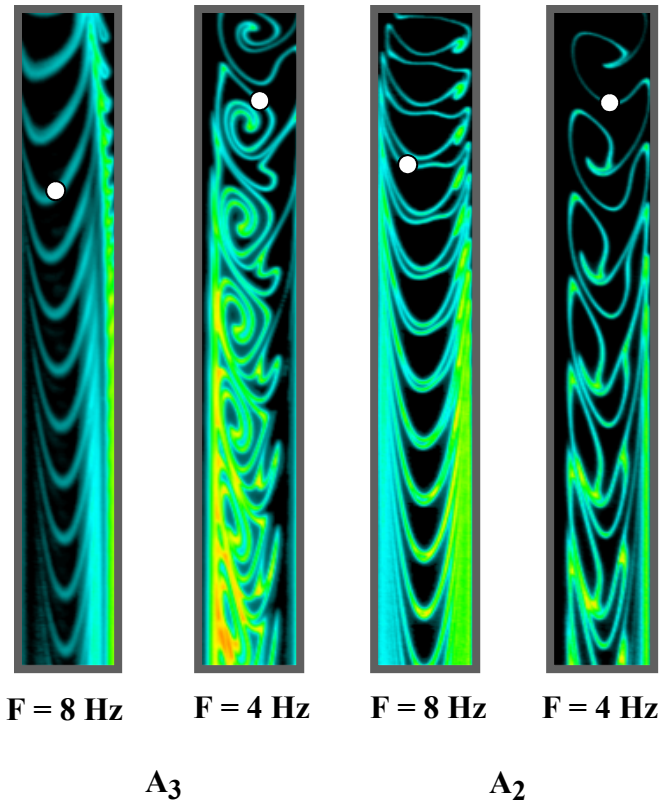

Figure 4-54. Position of the mixed fluid structure whose displacement is measured throughout a complete forcing cycle is marked by a solid circle.

will vary across the whole test section, the displacement measured here corresponds to only a portion of mixed fluid structure defined by x and y co-ordinates. Note that, this analysis is performed just to provide an estimate of the time period for which the flow exhibits stationary behavior.

Figure 4-55(a, b) depicts the phase resolved displacement and velocity of the mixed fluid structure for one complete forcing cycle corresponding to 4 and 8 Hz forcing case. In this analysis, each phase resolved displacement refers to the actual distance travelled by the mixed fluid structure over the phase duration $\Delta\phi = 0.052$. From figure 4-55(a, b), it is observed that forced flow at 4 Hz and 8 Hz forcing frequency exhibits stationary flow behavior such that mixed fluid structure remains stationary for 15.7 % of the forcing cycle. This means that, mixed fluid structure has zero displacement for 39 ms and 20 ms

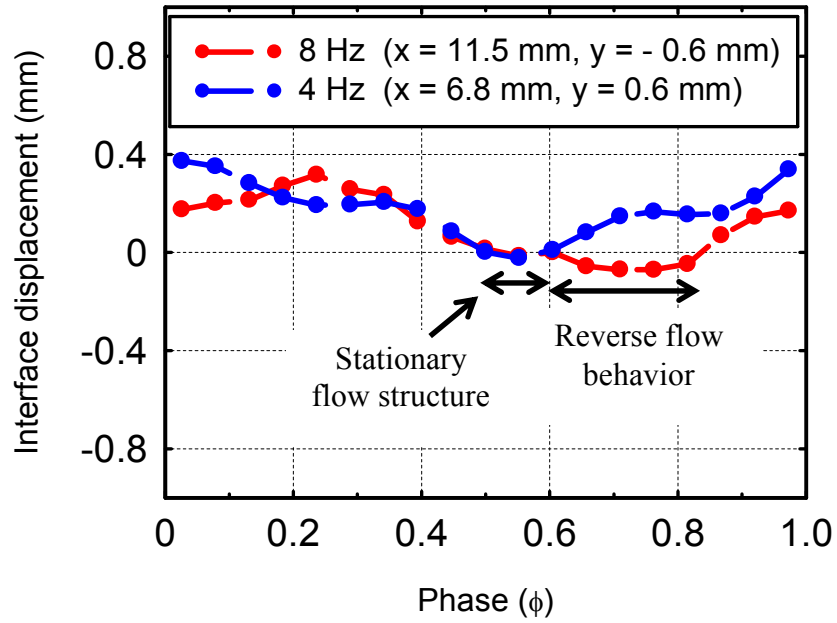

Figure 4-55(a). Phase resolved displacement of mixed fluid structure of forced flow at midspan corresponding to forcing amplitude A_3 = 60 μm and forcing frequency 4 and 8 Hz.

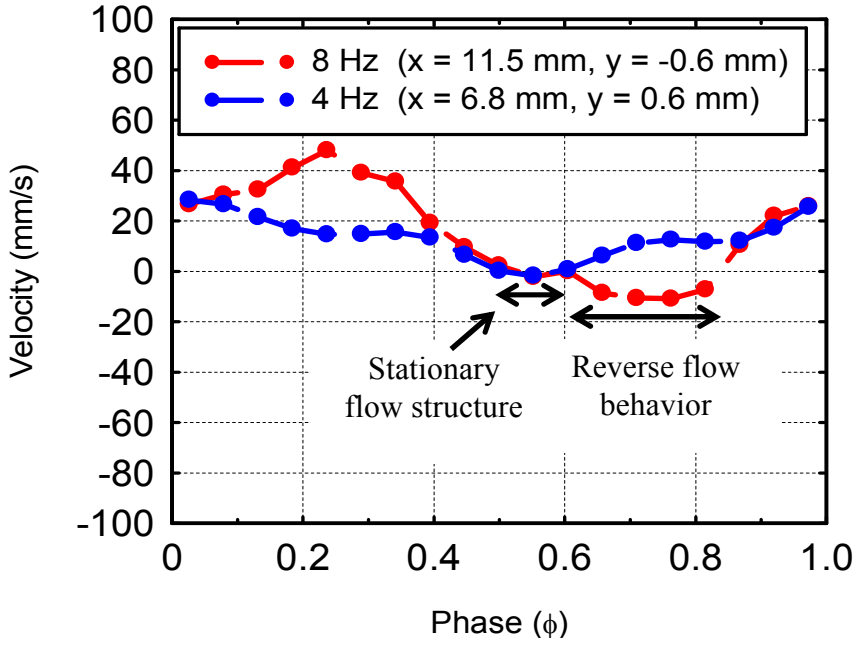

Figure 4-55(b). Phase resolved velocity of mixed fluid structure of forced flow at midspan corresponding to forcing amplitude A_3 = 60 μm and forcing frequency 4 and 8 Hz.

of the time period corresponding to 4 and 8 Hz forcing frequencies. In addition to stationary flow behavior, 8 Hz forced flow also exhibits the reverse flow behavior for 21 % of the time period i.e. 26 ms.

Similar analysis was also performed for lower forcing amplitude $A_2 = 40$ μm. Figure 4-56 (a, b) depicts the phase resolved displacement and velocity of the mixed fluid structure for one complete forcing cycle corresponding to 4 and 8 Hz forcing case and forcing amplitude $A_2 = 40$ μm. Due to lower forcing amplitude, 4 Hz forcing case shows stationary flow behavior for smaller amount of time period i.e. 26 ms. In case of 8 Hz forcing frequency, unlike to higher forcing amplitude, stationary flow behavior is observed for larger time period compared to reverse flow. Although a reverse flow is seen for 8 Hz forcing case, but a very small displacement is measured compared to the reverse flow displacement seen for higher forcing amplitude. Thus from figure 4-55 and 4-56 it could be observed that the stationary and the reverse flow behavior characteristics changes with forcing frequency and forcing amplitude.

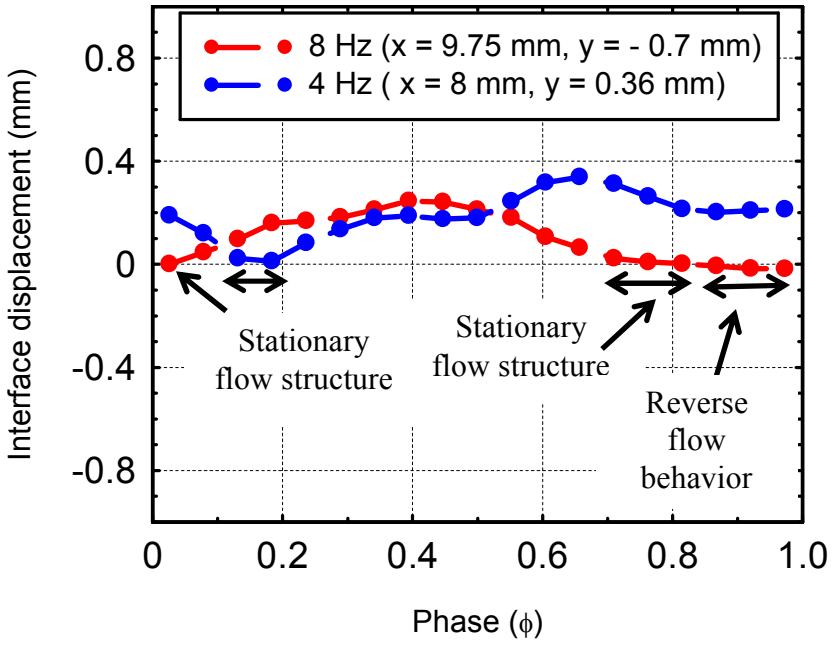

Figure 4-56(a). Phase resolved displacement of mixed fluid structure of forced flow at midspan corresponding to forcing amplitude A_2 = 40 μm and forcing frequency 4 and 8 Hz.

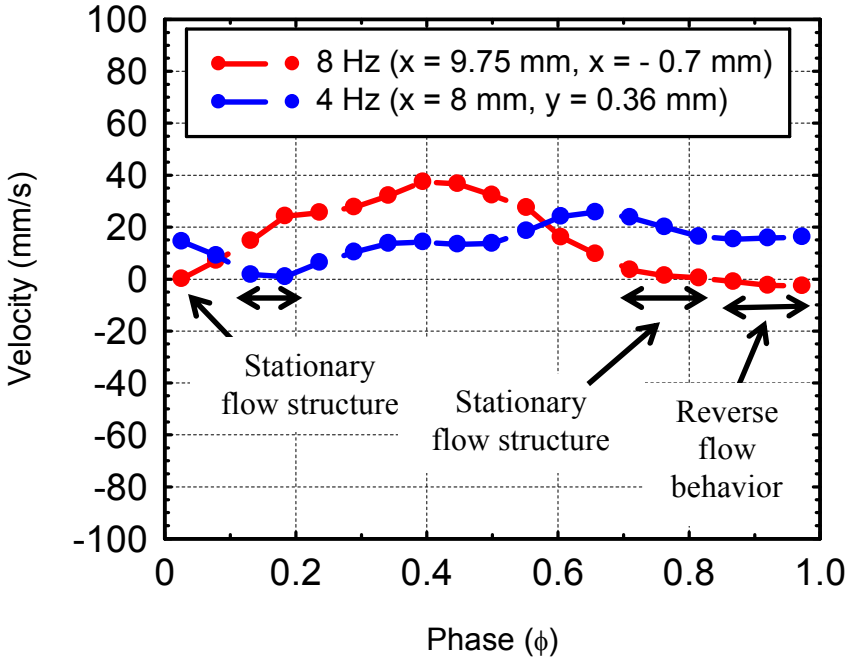

Figure 4-56(b). Phase resolved velocity of mixed fluid structure of forced flow at midspan corresponding to forcing amplitude A_2 = 40 μm and forcing frequency 4 and 8 Hz.

4.5. REVERSE FLOW CHARACTERISTICS

It was shown earlier in section 4.1.4 (see figure 4-26 to 4-29) that the higher forcing frequencies (10 to 25 Hz) exhibit very large streamwise RMS velocity corresponding to forcing amplitude A_3 = 60 μm. Such is the RMS velocity that the phase resolved streamwise velocity profiles showed the forward and the reverse flow characteristics. This means that the chemical product formed in the test section travels in reverse and forward direction (negative and positive x direction) within one forcing cycle. Thus it is possible that the chemical product travels even upstream of the splitter plate tip. This could be easily verified by imaging the chemical product in the upstream of the splitter plate. But due to limited optical access to the upstream of test section, a different approach was used to verify the presence of chemical product in the upstream of the splitter plate tip. An experiment was performed wherein during the data acquisition time, the forced flow (F = 12 hz, A_3 = 60 μm) was transitioned to unforced flow condition i.e. the forcing mechanism was stopped during the data acquisition. The recorded images during the data acquisition time monitored the time required by the forced flow concentration field to revert back to the unforced flow concentration field.

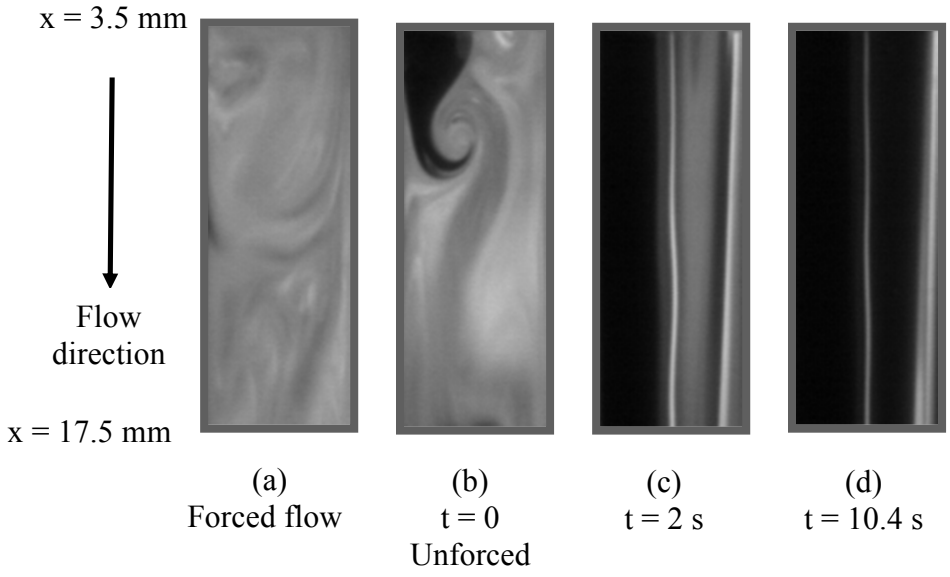

Figure 4-57. Streamwise chemically reacting LIF image sequence at midspan showing the transition of forced flow (F = 12 Hz and A_3 = 60 μm) to unforced flow condition.

Figure 4-57 highlights the LIF streamwise time series images which depicts the transition of the forced flow (F= 12 Hz and A_3 = 60 μm) to unforced flow condition. Note that the chemical product concentration field shown in figure 4-57 has arbitrary units since the concentration field is not normalized by the concentration field corresponding to stoichiometric ratio ξ_s.

Figure 4-57(a) shows the highly mixed forced flow corresponding to forcing frequency F = 12 Hz and forcing amplitude A_3 = 60 μm at the midspan. The chemical product at the time instant when the forcing mechanism is stopped is highlighted by figure 4-57 (b). This LIF image will be referred as t = 0 since it marks the beginning of the transition of the forced flow to unforced flow. The subsequent LIF images at t = 2 s and t = 10.4 sec from the beginning of transition event is shown by figure 4-57(c) and 4-

57(d). It could be observed from figure 4-57(c) that, although the forcing mechanism has been stopped, a large amount of chemical product is still found entering the test section from the flow stream which was forced. The inflow of chemical product in the test section after 2 seconds from stopping the forcing condition indicates the presence of the chemical product in the upstream of the channel. The occurrence of chemical product in the upstream of channel is due to the reverse flow behavior of the forced flow wherein chemical product travels upstream of the channel and once the forcing mechanism had stopped, it travels in the forward direction i.e. downstream of channel. At t = 10.4 sec (see figure 4-57(d)), if we neglect the near wall chemical product, almost zero product is seen on the forced flow stream and the concentration field appears similar to the unforced flow concentration field. Considering the time as t = 10.4 sec for the flow to revert back to unforced flow concentration field and the maximum streamwise velocity as U = 5.5 mm/s in the contraction chamber, the approximate upstream distance travelled by the chemical product from the splitter plate tip is 5.4 cm. Thus, the results presented above suggests that the highly mixed fluid forced cases exhibit reverse flow to such an extent, that the chemical product is found in the far upstream location from the splitter plate tip location.

4.6. MIXING PERFORMANCE CORRESPONDING TO VARIOUS FORCING FREQUENCIES AT FIXED VELOCITY AMPLITUDE

The results discussed in sections 4.1 and 4.2 relate to two different forcing amplitudes A_3 and A_2 over a frequency range 2- 25 Hz. Thus, by utilizing the database of the forced flow results obtained from the above mentioned conditions, the normalized RMS streamwise velocity is shown in figure 4-58 for each forcing frequency. In addition to A_3 and A_2, the normalized RMS velocity is also shown for two forcing frequencies (12 and 18 Hz) corresponding to forcing amplitude A_1. From figure 4-58, it can be observed that, forcing frequencies 8, 10, 12, 15, 18 and 22 Hz have the same velocity perturbation

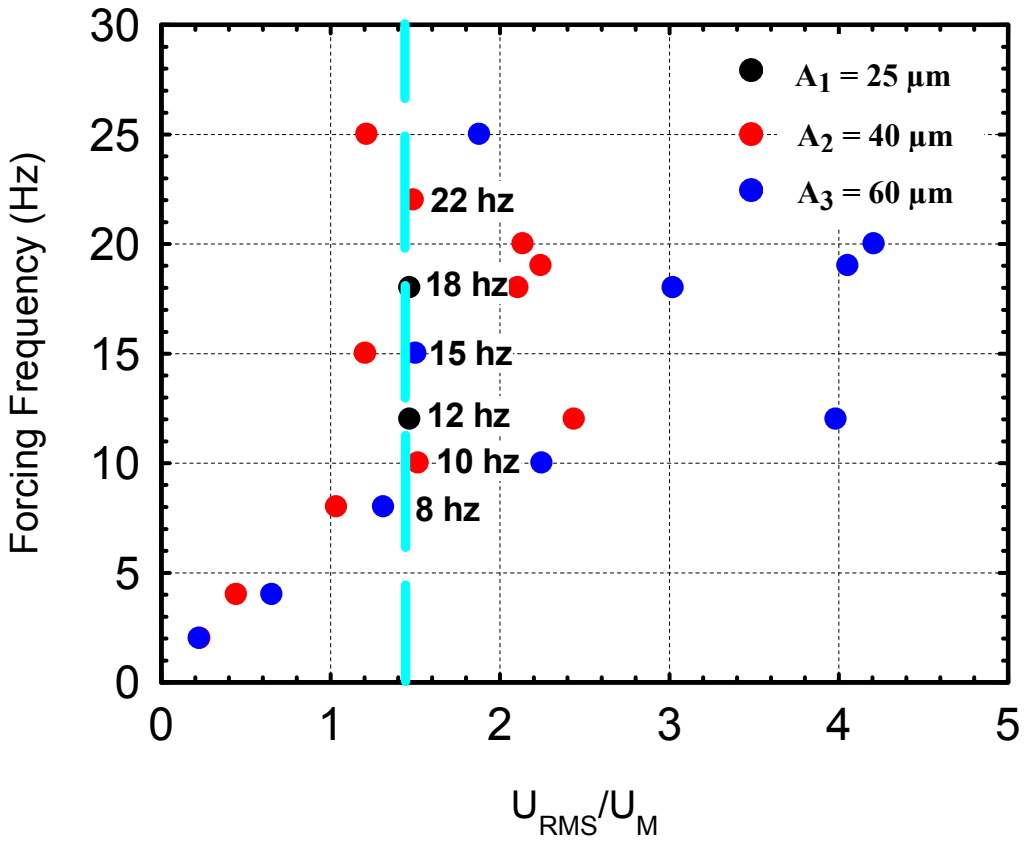

Figure 4-58. Normalized spatially averaged RMS streamwise velocity for various forcing frequencies and for a three different forcing amplitudes measured at x = 3 mm and z = 0**.**

amplitude $\frac{U_{RMS}}{U_M} = 1.45$. Thus, these forcing cases will be utilized to discuss the mixing performance of mixing layer facility at fixed velocity perturbation amplitude.

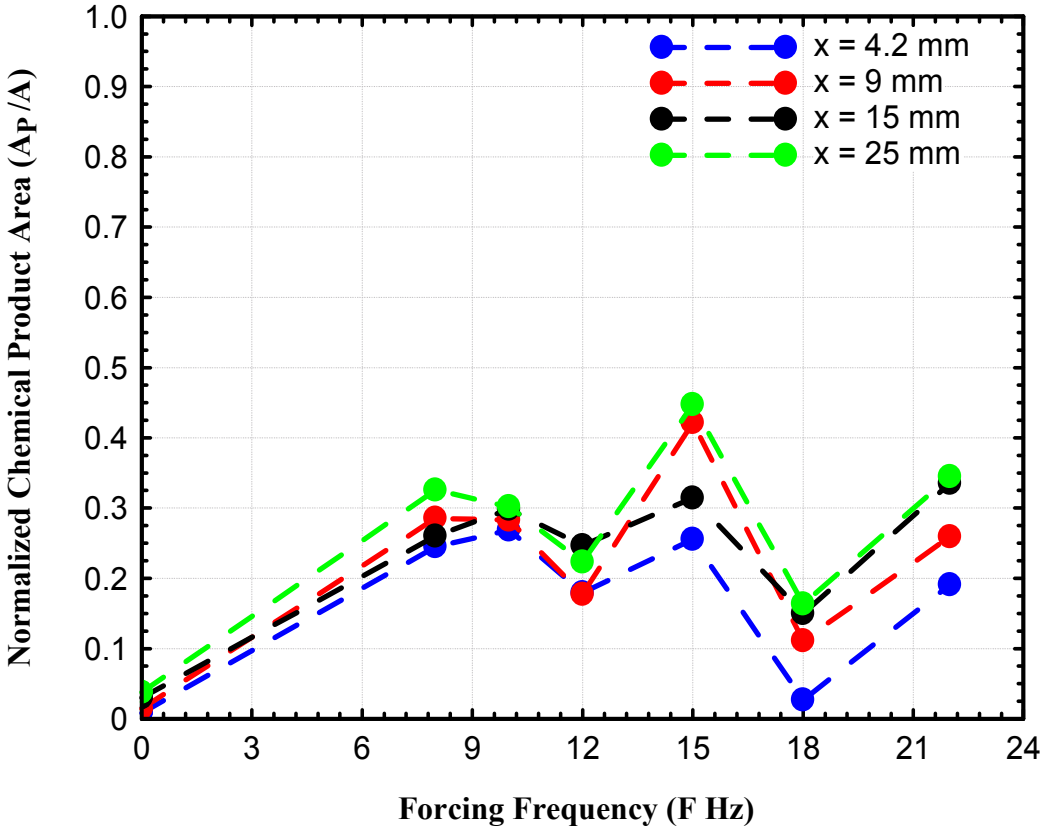

Figure 4-59. Normalized chemical product area for range of forcing frequencies measured at a fixed velocity perturbation amplitude $U_{RMS}/U_M = 1.45$ (U = 20 mm/s).

Figure 4-59 depicts the normalized chemical product area corresponding to forcing frequencies 8, 10, 12, 15, 18 and 22 Hz and fixed velocity perturbation amplitude $\frac{U_{RMS}}{U_M} = 1.45$ obtained from spanwise chemically reacting LIF measurements. For each forcing frequency the chemical product area is measured at four different streamwise locations (x = 4.2, 9, 15 and 25 mm). The instantaneous and average normalized chemical product concentration field of forcing frequencies 8, 10, 12, 15, 18 and 22 Hz is

highlighted in figures 4-8, 4-35, 4-60, 4-11, 4-61 and 4-62. Unlike figure 4-43, the change in chemical product with respect to forcing frequency for fixed velocity amplitude is shown in figure 4-59. It is observed that within the range of forcing frequency 8 to 22 Hz, the maximum chemical product is measured for 15 and 22 Hz while the lowest corresponds to 12 and18 Hz. In general, for the above mentioned forcing frequencies an inverted C-shaped mixed fluid structure of different size is observed. A larger size inverted C-shape structure is associated with the higher chemical product. Thus, as a result 15 Hz and 22 Hz cases show increased amount of chemical product compared to any other forcing frequency. One common feature among all of the forcing frequencies is the presence of unmixed fluid region. At $U_{RMS}/U_M = 1.45$ all of the forcing frequencies show the occurrence of unmixed fluid. The unmixed fluid region is apparent in the average normalized concentration fields highlighted in figure 4-8, 4-35, 4-60, 4-11, 4-61 and 4-62. Thus figure 4-58 depicts the selective behavior of mixing layer facility in enhancement of mixing with respect to forcing frequency at fixed velocity perturbation amplitude.

F = 12 Hz (Instantaneous normalized concentration field)

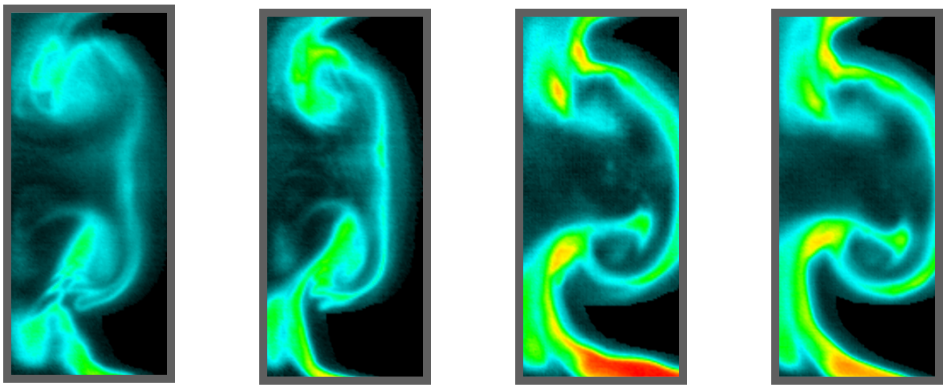

x = 4.2 mm x = 9 mm x = 15 mm x = 25 mm

F = 12 Hz (Average normalized concentration field)

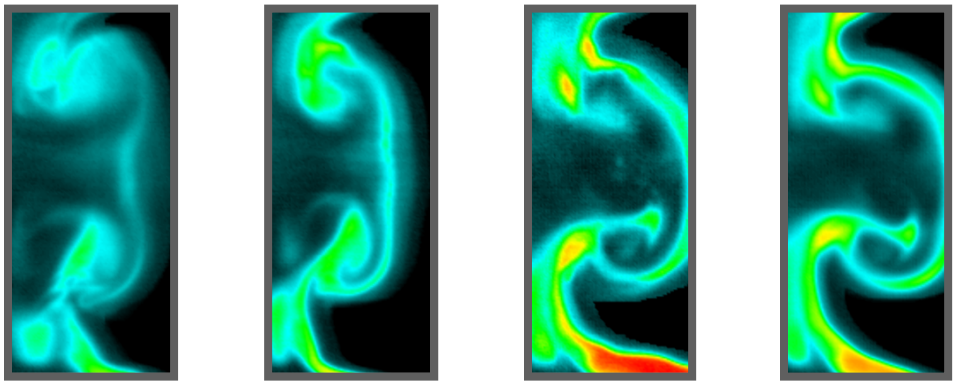

x = 4.2 mm x = 9 mm x = 15 mm x = 25 mm

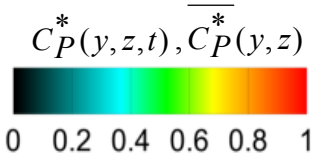

Figure 4-60. Instantaneous and average normalized chemical product concentration field at four different streamwise locations (F = 12 Hz, U = 20 mm/s and A_1 = 25 μm).

F = 18 Hz (Instantaneous normalized concentration field)

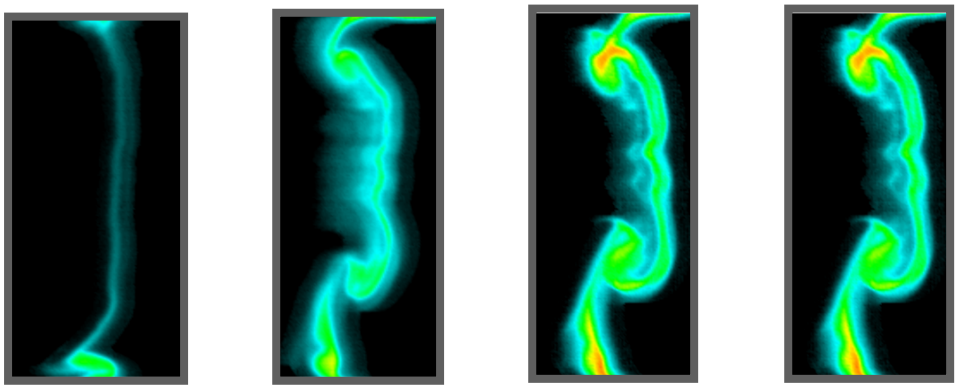

x = 4.2 mm x = 9 mm x = 15 mm x = 25 mm

F = 18 Hz (Average normalized concentration field)

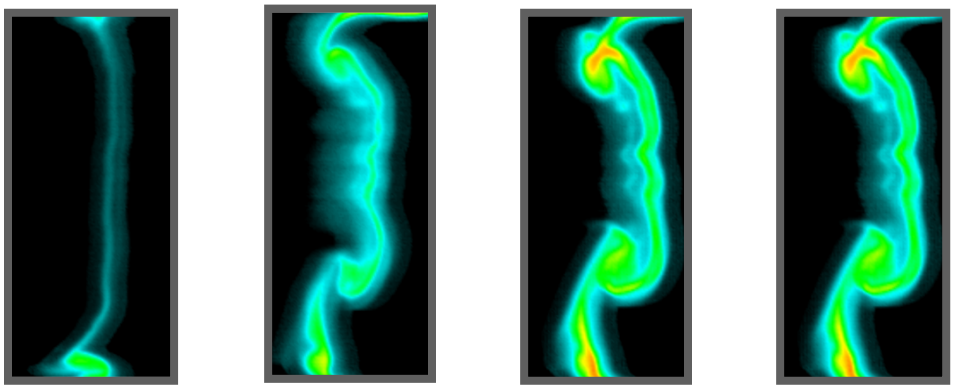

x = 4.2 mm x = 9 mm x = 15 mm x = 25 mm

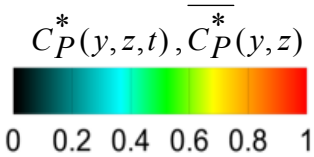

Figure 4-61. Instantaneous and average normalized chemical product concentration field at four different streamwise locations (F = 18 Hz, U = 20 mm/s and A_1 = 25 μm).

F = 22 Hz (Instantaneous normalized concentration field)

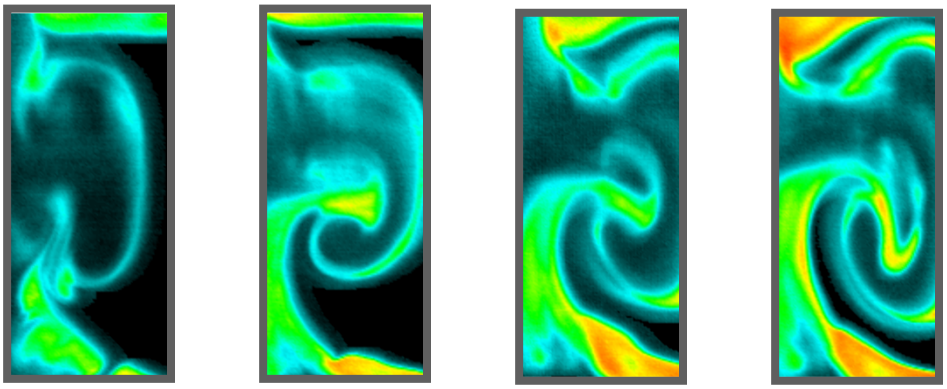

x = 4.2 mm x = 9 mm x = 15 mm x = 25 mm

F = 22 Hz (Average normalized concentration field)

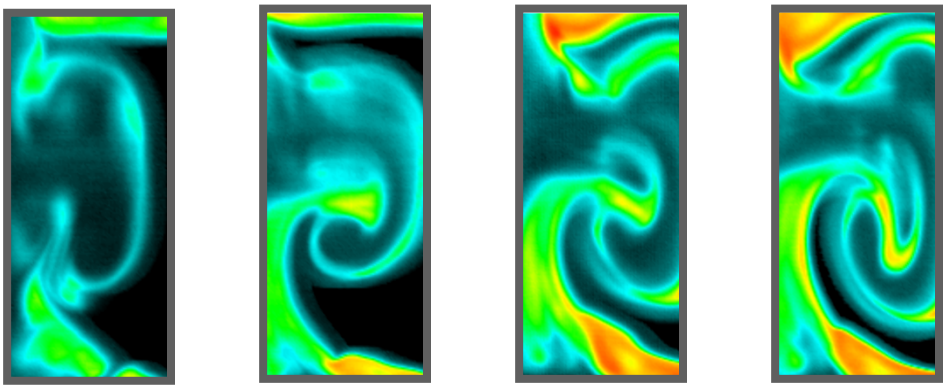

x = 4.2 mm x = 9 mm x = 15 mm x = 25 mm

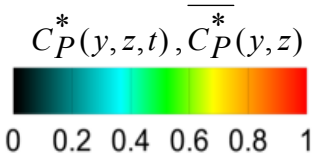

Figure 4-62. Instantaneous and average normalized chemical product concentration field at four different streamwise locations (F = 22 Hz, U = 20 mm/s and A_2 = 40 μm).

5. CONCLUSIONS

The effects of the periodic forcing in the small mixing layer facility on one of the flow streams were investigated. The mixing enhancement in the forced mixing layer facility was studied over a range of forcing frequencies (2 - 25 Hz) and forcing amplitudes A_1 = 25 μm A_2 = 40 μm and A_3 = 60 μm. The streamwise chemically reacting LIF technique was used to visualize the mixed flow structure at center span. The detail mixedness in the forced flow was quantified by performing spanwise (cross stream) chemically reacting LIF measurements at four different streamwise locations. In addition to chemically reacting LIF, non-reacting LIF (standard LIF) measurements were performed for few highly mixed fluid cases to find the composition distribution (pdf) of mixed fluid. The streamwise velocity dynamics within the forcing cycle was quantified by Molecular Tagging Velocimetry (MTV) performed at midspan. Following is the summary of the results:

1) The effect of forcing amplitude A_3 = 60 μm over the range of forcing frequencies (2-25 Hz) was such that it produces a unique interfacial mixed fluid structure for each forcing frequency. For lower forcing frequencies (2, 4 and 8 Hz) chemical product was found on the interfacial structures and it was observed to increase in the streamwise direction. Although the lower forcing frequency cases show the higher chemical product compared to an unforced flow, unmixed fluid was always found in the test section which was quantified using pdf of chemical product. Unlike the lower frequencies, a large amount of enhancement in the chemical product was observed when the flow was forced at higher frequencies (10, 12, 18,

19 and 20 Hz). Such was the dramatic increase in the chemical product that, there was no occurrence of unmixed fluid in the test section. The maximum chemical product area measured at four different streamwise locations was typically in the range 0.47 to 0.57. This defines the enhanced mixing efficiency of the mixing layer facility corresponding to the high forcing frequencies. Unlike the above mentioned high forcing frequencies, 15 and 25 Hz are other two high forcing frequencies for which a very low mixedness was measured.

To quantify the forcing amplitude in terms of velocity, MTV experiments were performed. Although the bellows amplitude was kept constant, as expected, each forcing frequency was found to have different RMS velocity at the entrance of the test section. A large RMS velocity was measured for higher forcing frequencies which also correspond to the highly mixed fluid cases. The RMS velocity for these cases was so large that a forward and a reverse flow characteristics were measured within a forcing cycle. Among the high forcing frequency cases, a lower RMS velocity was measured for 15 and 25 Hz forcing cases. This also explains the reason for these frequencies yielding lower chemical product area. The reason for selective increase of RMS velocity at the higher forcing frequencies is not known yet.

2) The effect of lower forcing amplitude on the mixedness in the small mixing layer facility was investigated by forcing the mixing layer at amplitude $A_2 = 40$ μm. At any given forcing frequency, the amount of mixing was found to be directly connected to the forcing amplitude. The measured chemical product was lower compared to the similar cases corresponding to higher forcing amplitude $A_3 = 60$

μm. Among the higher forcing frequencies (10 to 25 Hz) corresponding to A_2 = 40 μm, a lower amount of chemical product was measured for 15 and 25 Hz. The selective behavior of the mixing layer facility in terms of enhancement of mixedness at higher forcing frequencies was found to be consistent with forcing amplitudes A_2 and A_3. MTV experiments were also performed to find the forcing amplitude in terms of velocity. As expected, for any forcing frequency, a lower RMS velocity was measured compared to the similar cases of A_3 = 60 μm. As observed for forcing amplitude A_3, forward and reverse flow characteristics were also measured for forcing cases of A_2.

3) Non-reacting spanwise LIF measurements were performed for few selected forcing cases. The total pdf of the mixed fluid concentration of highly mixed cases showed asymmetric mixing characteristics such that it was biased towards the stream which was forced. It was interesting to note that although the total pdf was asymmetric, but the maximum occurrence of mixed fluid was measured for 50:50 mixed fluid compositions.
4) Stationary flow structure behavior was studied for certain forcing cases by utilizing the phase resolved streamwise LIF concentration fields. From the phase ordered sequence of concentration fields, it was found that, within the time period of one forcing cycle the flow structure appeared to be stationary for a certain fraction of the time period. As a result, an average concentration field showed a strong presence of a flow structure in addition to a smoothing effect. Here, the flow structure corresponded to the phases wherein the flow was stationary.

5) The database of forced cases obtained from forcing amplitudes A_1, A_2 and A_3 over a range of forcing frequencies 2- 25 Hz was also utilized to study the effect of varying forcing frequency and fixed forcing velocity amplitude on mixedness. It was found that mixing layer facility showed an enhancement in mixedness for only certain forcing frequencies. This shows the selective behavior of mixing layer facility in terms of enhancement in mixing with respect to forcing frequency.

6. FUTURE DEVELOPMENTS

Following are some of the improvements and the ideas to be explored in future:

1) For the highly mixed cases, a large reverse flow was noticed within the forcing cycle of perturbation. Such was the reverse flow behavior that chemical product was found to travel upstream of splitter plate. The experimental facility (mixing layer facility) has a limited optical access wherein flow cannot be imaged beyond x = 3 mm. Thus, the facility should be modified such that flow can be visualized near the splitter plate and in the contraction chamber. This will help to understand the mixing process in the upstream of the channel.
2) One of the objectives of this research was to determine the operating conditions and the characteristics of the highly mixed flow. It was found that a large amount of mixedness can be obtained for high forcing frequency and amplitude. For such highly mixed flow, although the total pdf was asymmetric, a maximum occurrence of 50:50 mixed fluid compositions was measured. From an engineering stand point, the highly mixed case might be very useful in a real microfluidic mixing device. Thus, the next logical step would be to utilize similar large forcing conditions to enhance the mixing in miniaturized devices. One such microfluidic Y-channel is shown in figure 6-1.

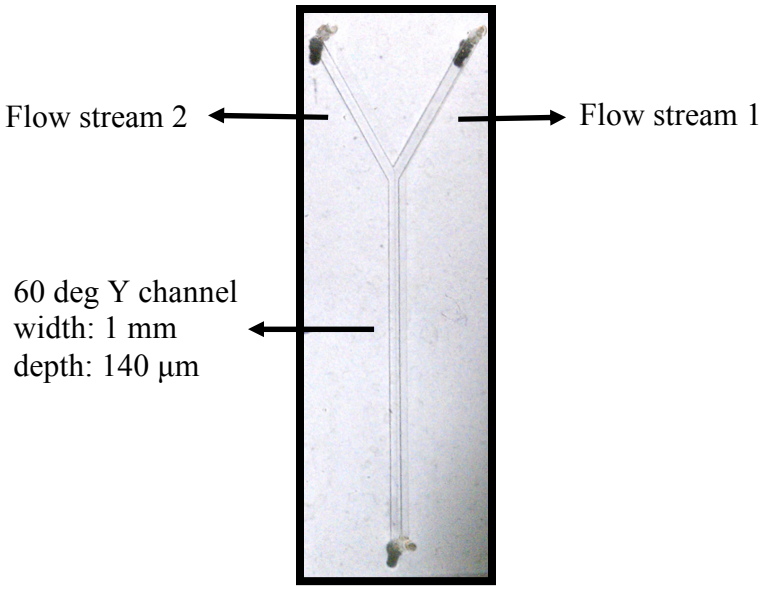

Figure 6-1. A sample microfluidic Y-channel

3) Incorporating a high forcing mechanism (high frequency and amplitude) proposed above might be very difficult in practical scenarios since microfluidic devices are known for their difficulty in fabrication. As shown in this dissertation, one could obtain appreciable amount of stretching and folding of interfacial structures even at low forcing amplitudes and frequencies. But one problem in low forced cases was that typically chemical product was seen to be 'sticking' near the wall and thus limiting its ability to mix as the flow travelled downstream of the channel. As a possible solution, it would be interesting to modulate the flow at low frequency and amplitude in a "*herringbone*" type channel. Through this method, one would not only increase the interfacial structures by forcing the flow but also allow the flow to mix more efficiently throughout its travel in the flow channel. Thus, this defines the hybrid approach wherein both active and passive mechanism would be used.

APPENDICES

APPENDIX A. DELAY TIME BETWEEN UNDELAYED AND DELAYED IMAGES USED FOR MTV EXPERIMENTS

Table A-1 depicts the delay and exposure time used for unforced as well as forced cases. An MTV measurement provides the velocity which is actually an average velocity over the delay time chosen for experiment. Thus, in general, smaller delay time was used for higher forcing frequency cases.

Consider an example wherein a velocity signal is periodically varying with a frequency of 25 Hz i.e. time period T = 40 ms. Figure A-1 and A-2 shows the filtering effect on this signal using two different time delays i.e. t_d = 2 ms and t_d = 10 ms. It can be observed from the figure that because of the larger time delay 10 ms (large time average window span) the sampled data points have noticeable deviation with respect to the original signal (blue solid line). While in case of 2 ms delay time, data points are sampled with relatively good fit with respect to the original signal. The delay time was chosen for all of the forced cases such that $t_d/T \leq 0.05$, which provided a minimum filtering effect of delay time on velocity measurement while performing MTV experiments.

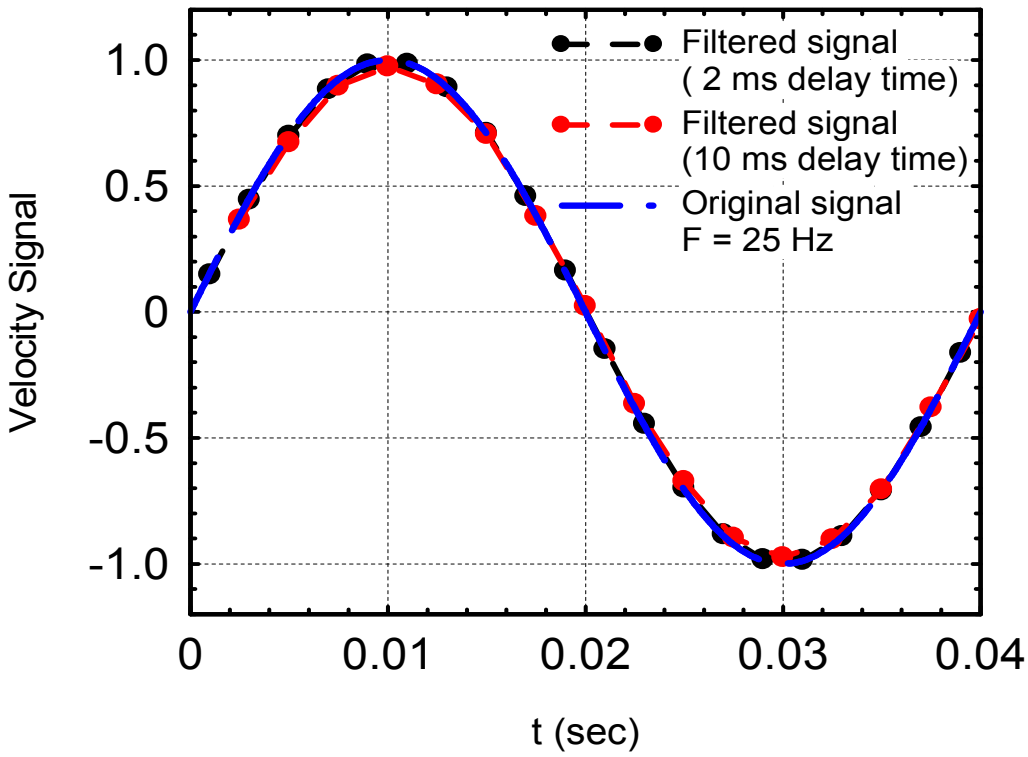

Figure A-1. Filtering effect on high frequency periodic signal

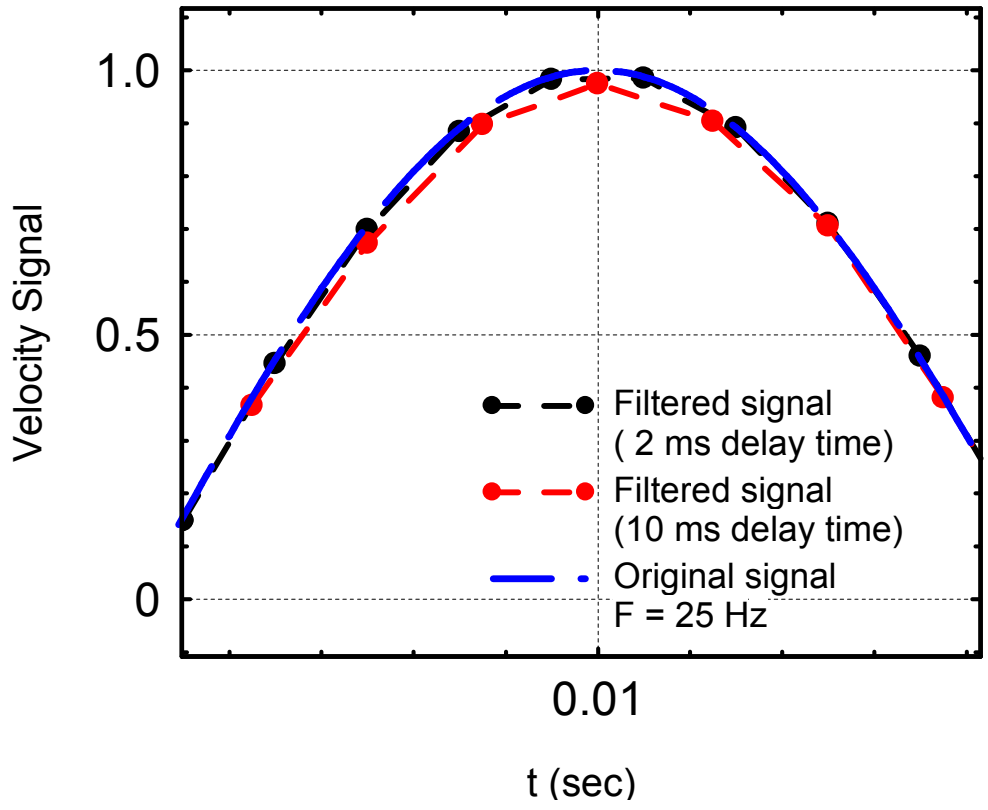

Figure A-2. Close-up view of filtering effect on high frequency periodic signal

Table A-1. Delay and Exposure time used for MTV experiments (U = 20 mm/s)

Frequency (Hz)	Amplitude	Delay (ms)	Exposure Undelayed (ms)	Exposure Delayed (ms)
Unforced	-	10	1	1
2	40 μm	10	0.1	0.4
	60 μm	10	0.1	0.6
4	40 μm	9	0.1	0.6
	60 μm	10	0.1	0.6
8	40 μm	7	0.1	0.3
	60 μm	4	0.1	0.3
10	40 μm	2.4	0.1	0.1
	60 μm	1.6	0.1	0.1
12	25 μm	2.5	0.1	0.1
	40 μm	1.5	0.1	0.1
	60 μm	1.2	0.1	0.1
15	40 μm	2.8	0.1	0.1
	60 μm	1.2	0.1	0.1
18	25 μm	2.5	0.1	0.1
	40 μm	1.5	0.1	0.1
	60 μm	1.0	0.1	0.1
19	40 μm	1.5	0.1	0.08
	60 μm	1	0.1	0.08

Table A-1 (cont'd)

20	40 µm 60 µm	1.2 1	0.1 0.1	0.08 0.08
22	40 µm	1	0.1	0.08
25	40 µm 60 µm	1.7 1.7	0.1 0.1	0.08 0.08

APPENDIX B. ESTIMATE OF PHOTOBLEACHING EFFECT

The model relating the number of active molecules (n) and the initial total number of dye molecules (n_0) after being exposed to light for a time (t) is given by (See Koochesfahani (1984), and the references therein)

$$n = n_0 \exp(-t/\tau_b) \tag{B-1}$$

The bleaching time constant τ_b is given as

$$\tau_b^{-1} = Q_b \phi_p \sigma \tag{B-2}$$

Where

Q_b - bleaching quantum efficiency (probability that a dye molecule will be bleached with the absorption of a single photon)

ϕ_p - laser photon flux

σ - dye absorption cross section

For the experiments described in this dissertation, bleaching time constant is 32 sec. This means that only 37% of molecules will be absorbing after 32 sec. The bleaching time constant is calculated based on $Q_b = 4 \times 10^{-6}$, $\phi_p = 3.67 \times 10^{19}$ photons/cm^2/sec, corresponding to 15 watts/ cm^2 power density at 488 nm and $\sigma = 2.14 \times 10^{-16}$ cm^2 (calculated from attenuation of 2×10^{-7} M).

APPENDIX C. CHEMICAL PRODUCT HISTOGRAM
(U = 20 mm/s, A_3 = 60 μm, F = 2 - 25 Hz, SPANWISE IMAGING)

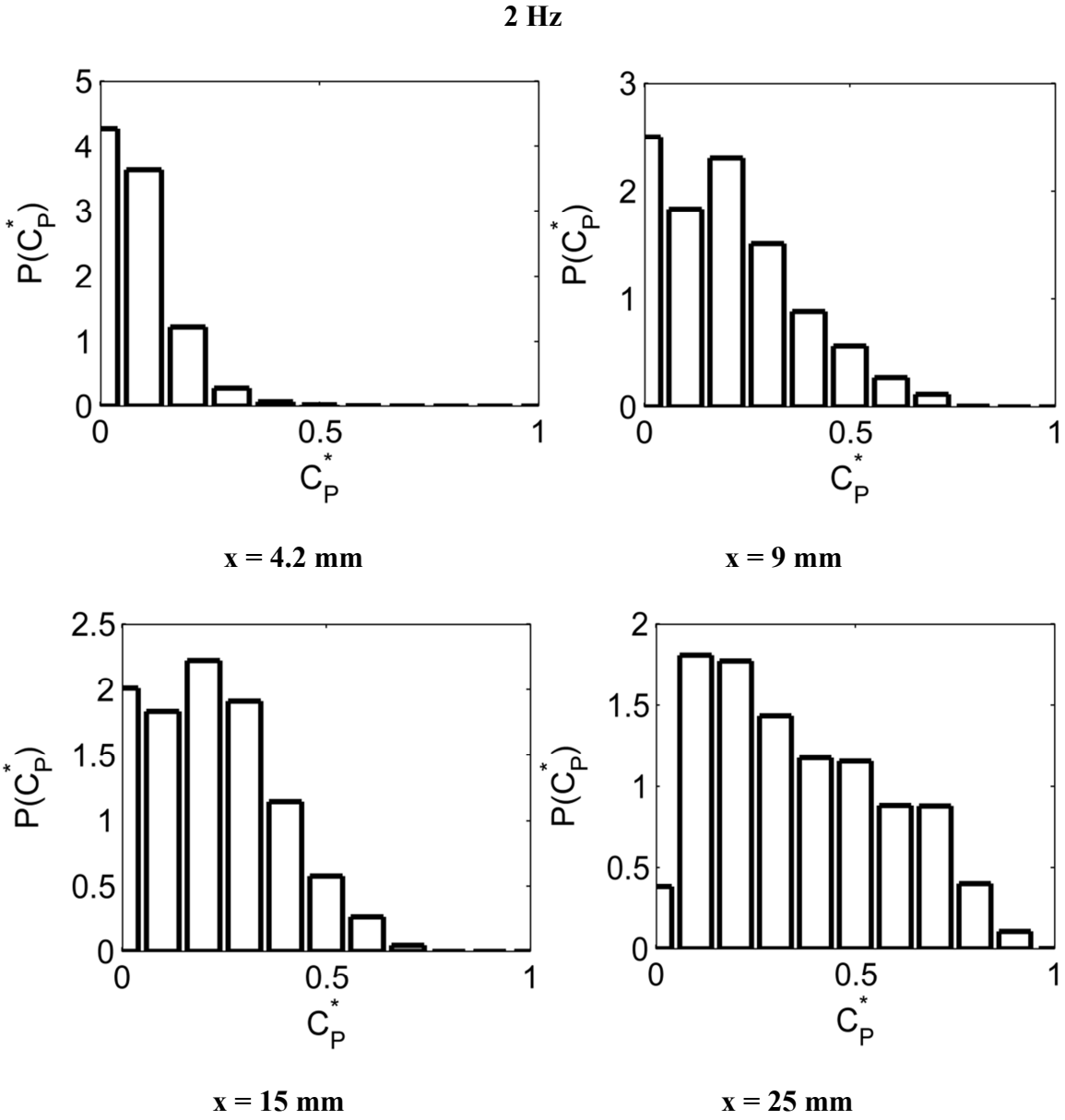

Figure C-1. Pdf of chemical product at four different streamwise locations (F = 2 Hz, U = 20 mm/s and A_3 = 60 μm).

4 Hz

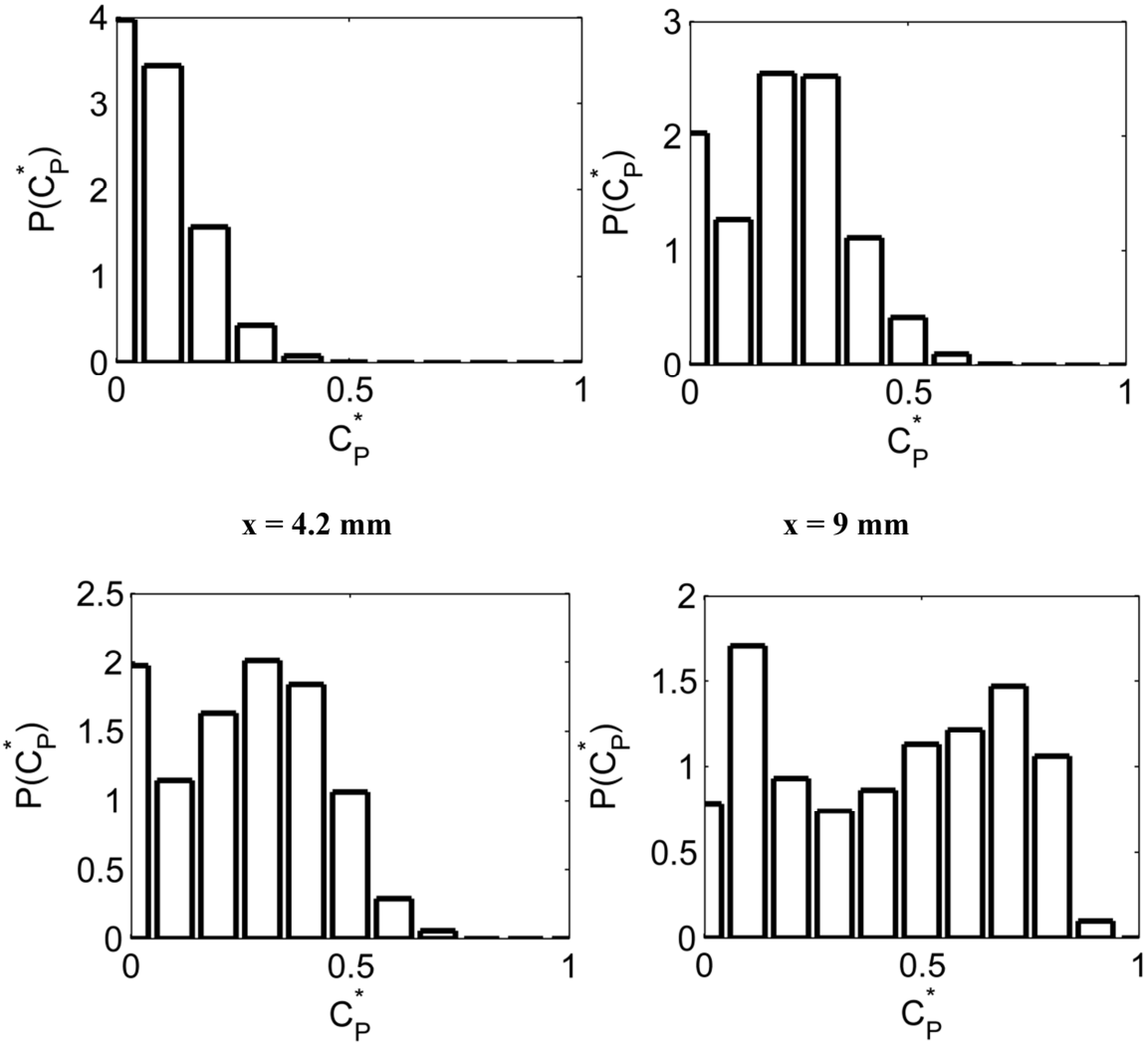

Figure C-2. Pdf of chemical product at four different streamwise locations (F = 4 Hz, U = 20 mm/s and A_3 = 60 μm).

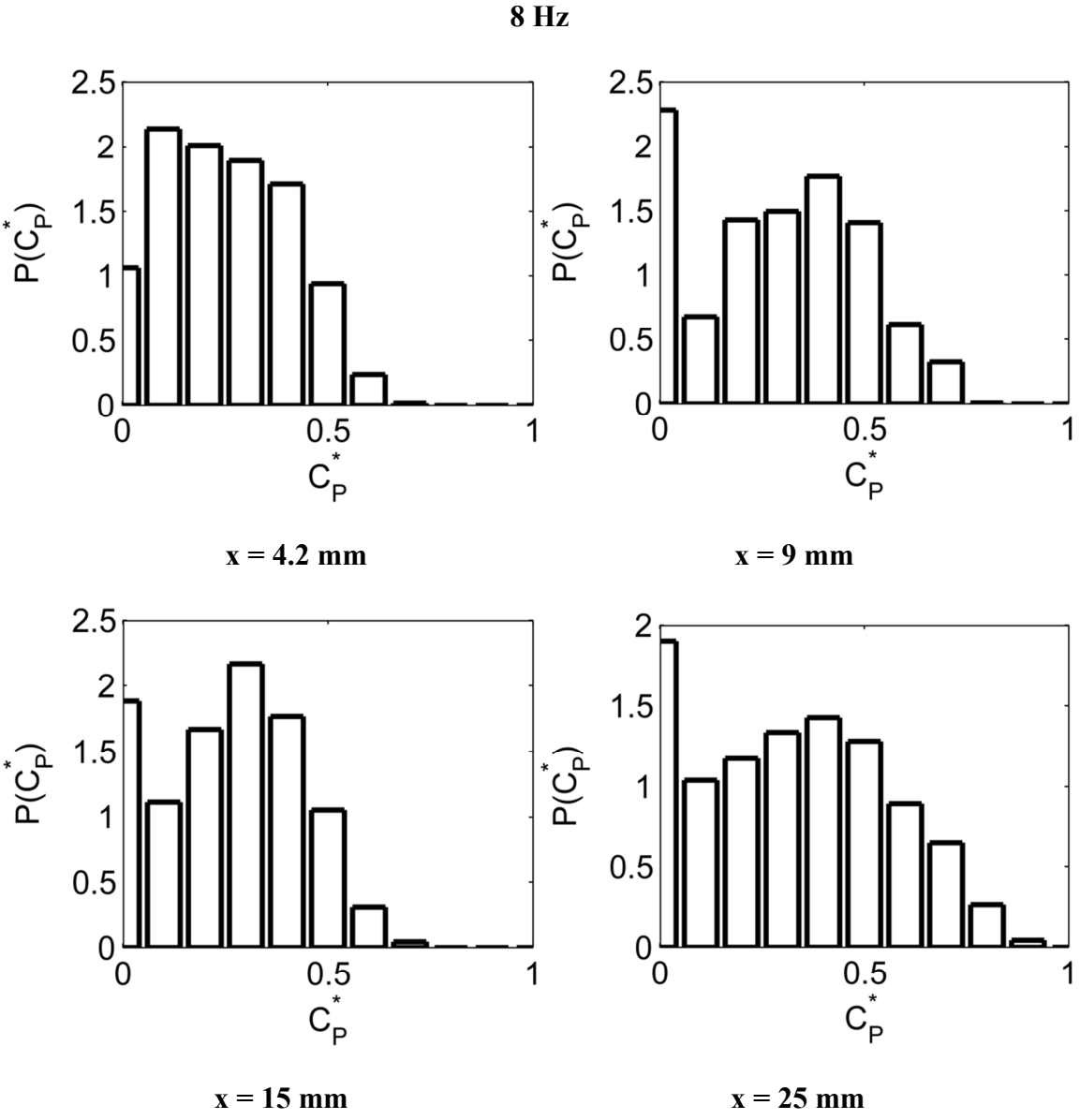

Figure C-3. Pdf of chemical product at four different streamwise locations (F = 8 Hz, U = 20 mm/s and A_3 = 60 μm).

10 Hz

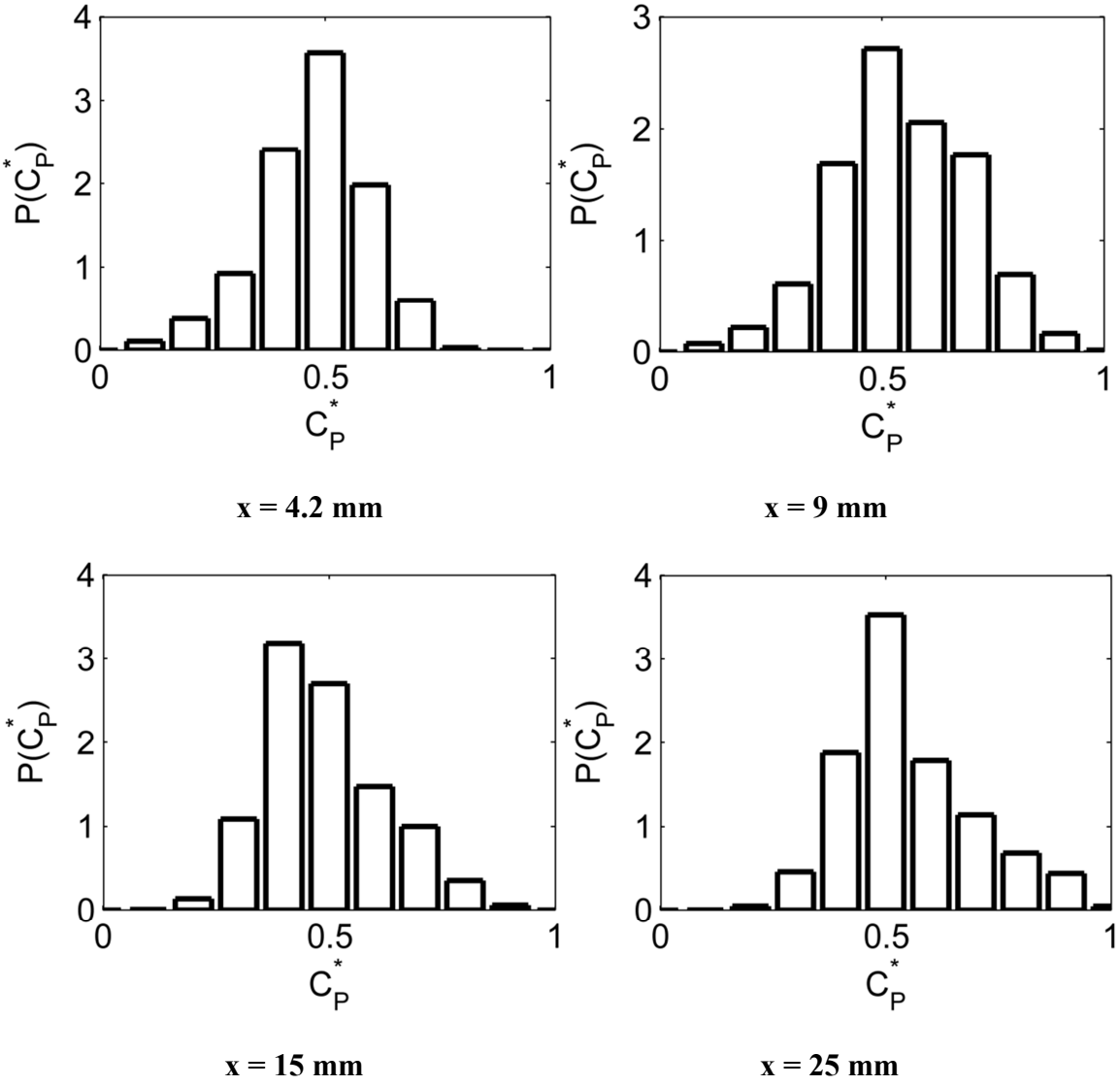

Figure C-4. Pdf of chemical product at four different streamwise locations (F = 10 Hz, U = 20 mm/s and A_3 = 60 μm).

12 Hz

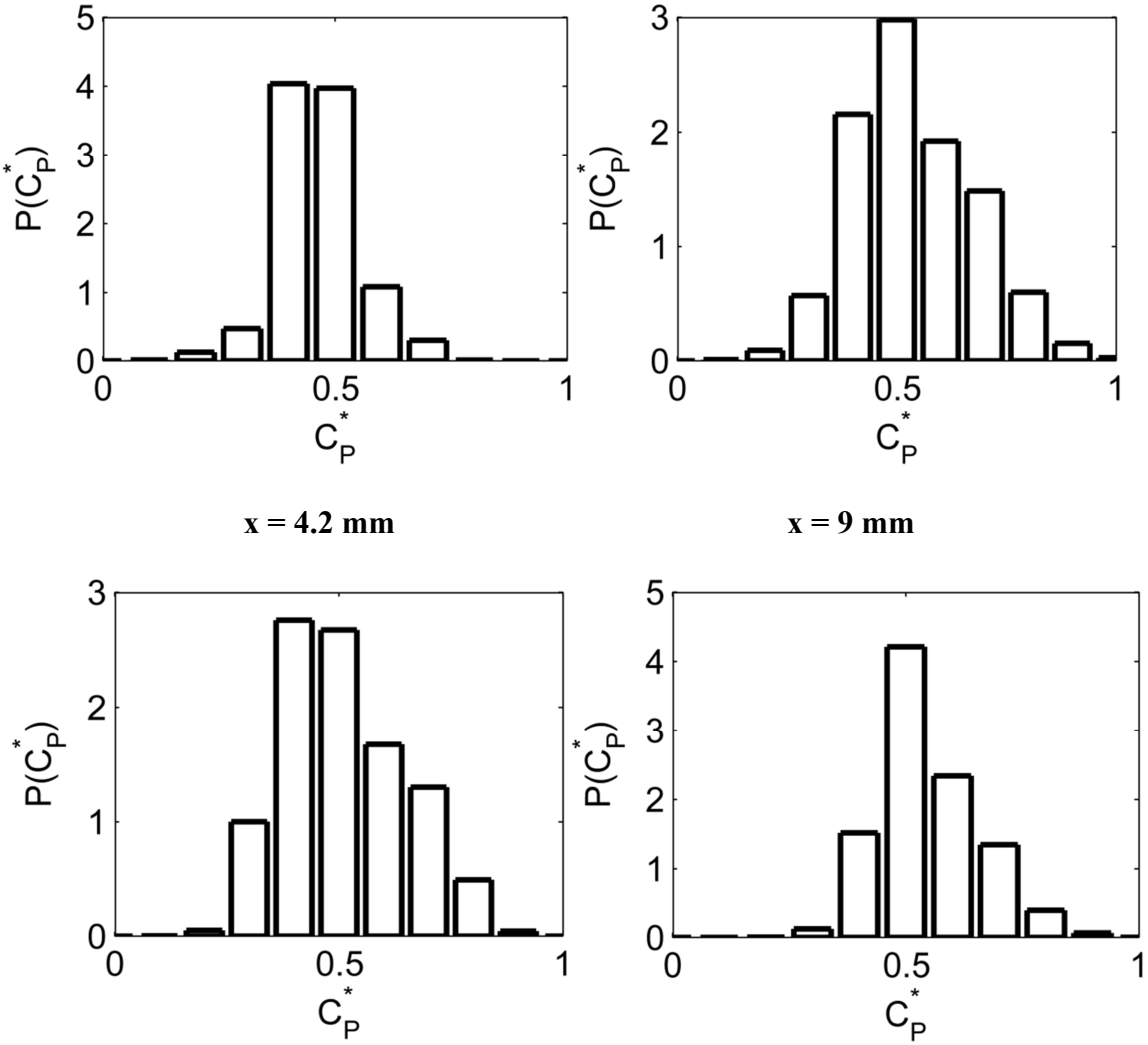

Figure C-5. Pdf of chemical product at four different streamwise locations (F = 12 Hz, U = 20 mm/s and A_3 = 60 μm).

15 Hz

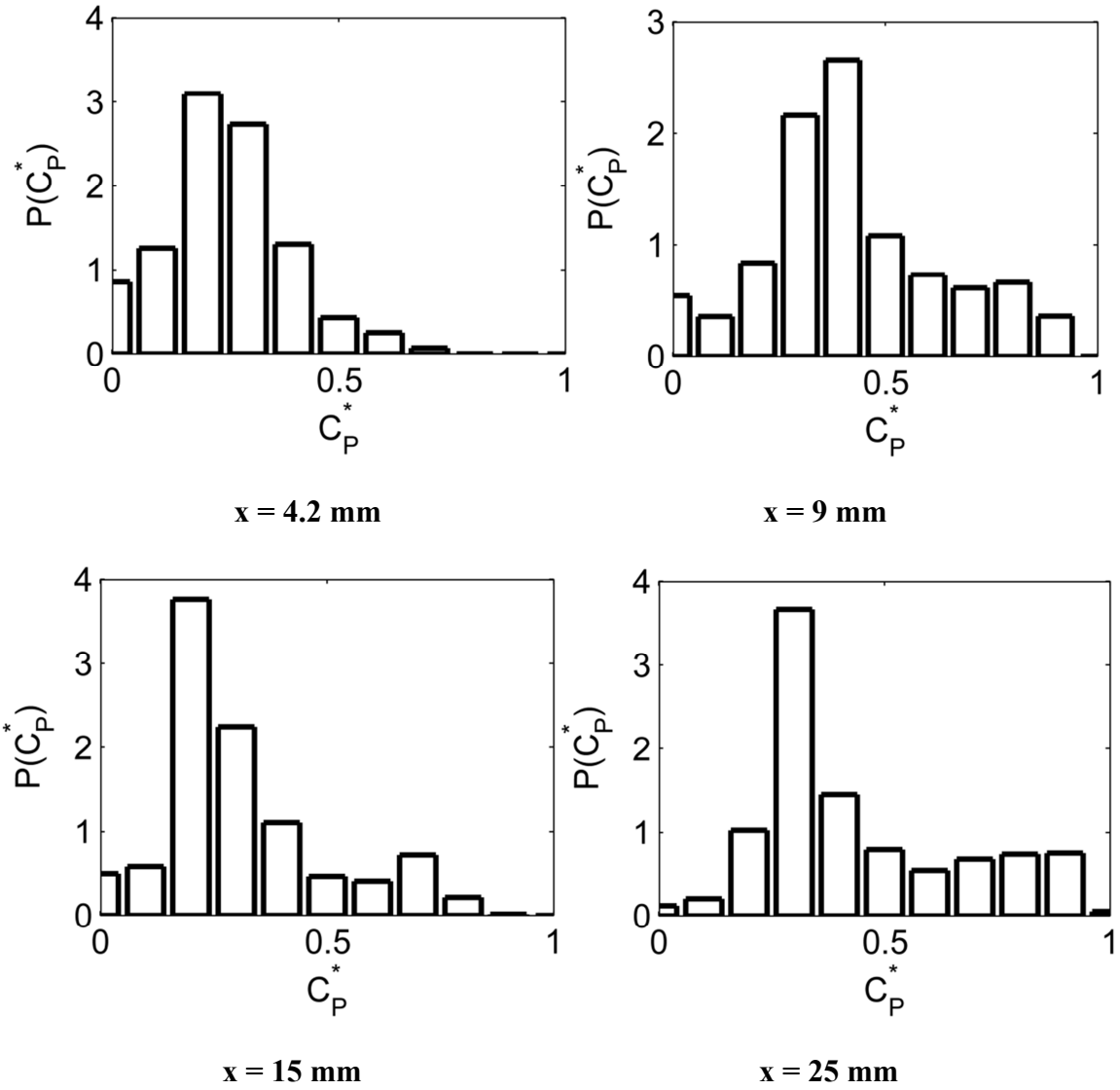

x = 4.2 mm **x = 9 mm**

x = 15 mm **x = 25 mm**

Figure C-6. Pdf of chemical product at four different streamwise locations (F = 15 Hz, U = 20 mm/s and A_3 = 60 μm).

18 Hz

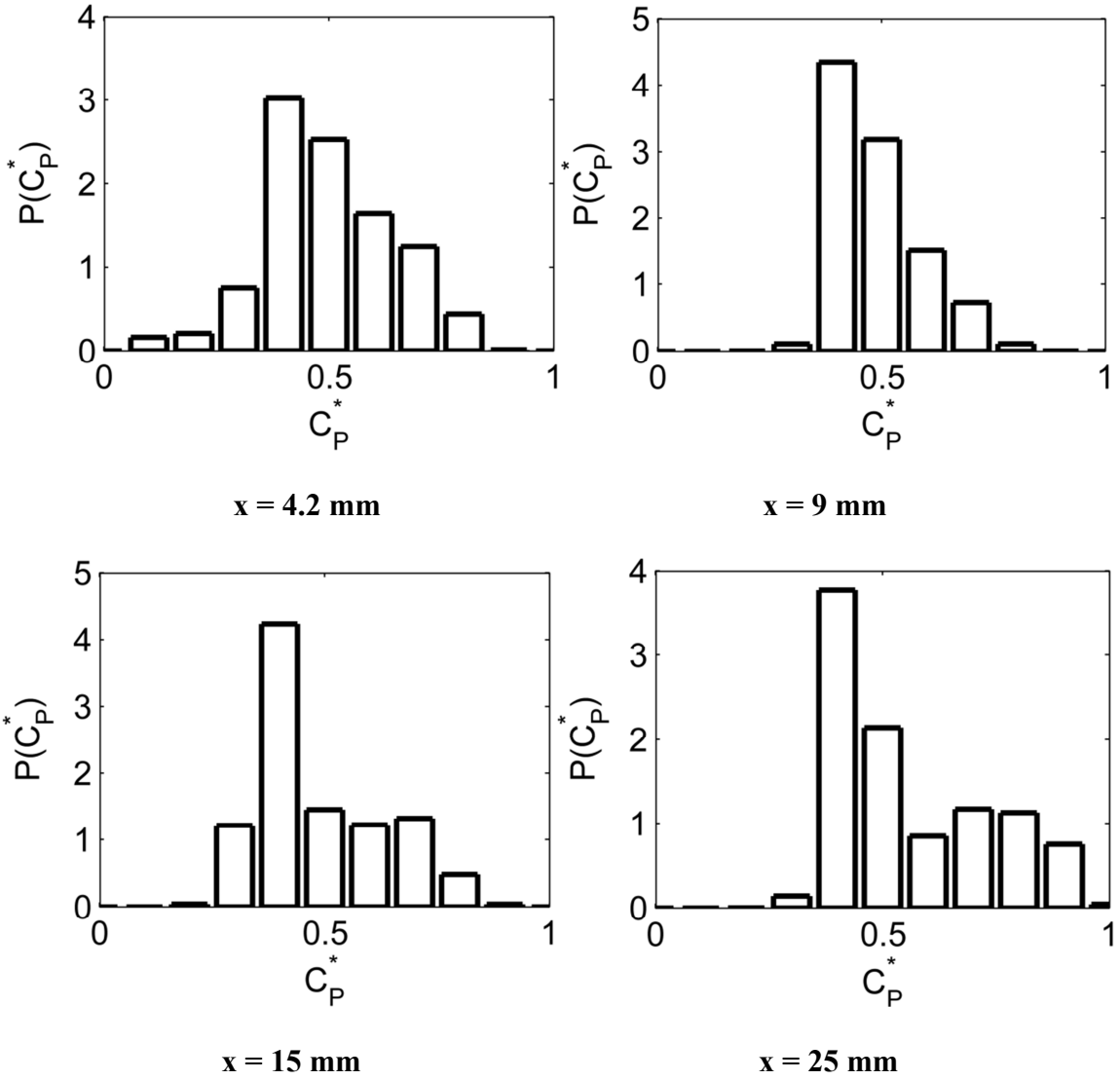

Figure C-7. Pdf of chemical product at four different streamwise locations (F = 18 Hz, U = 20 mm/s and A_3 = 60 μm).

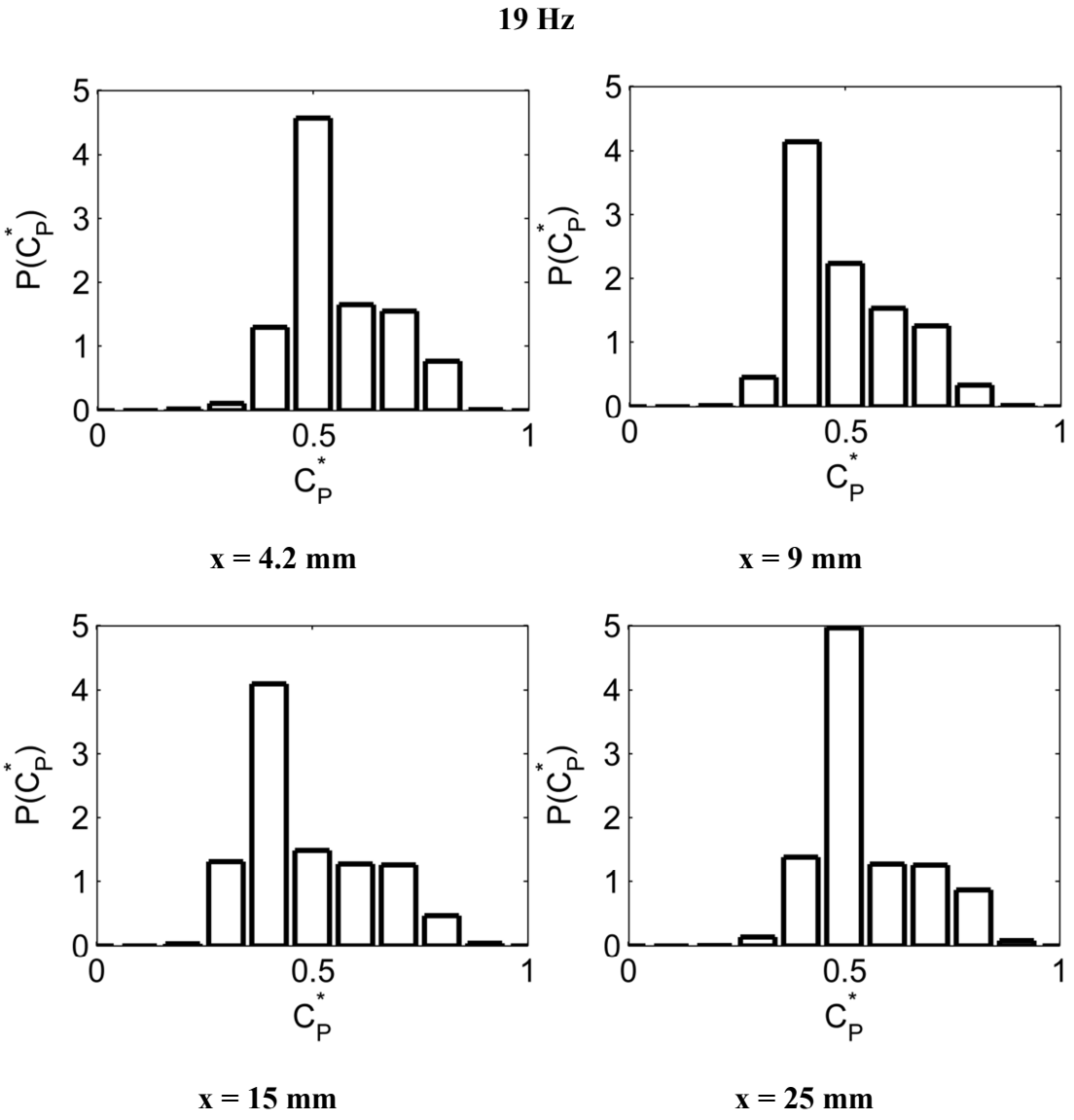

Figure C-8. Pdf of chemical product at four different streamwise locations (F = 19 Hz, U = 20 mm/s and A_3 = 60 μm).

20 Hz

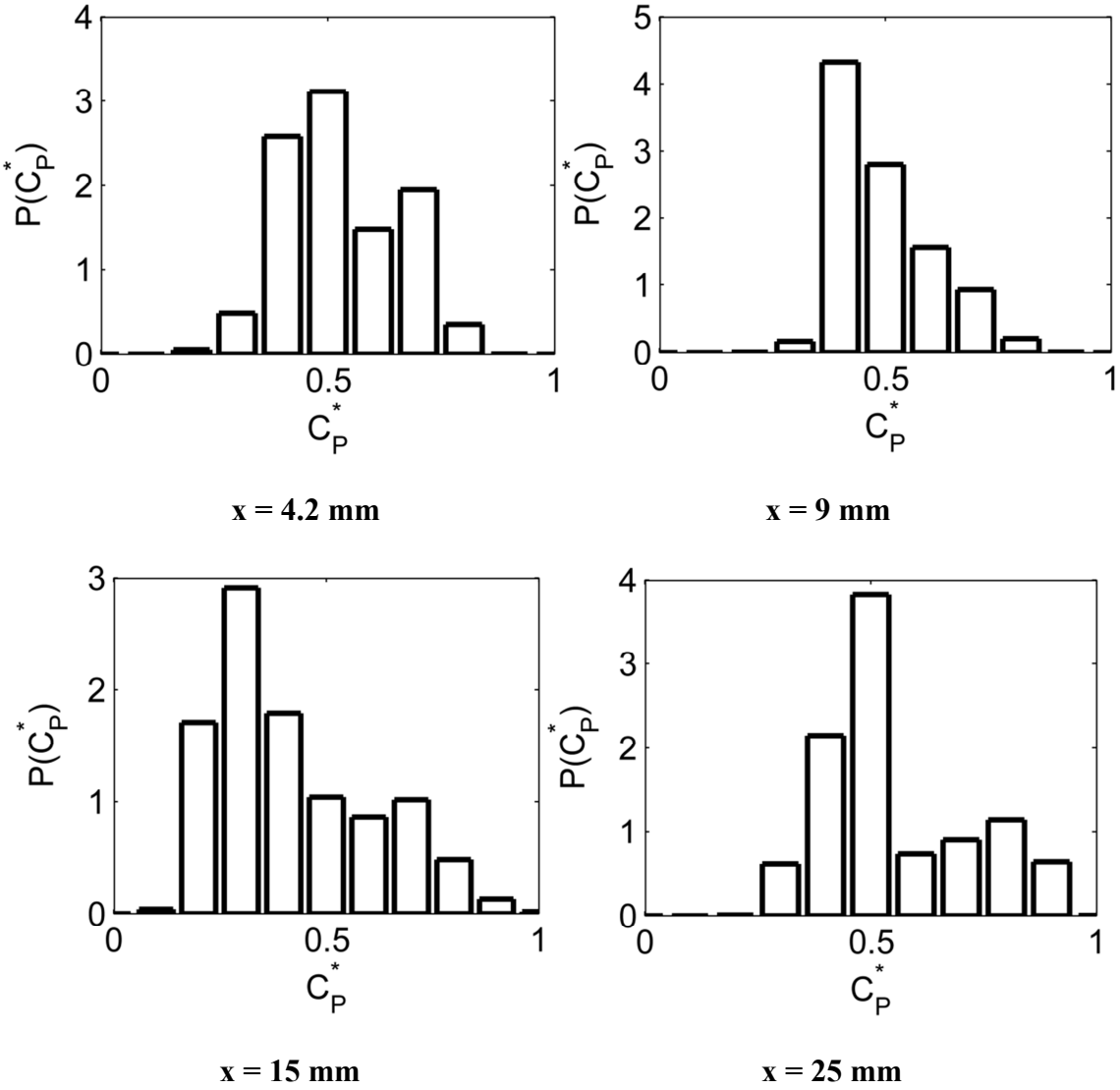

Figure C-9. Pdf of chemical product at four different streamwise locations (F = 20 Hz, U = 20 mm/s and A_3 = 60 μm).

25 Hz

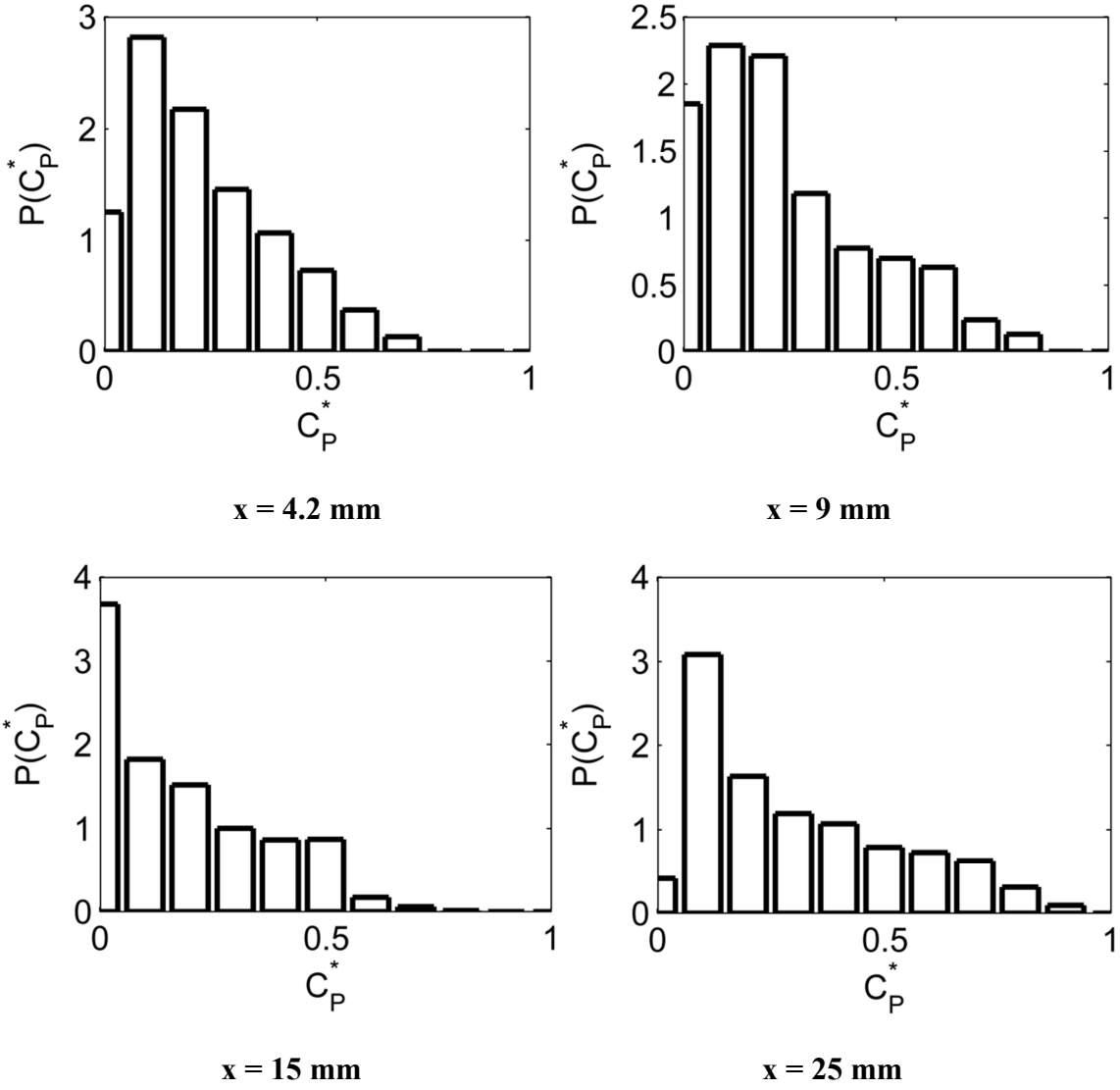

Figure C-10. Pdf of chemical product at four different streamwise locations (F = 25 Hz, U = 20 mm/s and A_3 = 60 μm).

APPENDIX D. CHEMICAL PRODUCT HISTOGRAM
(U = 20 mm/s, A_2 = 40 μm, F = 2 - 25 Hz, SPANWISE IMAGING)

2 Hz

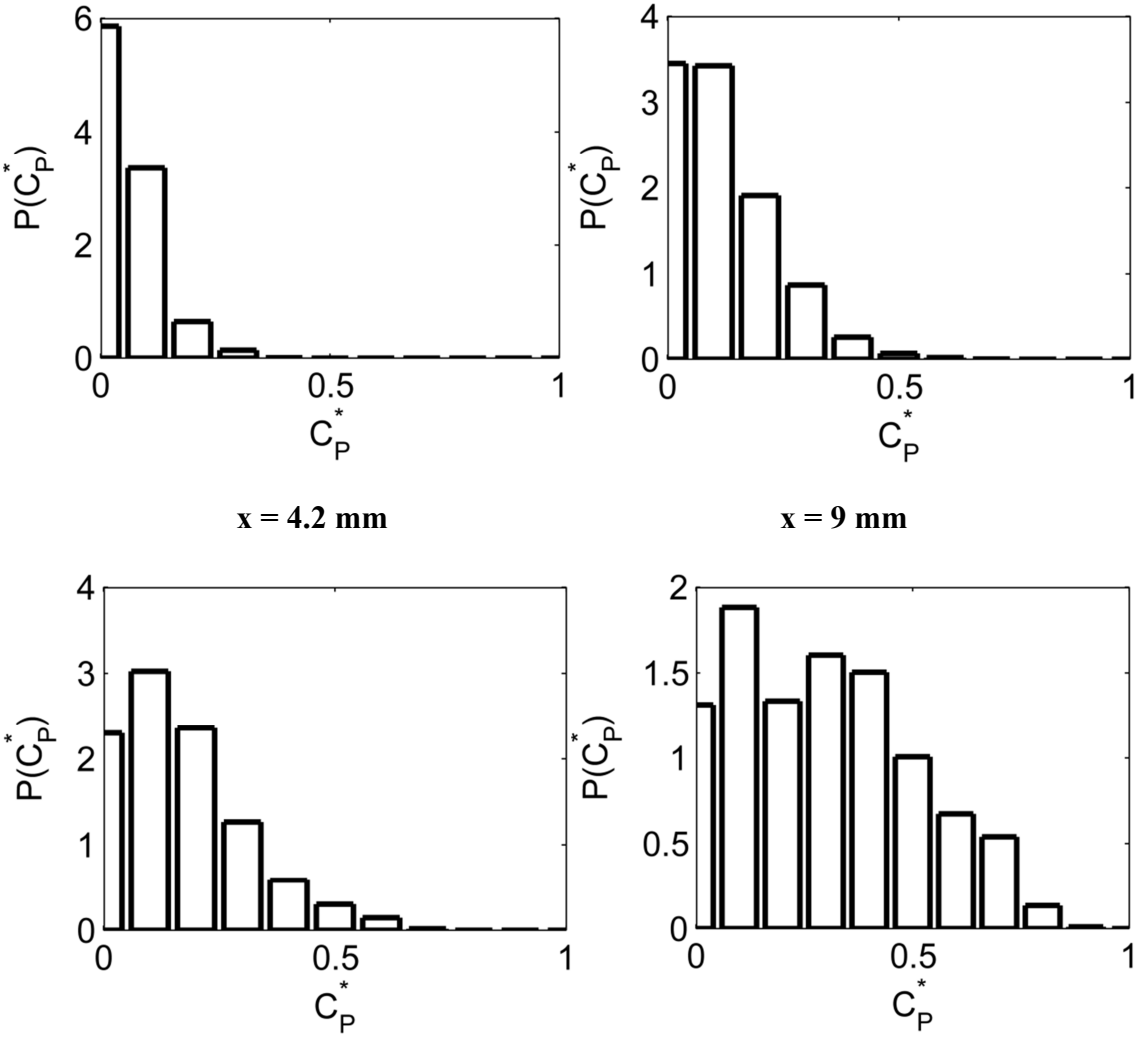

Figure D-1. Pdf of chemical product at four different streamwise locations (F = 2 Hz, U = 20 mm/s and A_2 = 40 μm).

4 Hz

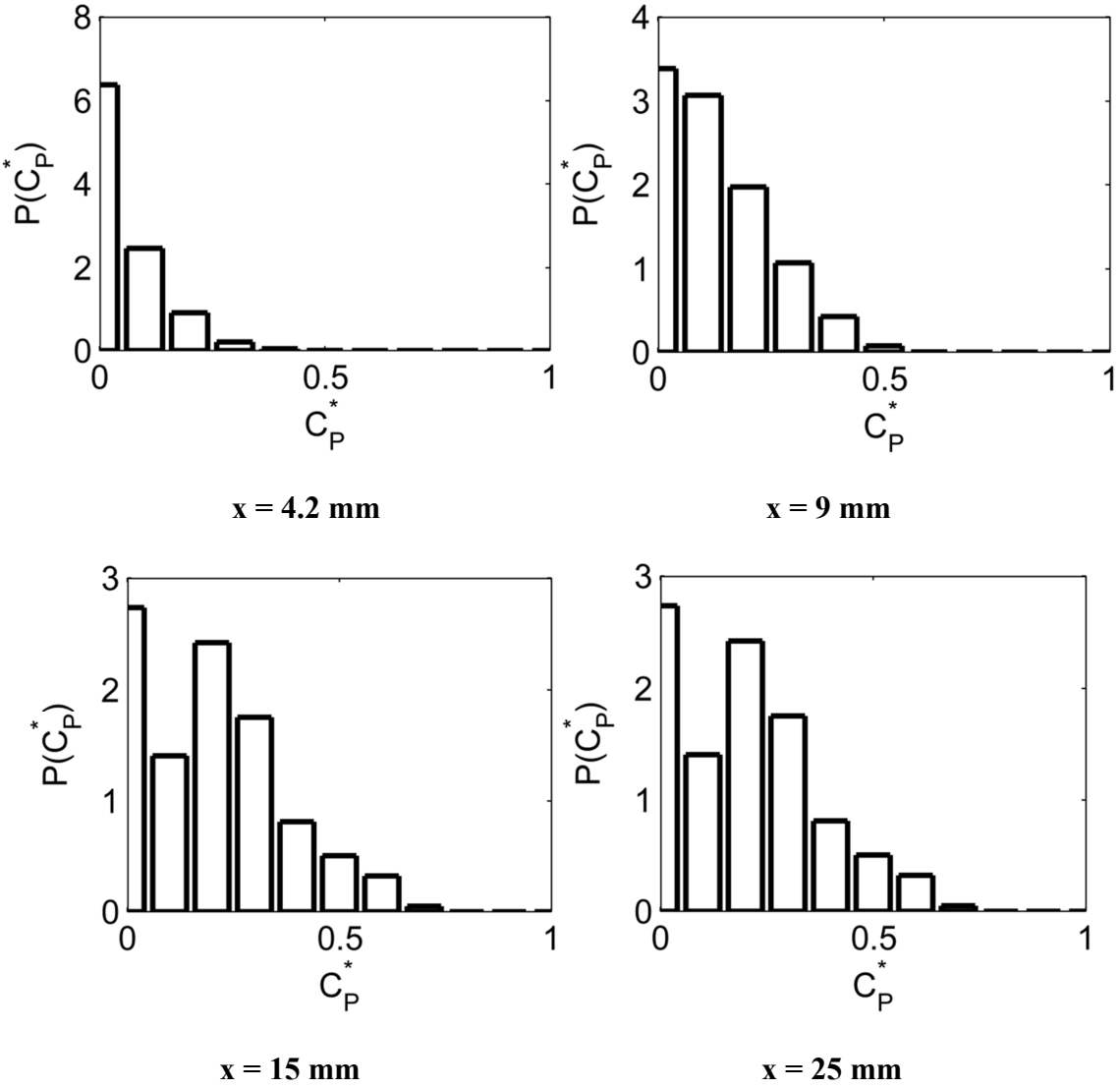

Figure D-2. Pdf of chemical product at four different streamwise locations (F = 4 Hz, U = 20 mm/s and A_2 = 40 μm).

8 Hz

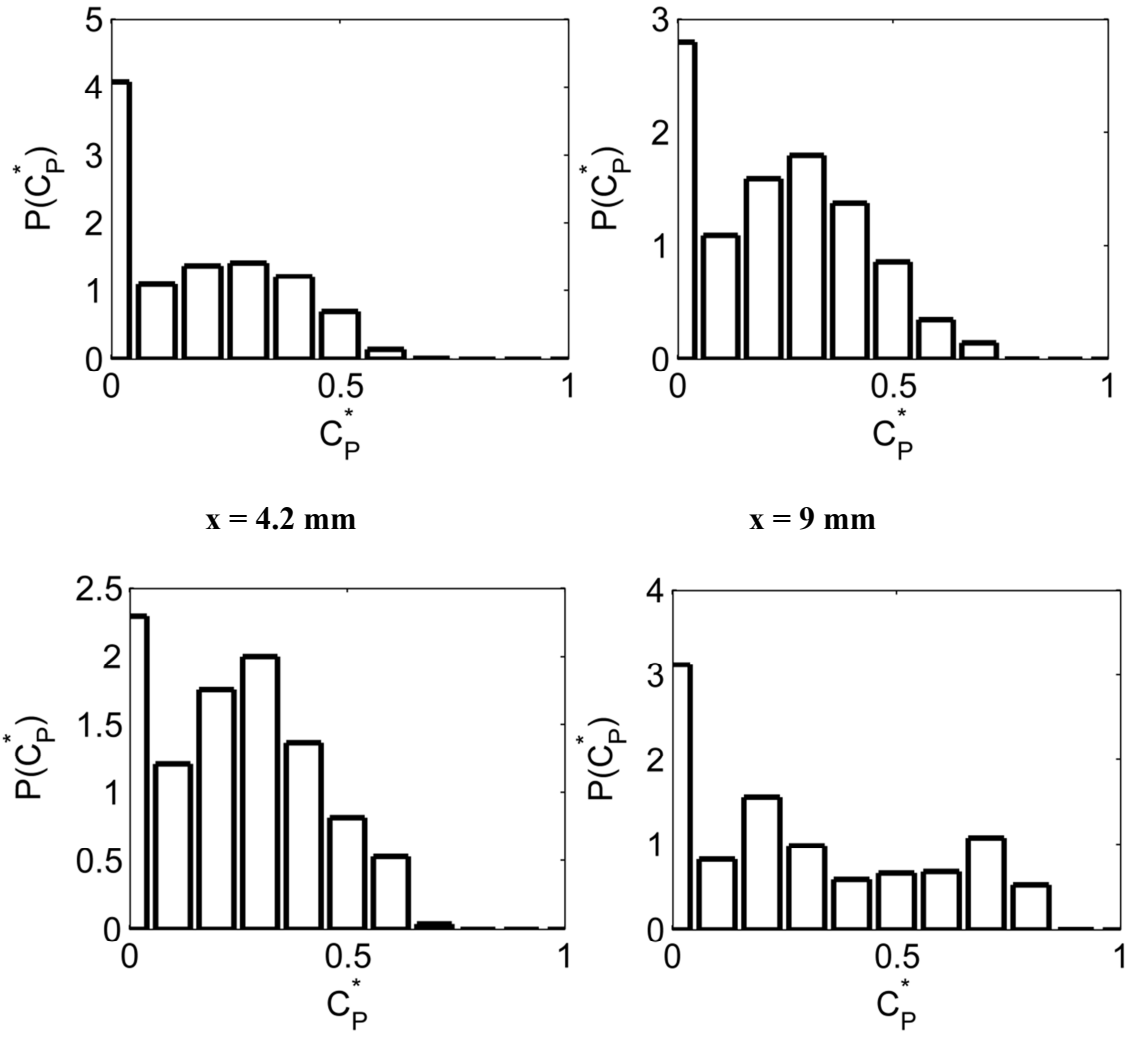

Figure D-3. Pdf of chemical product at four different streamwise locations (F = 8 Hz, U = 20 mm/s and A_2 = 40 μm).

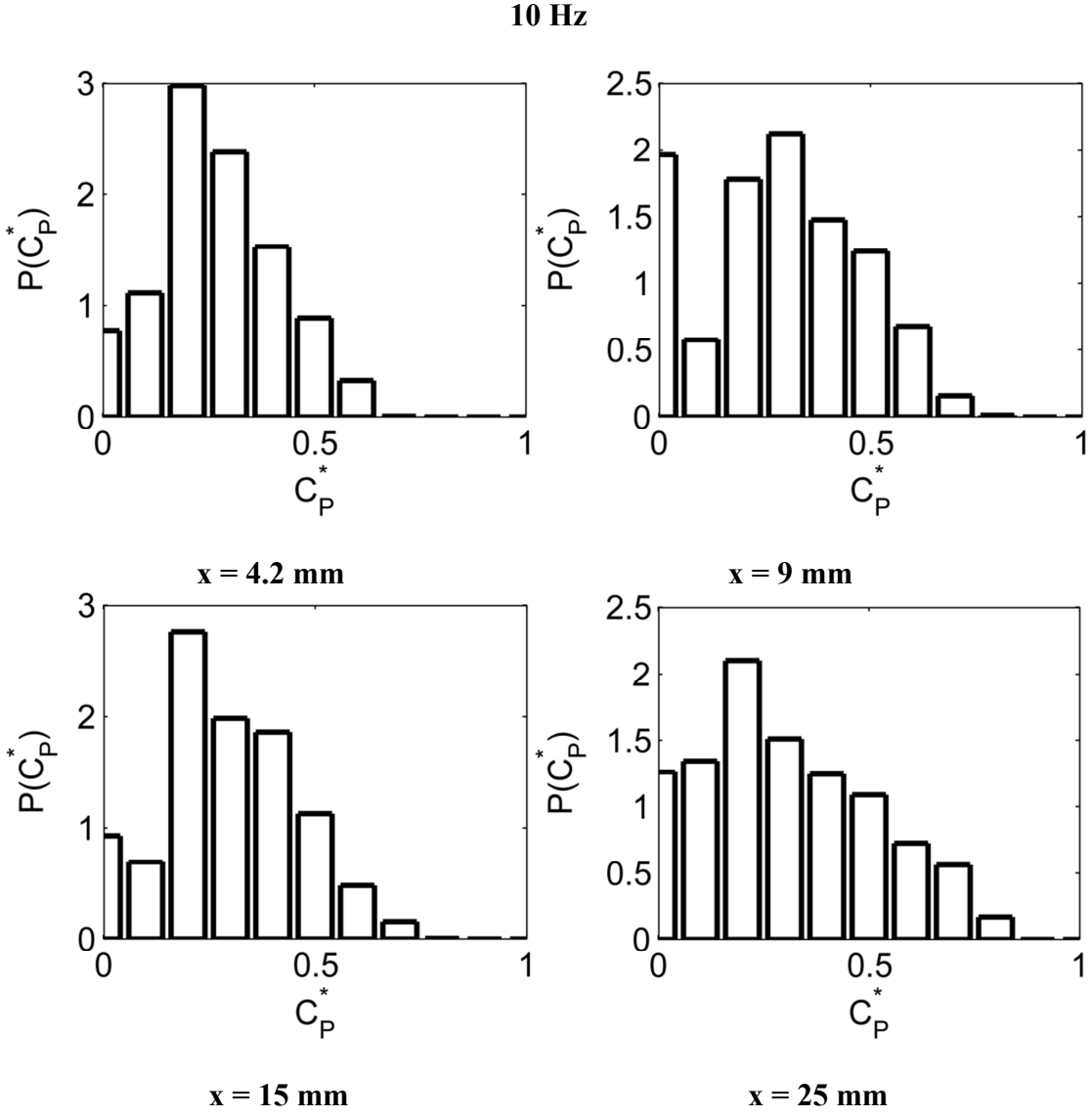

Figure D-4. Pdf of chemical product at four different streamwise locations (F = 10 Hz, U = 20 mm/s and A_2 = 40 μm).

12 Hz

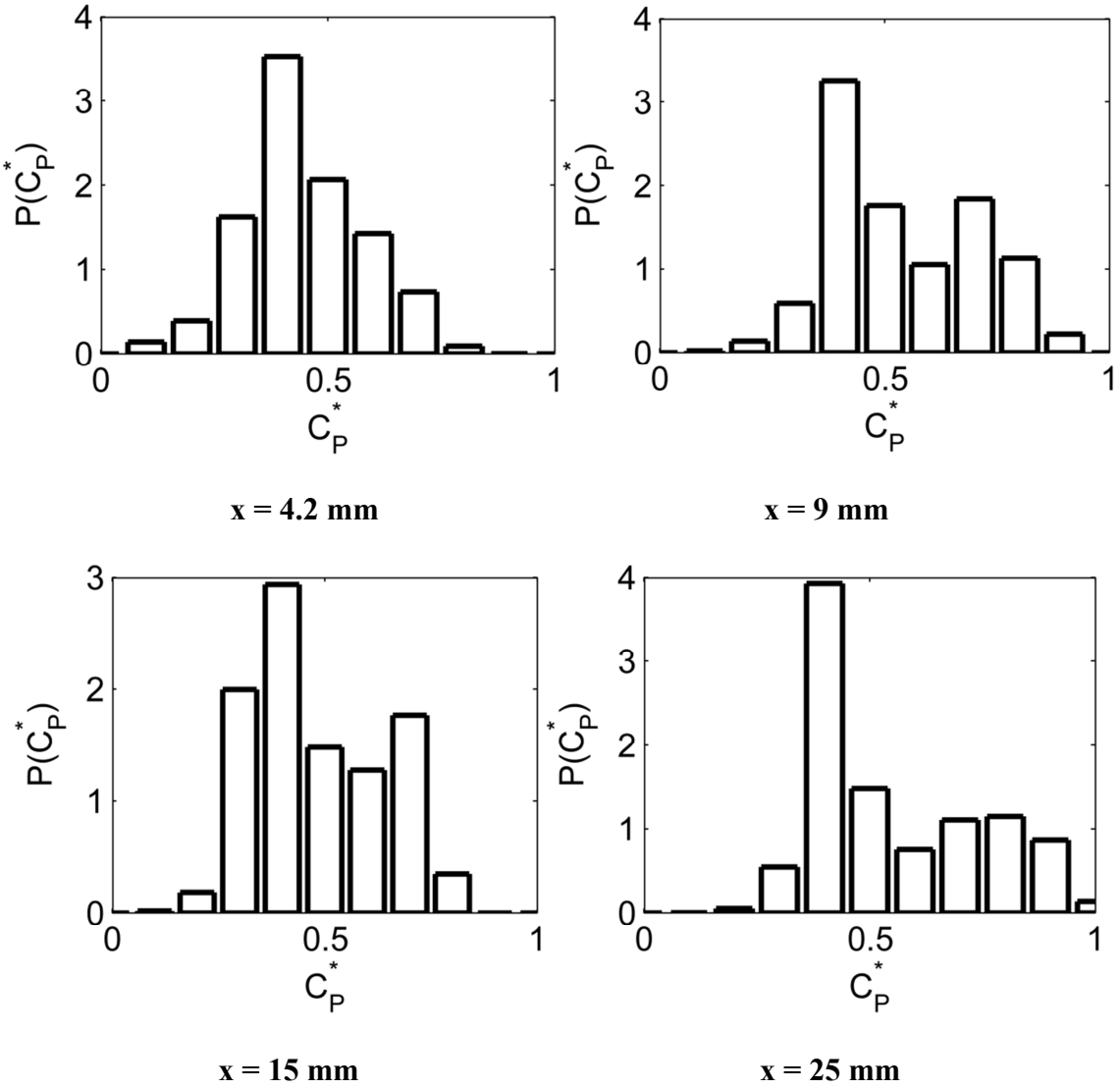

x = 4.2 mm **x = 9 mm**

x = 15 mm **x = 25 mm**

Figure D-5. Pdf of chemical product at four different streamwise locations (F = 12 Hz, U = 20 mm/s and A_2 = 40 μm).

15 Hz

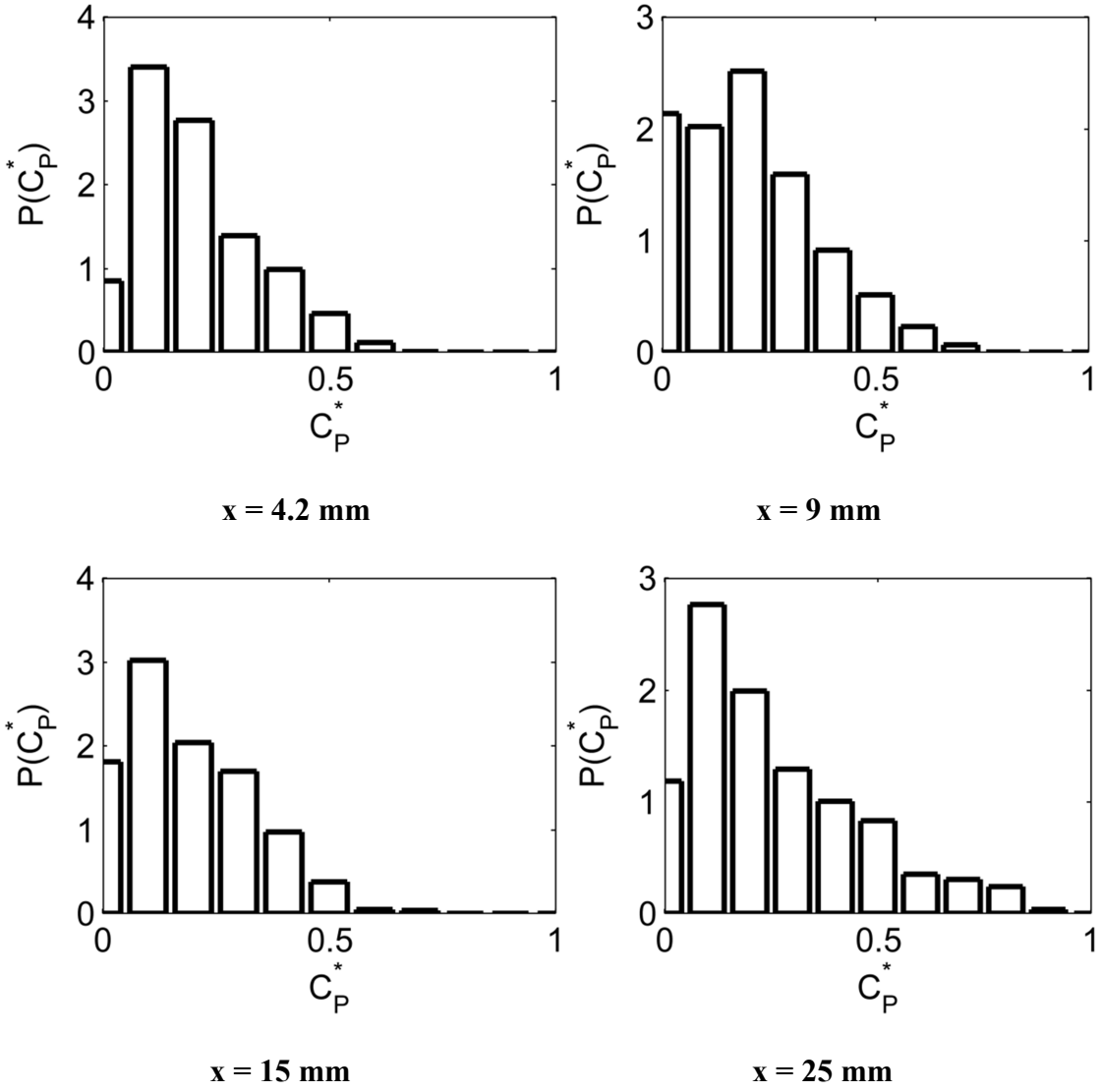

Figure D-6. Pdf of chemical product at four different streamwise locations (F = 15 Hz, U = 20 mm/s and A_2 = 40 μm).

18 Hz

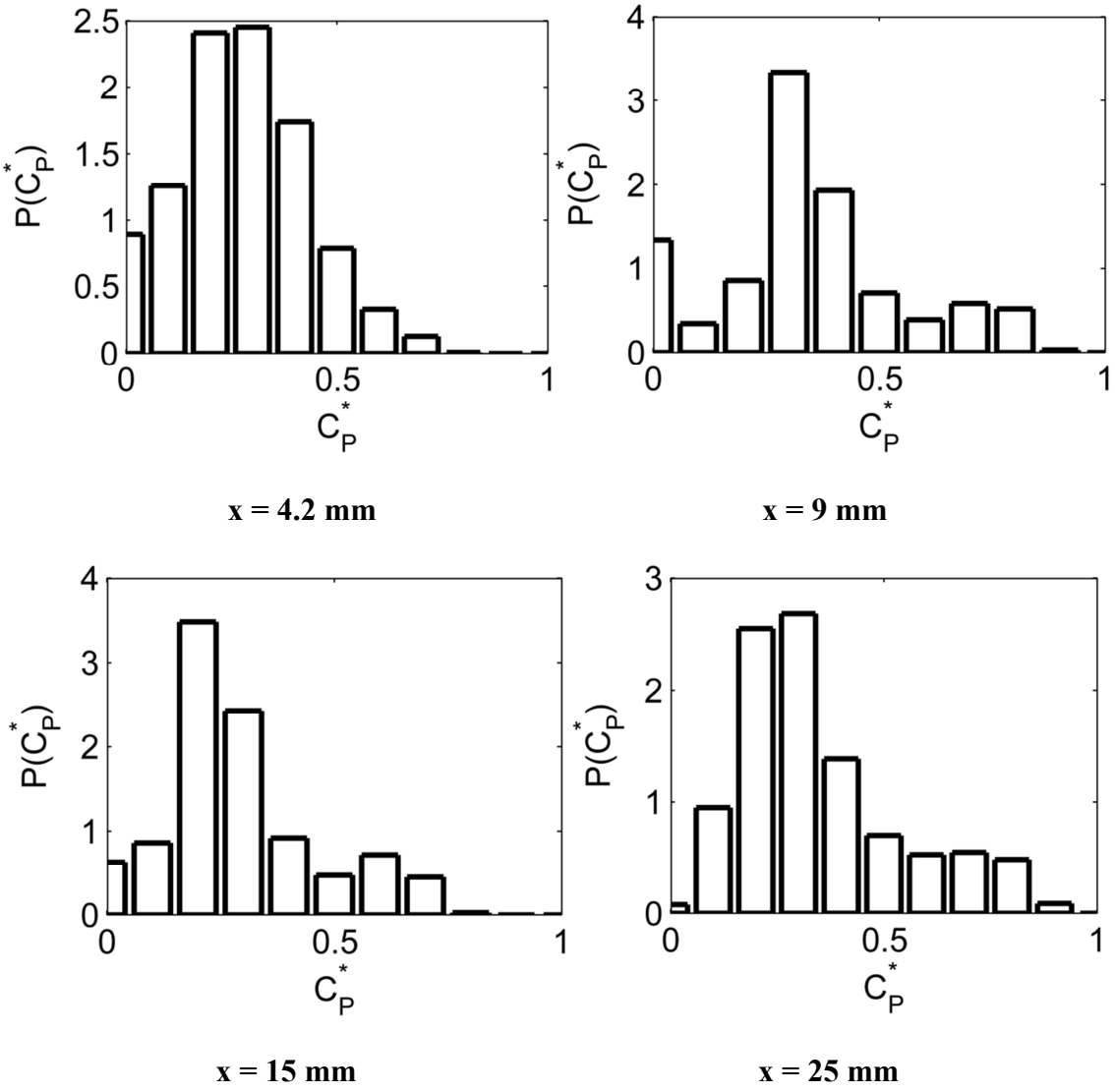

Figure D-7. Pdf of chemical product at four different streamwise locations (F = 18 Hz, U = 20 mm/s and A_2 = 40 μm).

19 Hz

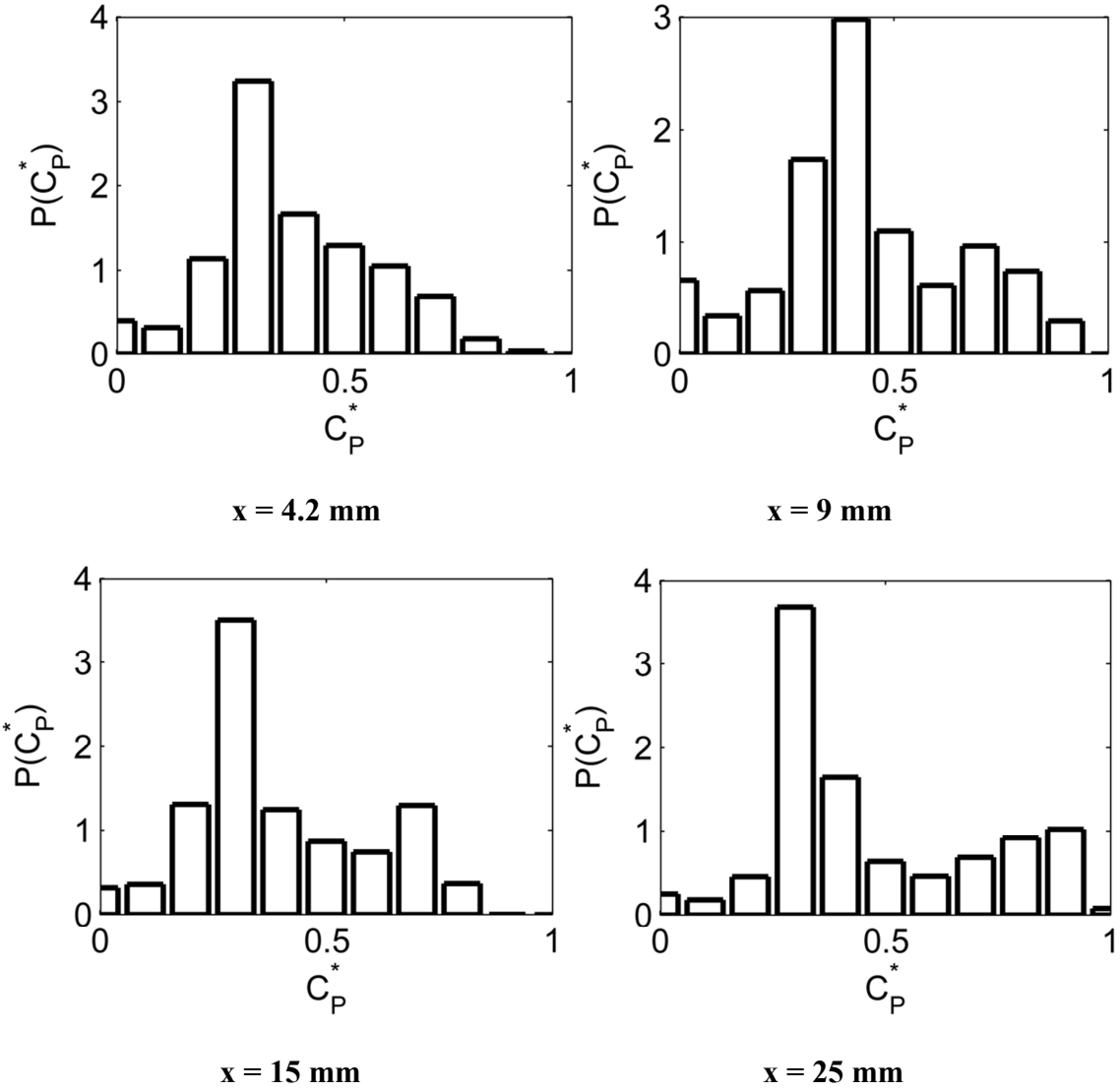

Figure D-8. Pdf of chemical product at four different streamwise locations (F = 19 Hz, U = 20 mm/s and A_2 = 40 μm).

20 Hz

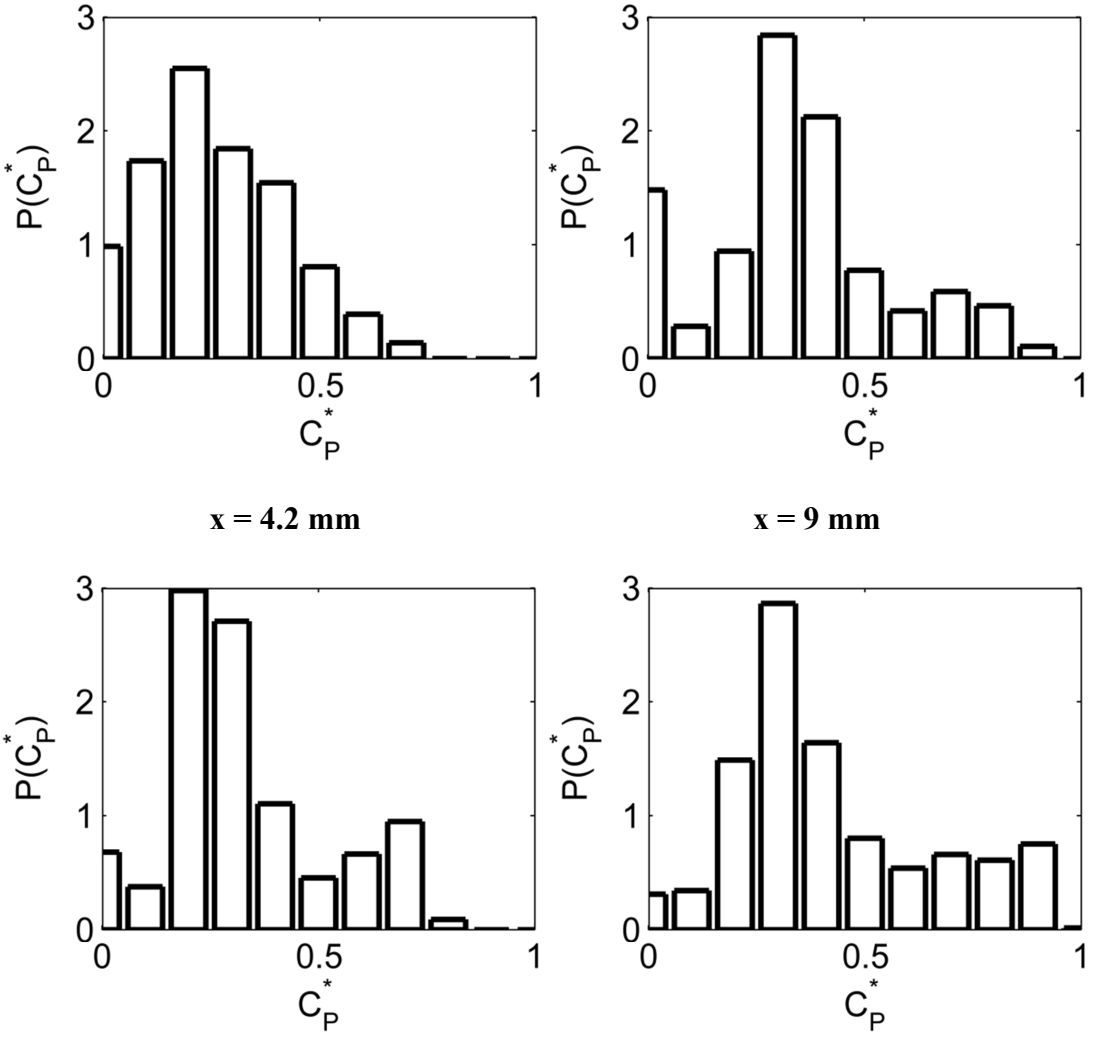

x = 4.2 mm **x = 9 mm**

x = 15 mm **x = 25 mm**

Figure D-9. Pdf of chemical product at four different streamwise locations (F = 20 Hz, U = 20 mm/s and A_2 = 40 μm).

25 Hz

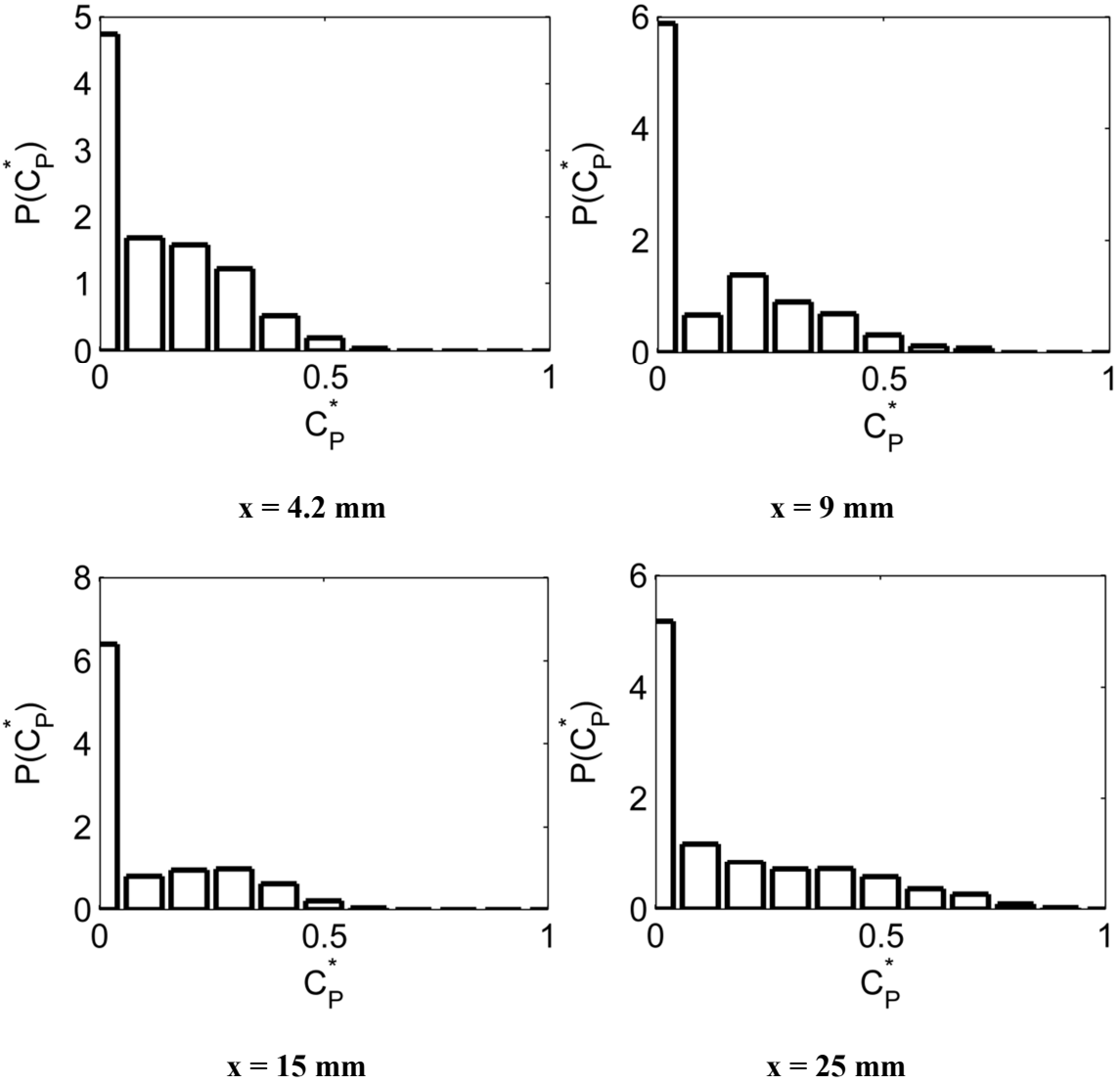

Figure D-10. Pdf of chemical product at four different streamwise locations (F = 25 Hz, U = 20 mm/s and A_2 = 40 μm).

BIBLIOGRAPHY

BIBLIOGRAPHY

Aref, H. (1984), "Stirring by chaotic advection." Journal of Fluid Mechanics, 143:1-21.

Aref, H. (1990), "Chaotic advection of fluid particles." Proc. R. Soc. Lond. A 434:273-289.

Aref, H. (2002), "The development of chaotic advection." Phys. Fluids, 14:1315-1325.

Bau, H. H., Zhong, J. and Yi, M. (2001), "A minute magneto hydro dynamic (MHD) mixer." Sensors and Actuators B, 79:207-215.

Breidenthal, R. (1981), "Structure in turbulent mixing layers and wakes using a chemical reaction." Journal of Fluid Mechanics, 109, pp. 1-24.

Campbell, C. J. and Grzybowski, B. A. (2004), "Microfluidic mixers: from microfabricated to self-assembling devices." Phil. Trans. R. Soc. Lond. A, 362:1069-1086.

Glasgow, I. and Aubry, N. (2003), "Enhancement of microfluidic mixing using time pulsing." Lab Chip, 3:114-120.

Koochesfahani, M. M. (1984), "Experiments on turbulent mixing and chemical reactions in a liquid mixing layer." Ph.D. Thesis, Caltech.

Koochesfahani, M. M. and Dimotakis, P. E., (1986), "Mixing and chemical reactions in a turbulent liquid mixing layer." Journal of Fluid Mechanics, 170, pp. 83-112.

Koochesfahani, M. M. and Dimotakis, P. E. (1989), "Effects of a downstream disturbance on the structure of a turbulent plane mixing layer."AIAA, 27, pp. 161-166.

Koochesfahani, M. M. and MacKinnon, C. G. (1991), "Influence of forcing on the composition of mixed fluid in a two-stream shear layer." Phys. Fluids A., 3(5), pp. 1135-1142.

Koochesfahani, M. and Nelson, R. (1997), "Molecular mixing enhancement in the confined wake of splitter plate." AIAA 97-2007.

Lin, K. W. and Yang, J. T. (2007), "Chaotic mixing of fluids in a planar serpentine channel." International Journal of Heat and Mass Transfer, 50:1269-1277.

Liu, R. H., Stremler, M. A., Sharp, K. V., Olsen, M. G., Santiago, J. G., Adrian, R. J., Aref, H. and Beebe, D. J. (2000), "Passive mixing in a three-dimensional serpentine microchannel." Journal of Microelectromechanical systems, 9, No.2, 190-197.

MacKinnon, C. G. and Koochesfahani, M. M. (1993), "Three-dimensional structure and mixing of a forced wake inside a confined channel." AIAA-93-0658.

Mengeaud, V., Josserand, J. and Girault, H. (2002), "Mixing processes in a zigzag microchannel: Finite element simulations and optical study." Anal. Chem., 74, 4279-4286.

Mensing, G. A., Pearce, T. M., Graham, M. D., and Beebe, D. J. (2004), "An externally driven magnetic microstirrer." Phil. Trans. R. Soc. Lond. A, 362:1059-1068.

Nelson, K. E. (1996), "Structure and mixing in a low Reynolds number forced wake in a confining channel." M.S. Thesis, Michigan State University.

Nguyen, N. T. and Wu, Z. (2005), "Micromixers- a review." J. Micromech. Microeng, 15: R1-R16.

Oster, D. and Wygnanski, I. (1982), "The forced mixing layer between parallel streams." Journal of Fluid Mechanics, 123, pp. 91-130.

Ottino, J. M. (1989), "The kinematics of mixing: stretching, chaos, and transport, Cambridge University Press.

Roberts, F. A. (1985), "Effects of a periodic disturbance on mixing in turbulent shear layers and wakes." Ph.D. Thesis, Caltech.

Roberts, F. A. and Roshko, A. (1985), "Effects of periodic forcing on mixing in turbulent shear layers and wakes."AIAA-85-0570.

Squires, T. and Quake, S. (2005), "Microfluidics: Fluid physics at the Nanoliter scale." Reviews of modern physics, 77, pp. 977-1026.

Stone, H. A., Stroock, A. D. and Ajdari, A. (2004), "Engineering flows in small devices: Microfluidics toward a lab-on-a-chip." Annu. Rev. Fluid Mech, 36:381-411.

Strook, A. D., Dertinger, S. K.W., Ajdari, A., Mezic, I., Stone, H. A. and Whitesides, G. M. (2002), "Chaotic mixer for microchannels." Science, 295, 647 (2002).